CrystEngComm

Accepted Manuscript

ROYAL SOCIETY OF CHEMISTRY

www.rsc.org/crystengcomm

Journal Name

CrystEngComm

Dynamic Article Links ►

Cite this: DOI: 10.1039/c0xx00000x

www.rsc.org/xxxxxx

ARTICLE TYPE

Hybrid Vanadates Constructed from Extended Metal-Organic Arrays. Crystal Architectures and Properties.

Roberto Fernández de Luis,[a,b] Joseba Orive,[a] Edurne S. Larrea,[a] M. Karmele Urtiaga,[a] María I. Arriortua[a,b]*

Received (in XXX, XXX) Xth XXXXXXXXX 20XX, Accepted Xth XXXXXXXXX 20XX

DOI: 10.1039/b000000x

The hybrid vanadates exhibit structural archetypes between the hybrid zeotypes in which the inorganic framework is surrounding an organic cation acting as a template, and metal-organic frameworks which crystal structures are constructed from metal nodes or clusters linked by organic bridges. Here we present the summary of the work carried out in hybrid vanadates constructed from extended metal-organic arrays. The crystal structures are systematically described and classified according to the dimensionality of the inorganic and metal-organic frameworks. Finally, the magnetic, thermal and catalytic properties of different structural archetypes are discussed.

Introduction

The research in the area of open framework materials has become progressively an important field since the discovery of the Stilbite mineral by Crönsted[1] and the synthesis of artificial zeolites by Barrer and Milton. Later, Flamingen *et. al.* proposed the substitution $Si^{4+} \rightarrow Al^{3+} + P^{5+}$ opening a new route to synthesize microporous aluminophosphates.[2] Since these pioneer works, the search for open framework materials has extended to other anions, such as oxyfluoride, phosphite,[3] arsenate, germanate,[4] sulphate, or sulphite, among others.[5] The crystal structures of these compounds are generally formed by the combination of tetrahedral or pseudotetrahedral oxoanions and transition metals in six, five or four coordination polyhedra, sharing vertices between them. Usually, organic amine molecules are used as templates, structure directing agents, or space filling, enhancing the interaction with the inorganic framework, and increasing the thermodynamic stability of the hybrid compounds through the establishment of hydrogen bonds, van der Walls and/or other weak interactions. One of the barriers that hinder the synthesis of real porous materials from these inorganic-organic zeotypes is that the anionic skeleton often collapses during the extraction of the cationic template, owing to the strong electrostatic host-guest interactions, which energetically represent an important contribution to the lattice energy.

The present interest is focused on the construction of metal-organic frameworks (MOFs) through the combination of rigid polyhedral secondary building units of metal ions or clusters connected by organic ligands. There are other auxiliary components, such as blocking ligands, counter-anions, and non-bonding guest or template molecules. The structures and properties of coordination polymers can be well-designed and systematically tuned by the judicious choice of metal-based building blocks and organic linkers, in principle.[6]

This work is focused on hybrid vanadates (here and after HV), a family of inorganic-organic materials sharing structural characteristics of MOFs and zeolite type compounds. HV combines vanadium oxide based structural units, with discrete or polymeric metal-organic subunits. In the first studies on HV, the use of chelating amines avoided the increase of the framework dimensionality through metal-ligand-metal links. So the discrete metal-organic units were linked through the vanadium oxide subunits (hear and after VOS) giving rise to 0D, 1D, 2D or 3D inorganic scaffolds. In that regard, the work of Zubieta *et. al.*[7] is mainly focused on the construction of HV from organic components that usually act chelating the secondary metal centres. In HV the secondary metal centres are defined as these metal cations that are connected to the organic ligands, and usually also to the VOS. A schematic example of HV combining metal-organic discrete units linked through VOS is shown in Fig. 1. The molecular complexes generated by the metal centres and the chelating ligands are connected by the VOS, giving rise to a 1D crystal structure.

The use of bridging ligands allows to combine the inorganic substructures (defined as the framework constructed from the VOS and the secondary metal centres) with metal-organic subnets, giving rise to more complex crystal architectures. Indeed, as it is observed in Fig. 1, metal centres of a square planar metal-organic net can be connected through the VOS, giving rise to a crystal structure combining both 2D inorganic and metal-organic arrays. As in MOFs, the interpenetration or catenation phenomena of the nets are observed in several HV. Moreover, the linkage of these interpenetrated or catenated nets through the VOS gives rise to self-catenated structures.[8]

Since the pioneer work of Zubieta *et al.*[7] a great number of transition hybrid vanadium oxides containing polymeric metal-organic substructures have been reported. Therefore, a generalized highlight comprising the wide range of HV containing extensive metal-organic substructures, reported during the last years, and even a descriptive systematization of these architectures is urgent. The hybrid vanadium oxides constructed from chelating ligands are deeply described in the literature. They possess several common characteristics with the HV containing bridging ligands, so we are going to discuss these points during the descriptions of the crystal structures.

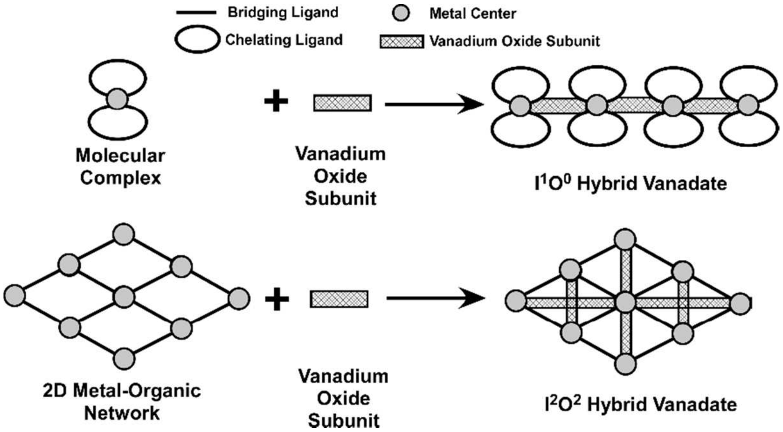

Fig. 1 Schematic representation of the combination between coordination metal-organic complexes plus vanadium oxide subunits (top), and the combination of extended metal-organic nets with vanadium oxide subunits (bottom).

This highlight is divided into four sections dealing with: i) a brief discussion about the crystal chemistry, ii) classification, iii) crystal structure archetypes and iv) thermal, magnetic and catalytic properties of HV.

1.- Hybrid Vanadates Archetypes: From Zeotypes to MOFs

Despite the difficulties to control the final crystal architectures in HV, the analysis of the synergetic interactions between the inorganic and organic components allows a partial degree of "crystal engineering", towards more open or condensed structural archetypes. Three are the main factors that define the obtained crystal structures in HV: i) the coordination preferences and oxidation state of the secondary metal centres; ii) the length, geometry, degree of flexibility and relative position of the donor groups of the ligand and iii) the structural influence of the vanadate anion on the framework organization and assembly adopted by the different metal–organic moieties.

The coordination preferences and geometry of the metal centres is a key issue, just as in classical coordination chemistry. A systematic search in the CSD (Cambridge Structural Database) reveals the existence of 218 different crystal structures for HV in which the metal centres are linked through M-O-V linkage to the VOS. Up to now, Mn(II), Fe(II), Co(II), Ni(II), Cu(II), Cu(I), Zn(II), Ag(I) and Cd(II) secondary metal centres have been used to obtain HV.

Ni(II), Co(II), Mn(II) and Cd(II) cations in HV usually present regular octahedral coordination environments, although a few examples of HV with five coordinated Co(II) cations are known. The great diversity of coordination modes, octahedral, five-coordinated and tetrahedral, for Cu(II) and Zn(II) atoms allows obtaining several crystal structures with different metal coordination environments. This fact makes more difficult the prediction of the structural archetypes obtained with these cations, but enlarge the rich structural diversity of Zn(II) and Cu(II) vanadates in comparison with those obtained from cations possessing regular octahedral coordination spheres. For Cu(I) and Ag(I) the coordination spheres are less predictable, but with certain types of ligands, these ions are only able to support the formation of one-dimensional metal-organic substructures due to their linear coordination.

The length, geometry and position of the donor groups of the ligand determine its role in the construction of the final crystal structure. Chelating ligands, such as 2,2-bipyridine,[9,10] 1,10-phenanthroline[11,12] or terpyridine,[13,14] give rise to discrete metal-organic units. On the other hand, dipodal or multi-podal bridging ligands such as pyrazine, 4,4´-bipyridine, or 1,2-di(4-pyridyl)ethylene allow obtaining extended metal-organic nets (see Tables 1-3). These polytopic organic amino ligands serve to link the metal sites propagating the structural information expressed by the metal coordination preferences through the extended structure. Figs. 2 and 3 show the dipodal and multipodal amino ligands found in HV with extended metal-organic frameworks. The ligands combining both amino and carboxylate donor groups have been also used in the synthesis of HV, allowing an increase in the connectivity of the metal centres through the organic ligand. Another interesting strategy is to use unsymmetrical ligands to obtain non centro-symmetric microporous compounds. The most common ligands containing carboxylate groups observed in HV are depicted in Fig. 4.

On this point, the transition metal HV constructed from dipodal ligands have common characteristics with MOFs, because of the generation of metal-organic sub-structures through the linkage of metal and ligands. Usually the VOS are located in the channels of the metal-organic framework, and directly linked to the secondary metal centres. The combination of metal-organic nets based on nitrogen donor dipodal bridging ligands and VOS, has become also a great chemical strategy to synthesize self-catenated and/or highly connected nets.[15] One of the keys to explain the crystal chemistry of HV is the connectivity between the metal-organic subnets and the VOS, in addition to the VOS role itself.

Vanadium commonly adopts V(V), V(IV) or V(III) oxidation states. The coordination environments, as well as the V-O bond distances, are clearly related to the vanadium oxidation state. The coordination environment of V(III) is a regular octahedron. V(IV) exhibits five or six coordination environments, while V(V) ranges from six to four coordination. The most common coordination environment shown by vanadium atoms in HV are the regular tetrahedron and the distorted square pyramid. Similarly, the most common oxidation state of vanadium atoms in HV is V(V), but several architectures containing five coordinated mixed valence V(V)/V(IV) have been reported. For an extensive work about the oxidation states and coordination environments of vanadium, the reader should refer to the work of Schindler *et al.*[16]

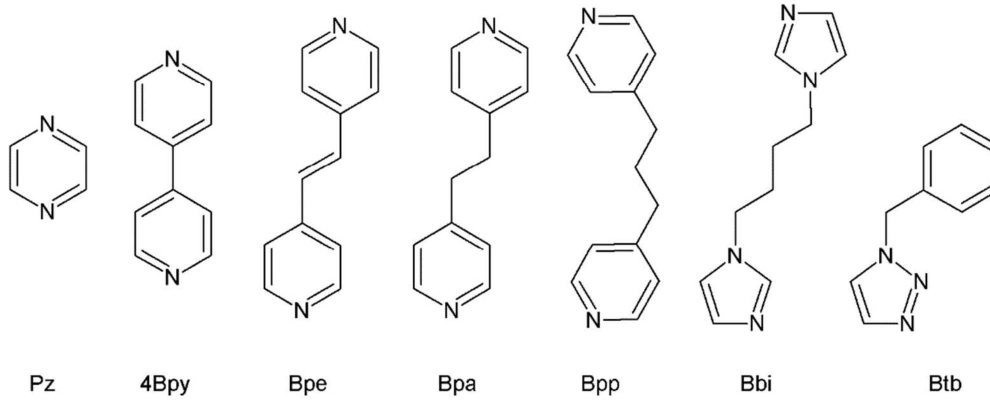

Fig. 2 Bipodal organic ligands observed in HV: Pz (pyrazine), 4Bpy (4,4´-bipyridine), Bpe (1,2-di(4-pyridyl)ethylene), Bpa (1,2-di(4-pyridyl)ethane), Bpp (1,3-bis(4-pyridyl)propane), Bbi (1,4-bis(imidazol-1-yl)butane), Btb (1,4-bis(triazol-1-ylmethyl)benzene).

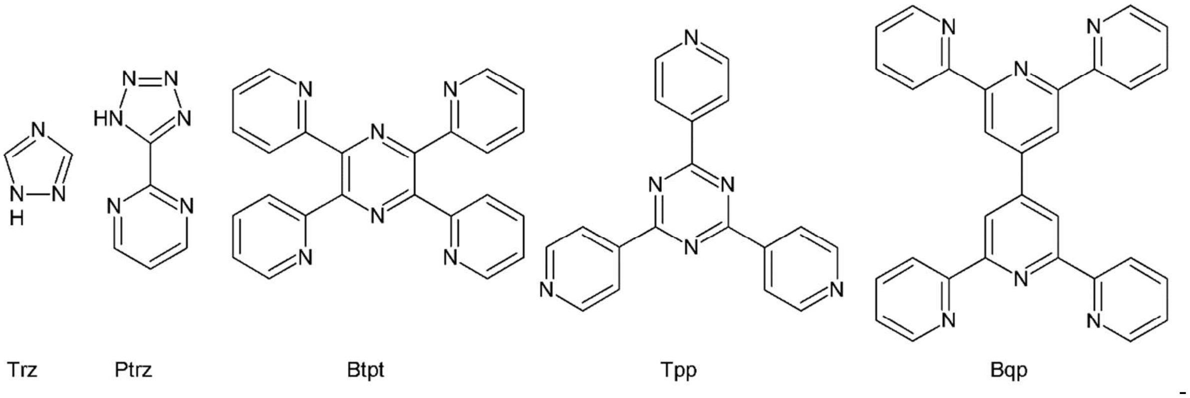

Fig. 3 Multi-podal organic ligands observed in HV: Trz (1,2,4-Triazol), Ptrz (5-(Pyrimidin-2-yl)tetrazol), Btpt (tetra-2-pyridylpyrazine), Tpp (2,4,6-tri(4-pyridyl)-1,3,5-triazine), Bqp (6',6"-Bis(2-pyridyl)-2,2':4',4":2",2'"-quaterpyridine).

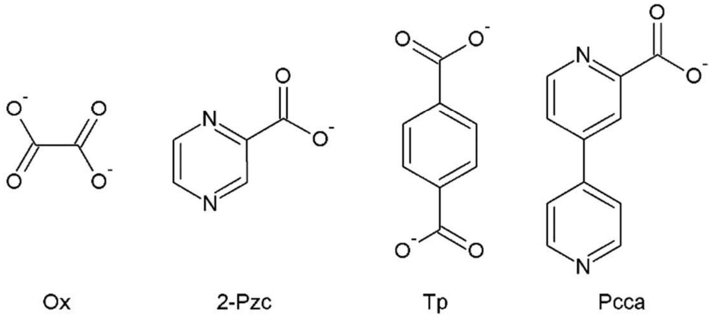

Fig. 4 Multi-podal carboxylic organic ligands observed in HV: Ox (oxalate), 2-Pzc (2-pyrazinecarboxylate), Tp (terephthalate), Pcca (4,4´-bipyridine-2-carboxylate).

Vanadium polyhedra may fuse to provide different VOS, such as discrete oligomers (dimers, cycles or clusters), 1D chains or 2D layers constructed from the same polyhedron or mixtures of various polyhedral types. The most comprehensive study of inorganic structures was provided by Wells in the book *Structural Inorganic Chemistry*,[17] but no specific information about vanadium oxides was included. Later works of Zavalij and Whittingham,[18] and Zubieta *et al*.[7] are extensive studies of the structural chemistry of vanadium oxides with open frameworks and the influence of organic components on vanadium oxide architectures, respectively. Zavalij and Whittingham[18] deeply describe, and systematize the VOS, classifying them according to the coordination environment of vanadium polyhedra and the connectivity between them.

In HV containing bridging ligands, more polymerized VOS, constructed from six coordinated vanadium seem to be avoided, while more open subunits constructed from VO_4 tetrahedra and/or VO_5 polyhedra are favoured. In that regard, the most common VOS are the metavanadate $(VO_3)^-$ chains and the $\{V_4O_{12}\}$ cycles, both formed by corner-sharing (VO_4) tetrahedra. Both units possess the ability to link to metal centres or to other VOS in different directions of the crystal structure. In this sense, the $\{V_4O_{12}\}$ cycle can act as two, four or six connector. Besides the $\{V_4O_{12}\}$ cycles different $\{V_xO_y\}$ cyclic discrete units have been observed, depending on the number of polyhedra that compose them, $\{V_2O_7\}$, $\{V_5O_{15}\}$, $\{V_6O_{18}\}$, $\{V_8O_{25}\}$, $\{V_{10}O_{30}\}$, $\{V_{12}O_{36}\}$, among others (Fig. 5).

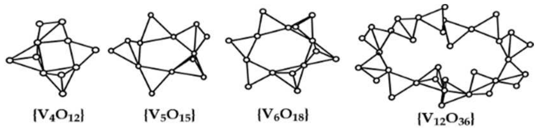

Fig. 5 Several vanadium oxide cycles observed in hybrid vanadates.

With regard to the metavanadate chains, they also could act as multidirectional connectors. This unit possesses certain degree of adaptability to the crystal environment, due to the reorientation and reorganization ability of the (VO_4) tetrahedra. Fig. 6 shows some metavanadate chains belonging to different vanadates. The number of tetrahedra that, by translation, gives rise to the whole chain increases progressively from two, in $Ba(VO_3)\cdot 2H_2O$,[19] to twelve, in $\{Ni(en)_3\}(VO_3)_2$,[20] depending on the connectivity between the metavanadate chains and its crystal environment.

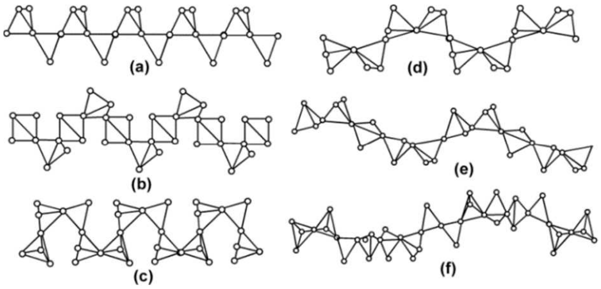

Fig. 6 Metavanadate chains of corner-sharing VO_4 tetrahedra. (a) $Ba(VO_3)\cdot 2H_2O$,[19] (b) $NH_3(CH_2)_4NH_3(VO_3)_2$,[21] (c) $M(Hdpa)V_4O_{12}$ (M=Co, Ni),[22] (d) $Cu(2Bpy)V_2O_6$,[23] (e) $Co_3(Bpp)_4V_6O_{18}\cdot 2H_2O$,[24] (f) $\{Ni(en)_3\}(VO_3)_2$[20].

There is also a very rich crystal chemistry of vanadate chains and layers constructed from five and six-coordinated vanadium atoms, but these structural subunits are not commonly observed in HV constructed from bridging ligands. The reader should consult the work of Zavalij and Whittingham[18] for a more thorough study about VOS in open framework vanadates. Only one kind of metavanadate chains constructed from five coordinated vanadium has been reported. This consists of edge-sharing (VO_5) square pyramids, as observed in Fig. 7.

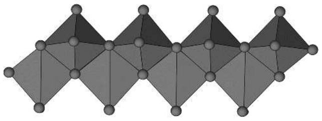

Fig. 7 Metavanadate chains of edge-sharing (VO_5) square pyramids.

The structural diversity of inorganic-organic vanadates is not only based on the great variety of VOS, but also on their ability to link to each other giving rise to more complex one, two- or three-dimensional architectures. There are several vanadates whose crystal structures are constructed from the combination of some of the previously described VOS. Examples of them are the chains constructed from corner-sharing $\{V_6O_{18}\}$ cycles, the chains formed by the connectivity between $\{V_4O_{12}\}$ cycles and $\{V_2O_7\}$ dimers,[25,26] sheets of corner-sharing VO_4 polyhedra or metavanadate chains combined with $\{V_2O_7\}$ dimers (for more information see Tables 1-6). There are also a few examples of HV constructed from vanadium oxide V_xO_y layers. These layers can be described as the combination of corner-linked metavanadate chains of edge-sharing VO_5 polyhedra, as the ones observed in Fig. 7.

2.- Classification of Hybrid Vanadates

The works of Zavalij and Whittingham[18] and Zubieta *et. al*[7] summarize the crystal chemistry of these materials. They proposed two different but complementary classifications. Zavalij and Whittingham based their classification of the open framework vanadium oxides on the coordination environment of the vanadium atom. Seven categories can be distinguished according to the presence of tetrahedra (T), square pyramids (SP) and/or octahedra (O) into the crystal structures. As a complementary point of view, Zubieta *et al.* take into account the role of the metal-organic or organic moiety into the crystal structure, distinguishing four different classes of HV:

a) Compounds in which the organic component or a metal-organic discrete coordination complex acts as an isolated cation, compensating the charge of the vanadium oxide host.
b) Phases in which the organic molecule serve as a ligand directly attached to the oxide array.
c) Transition metal HV in which the organic ligand is coordinated to the transition metal and this secondary metal linked to the VOS through oxygen bridges. The organic ligand coordinates only one metal centre, preventing the propagation of the crystal structure through the organic linkers.
d) HV constructed from extended metal-organic nets (one-, two- or three-dimensional) linked through the metal centre to VOS.

The classification of Zubieta *et. al.*7 lies within the previous one described by Cheetham *et. al.*[27] for hybrid inorganic-organic compounds. These authors proposed a classification based on a $\mathbf{I^nO^m}$ code, in which the $\mathbf{I^n}$ takes into account the dimensionality of the inorganic substructure (n= 0, 1, 2, 3) and $\mathbf{O^m}$ refers to the dimensionality of the metal-organic array (m= 0, 1, 2, 3). In this classification, for example, the zeolite type compounds constructed from three dimensional inorganic skeletons containing isolated organic cations, are classified as $\mathbf{I^3O^0}$ materials, while the coordination polymers formed by inorganic clusters linked through organic ligands are included in the $\mathbf{I^0O^3}$ archetype. It is clear that many systems combine both inorganic and metal-organic extended arrays, for example, there are several MOFs constructed from inorganic chains connected by organic linkers ($\mathbf{I^1O^1}$), or coordination polymers containing inorganic layers pillared by organic ligands directly attached to the metal centres generating also metal-ligand-metal one dimensional arrays ($\mathbf{I^2O^1}$).[28] Fig. 8 (a) summarizes the structural classes described by Cheetham *et. al.*[27] while in Fig. 8 (b) the occurrence of each structural class observed in HV is represented.

Cite this: DOI: 10.1039/c0xx00000x

www.rsc.org/xxxxxx

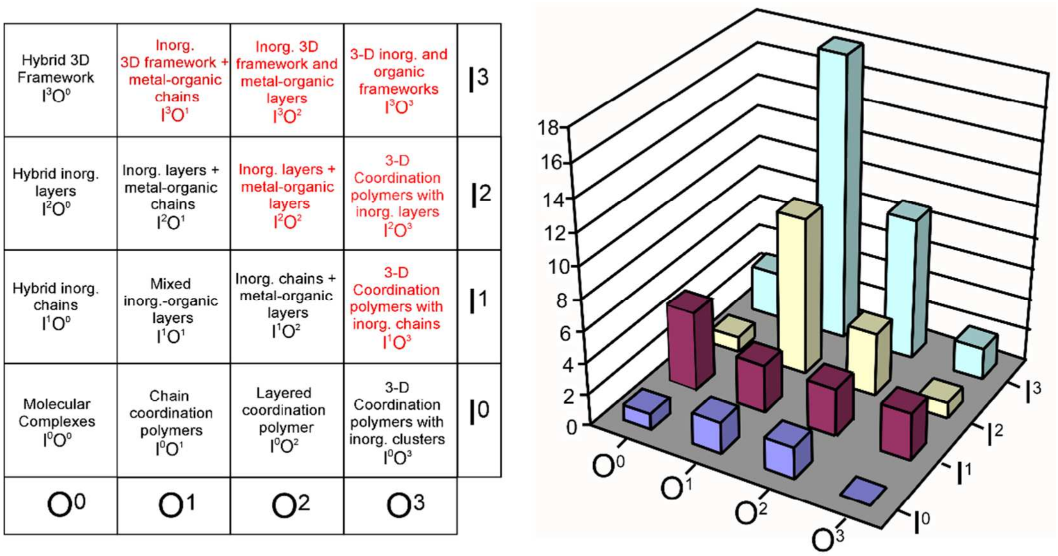

Hybrid 3D Framework I^3O^0	Inorg. 3D framework + metal-organic chains I^3O^1	Inorg. 3D framework and metal-organic layers I^3O^2	3-D inorg. and organic frameworks I^3O^3	I3
Hybrid inorg. layers I^2O^0	Inorg. layers + metal-organic chains I^2O^1	Inorg. layers + metal-organic layers I^2O^2	3-D Coordination polymers with inorg. layers I^2O^3	I2
Hybrid inorg. chains I^1O^0	Mixed inorg.-organic layers I^1O^1	Inorg. chains + metal-organic layers I^1O^2	3-D Coordination polymers with inorg. chains I^1O^3	I1
Molecular Complexes I^0O^0	Chain coordination polymers I^0O^1	Layered coordination polymer I^0O^2	3-D Coordination polymers with inorg. clusters I^0O^3	I0
O0	O1	O2	O3	

(a) (b)

Fig. 8 (a) Cheetham *et. al.* classification for inorganic-organic materials. The red boxes have been completed taking into account the structural archetypes observed in hybrid vanadates (b) Number of hybrid vanadates constructed from bridging ligands classified according to Cheetham *et. al.* nomenclature.

Cheetham *et. al.* proposed a very interesting question in their work: "The question arises as to whether there are materials that could be classified within the empty boxes in the upon right part of the table (red boxes in Fig. 8(a))… we currently known no of such materials, but the possibility exists that these may be found in compounds that have not yet been discovered". Concerning this discussion, Natarajan and Mandal (See Ref. 2(d)) gave a premonitory answer to this question in their work entitled "Open-Framework Structures of Transition-Metal Compounds" suggesting that "the limits are not the imagination and creativity of the researchers but the lack of understanding of the subtler forces involved in the formation of such structures... in the light of this, it should be possible to prepare compounds based on other anions, such as VO_4^{3-}, MoO_4^{2-} or ReO_4^-. A combination of these anionic ligands with transition metals would open the exciting possibilities for new properties and also expand the scope of research in this area".

The great crystallochemistry of the HV exhibit several intermediate structural archetypes combining extended metal-organic and inorganic arrays from zeolitic types (**I^3O^0**) to coordination polymers (**I^0O^3**). There are several examples of HV with complex structures lying in the previously empty boxes of the Cheetham *et. al.* classification. As it is shown in Fig. 8 (b), the analysis of the crystal structures reveals that **I^3O^2**, **I^3O^1**, **I^2O^2** and **I^2O^1** architectures the most common ones in HV. In the same way that in metal-organic frameworks, the main factors that influence the dimensionality of the metal-organic substructure are the secondary metal coordination environment and ligand-metal connectivity. But, in HV, the VOS plays a crucial role, connecting the metal centres belonging to the metal-organic substructure, and hence, giving rise to a higher dimensionality of the inorganic framework and a greater degree of complexity in the crystal structures.

Fig. 9 outlined the simplification of the main structural archetypes observed in HV in function of the metal-organic and inorganic substructures dimensionalities, according to the Cheetham *et. al.* terminology, within each of the **I^nO^m** groups. The inorganic scaffold (**I**) is defined by the linkage of the VOS and the secondary metal centres, while the metal-organic substructure (**O**) is built up from the secondary metals and the organic linkers. It is also necessary to incorporate the information of the whole crystal structure dimensionality into the Cheetham **I^nO^m** code, since the same combination of inorganic and metal-organic moieties could give rise to crystal structures with different dimensionalities, as shown in Fig. 9. For this reason, another code based on the overall dimensionality which takes into account the interaction between both subnets has been introduced. For example, the **I^1O^2** compounds are described also as 1D + 2D → 3D. When the crystal framework contains interpenetrated or polycatenated metal-organic subnets, the metal-organic substructure dimensionality will be denoted as (2D + 1D), that would represent a crystal structure that contains metal-organic layers polycatenated with metal-organic chains.

Cite this: DOI: 10.1039/c0xx00000x
www.rsc.org/xxxxxx

ARTICLE TYPE

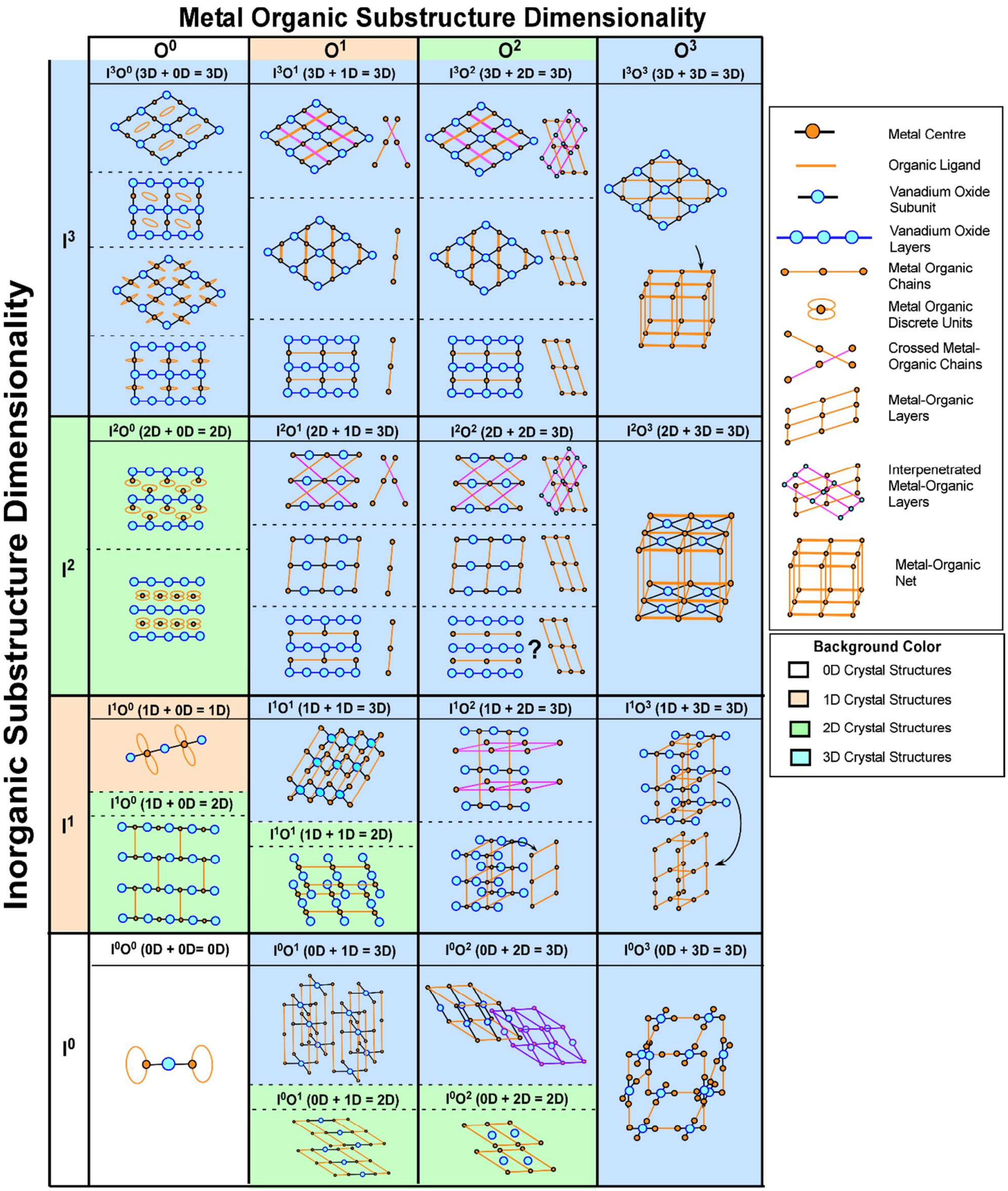

Fig. 9 Schematic representation of the different structural archetypes observed in hybrid vanadates

Cite this: DOI: 10.1039/c0xx00000x

www.rsc.org/xxxxxx

ARTICLE TYPE

In order to better distinguish the metal-organic substructure and the VOS, the simplified models have been represented with different colours, orange and pink for metal-organic part and blue for VOS as stated in the legend of Fig. 9. Within several **I^{n}O^m** archetypes a picture of the metal-organic substructure simplification has been depicted next to the simplified model. The metal centres and VOS have been simplified as nodes of the nets, while the ligands have been represented as connectors between metal centres. In the specific case of chelating ligands, one line connects twice one metal centre. The vanadium oxide layers have been simplified as connected VOS.

The background colour in Fig. 9 is related to the crystal structure dimensionality within the different structural archetypes. On the other hand, we have observed that crystal structures classified within the same **I^{n}O^m** code could present different structural organizations of the metal-organic and inorganic skeletons. A clear example in that regard is that of the **I^{2}O^0** architectures, with two different subclasses crystal archetypes constructed from different arrangement of the metal-organic discrete units and the vanadium oxide layers. In the first architecture the organic ligand is chelating the metal centre, and this one is linked directly to the VOS, while in the second type, discrete metal-organic units are disposed between the vanadium oxide layers (see Fig. 9, **I^{2}O^0** box).

In the following section the crystal structures observed for each **I^{n}O^m** archetype will be described and discussed. The main discussion of this highlight will be focused on HV constructed from bridging ligands, but for the sake of comparison, several examples of HV constructed from chelating ligands have been also briefly mentioned.

In Tables 1 to 6, most of the HV constructed from dipodal and multi-podal organic ligands are included. The VOS and metal-organic substructure are briefly described. The coordination environment and oxidation state of the vanadium atoms are also mentioned. The crystal structures have been classified according to the metal-organic and inorganic substructure dimensionalities, as it has been previously explained. The CSD "Cambridge Structural Database" reference codes for the compounds are also shown when available.

3. -Crystal Architectures

3.1.- I^{3}O^m (m=0–3) Architectures: Hybrid Vanadates Archetypes Containing Three-Dimensional Inorganic Scaffolds.

The **I^{3}O^m** crystal architectures are characterized by three-dimensional inorganic substructures constructed from linkages between the secondary metal centres and the VOS. According to the metal-organic substructure dimensionality, four archetypes of **I^{3}O^m** crystal structures can be distinguished: **I^{3}O^0**, **I^{3}O^1**, **I^{3}O^2** and **I^{3}O^3**.

Among the **I^{3}O^0** architectures, there are four different types of structures shown in the Scheme 1. The HV belonging to the two first types (Scheme 1 (a) and (b)) possess organic molecules not bonded to the inorganic substructure, so, in fact, the metal-organic substructure, does not exist. In this sort of structures, the organic molecule is positively charged and acts compensating the charge of the inorganic skeleton. The main difference between the types observed in the Scheme 1 (a) and (b) in the VOS. In the concrete case of the (b) type the structures are constructed from vanadium oxide layers. These compounds are structurally similar to aluminophosphates or transition metal phosphates, arsenates, phosphites, germanates, etc. Several examples of HV belonging to this group are known, such as $\{Mn_3(en)\}(V_4O_{16})$,[29] $[\{Ni(enMe)_2\}_{0.5}(V_6O_{14})]\cdot(H_2enMe)_{0.5}$,[30] $[(N(CH_3)_4]_2[Co(H_2O)_4(V_{12}O_{28})]$,[31] $[enH_2][Mn_3(V_2O_7)_2(H_2O)_2]$,[32] and $[C(NH_2)_3]_2[M^{II}(H_2O)_4(VO_3)_4]$ 4H$_2$O, M=Ni, Co, Mn.[33]

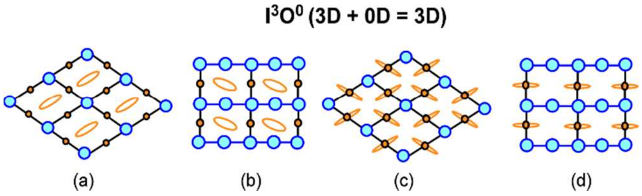

Scheme 1 Structural types in **I^{3}O^0** group.

In the other two types of **I^{3}O^0** vanadates (Scheme 1 (c) and (d)), the organic molecule is chelating the metal centre and, therefore, the dimensionality of the metal-organic substructure does not extend, being 0D. Two examples of this architecture are $[\{Ni(Ht)\}(VO_3)_2]\cdot0.33H_2O$ (**Fig 10**) and $[\{Cu(Ht)\}(VO_3)_2]\cdot0.33H_2O$, (Ht= 5,5,7,12,12,14-hexamethyl-1,4,8,11-tetraazacyclotetradecane) vanadates.[34] The equatorial plane of the nickel(II) and copper(II) atoms consists of four nitrogen atoms belonging to the Ht organic ligand. The axial oxygen atoms of the secondary metal centre are shared with the metavanadate chains, generating porous 3D frameworks, whose channels are filled by crystallization water molecules.

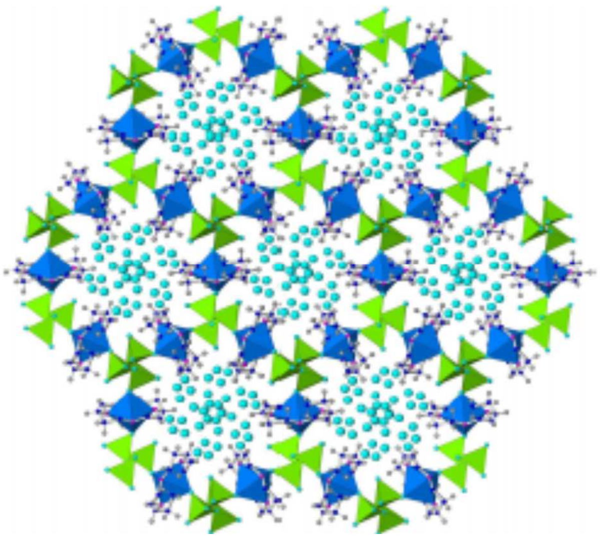

Fig. 10 Crystal structure of $[\{Ni(Ht)\}(VO_3)_2]\cdot0.33H_2O$ (green polyhedra: metavanadate chains constructed from corner-linked VO$_4$ tetrahedra, blue polyhedra: NiN$_4$O$_2$ octahedra, cyan spheres: crystallization water molecules).[34]

Another **I^3O^0** (b) type compound is the $\{Cu_2(Pz)\}(V_4O_{12})$[42] HV, in which two copper(II) atoms are linked through the Pz ligand generating discrete metal-organic units. Within this category a great number of HV with chelating ligands such as ethylenediamine, *N*,*N*-bis(3-aminopropyl)ethylenediamine, 1,3-diaminopropane, among others, have been reported.[35]

Two interesting examples of **I^3O^0** group containing bridging oxalate ligands are the (en)$[\{Co_2(Ox)\}(V_4O_{12})]$ and $(H_2pn)[Mn_2(Ox)(V_4O_{12})]$ HV.[77,78] These compounds combine discrete metal-oxalate dimers linked through the $\{V_4O_{12}\}$ cycles giving rise to 3D + 0D → 3D inorganic-organic scaffolds. The protonated amines act as templates compensating the negative charge of the inorganic-organic skeleton, stabilizing the framework *via* weak interactions.

Table 1 Hybrid vanadium oxides constructed from pyrazine and pyrimidine (The coordination environment of the vanadium cations has been briefly described as 4-c, 5-c, and 6-c for tetrahedral, square pyramid and octahedral coordination spheres. In the same sense the oxidation states for the vanadium atoms have been depicted as V(V) and V(IV)).

Compound	**Vanadium oxide subunit**	**Metal-organic subnet**	**Class.**	**Ref.**
Pyrazine (Pz)				
$\{M(Pz)\}(VO_3)_2$ M= Ni, Co	Metavanadate chains. 4-c V(V)	M(Pz) crossed chains (1D)	I^3O^1 3D+1D→3D	POCNIF [36] QOXFEO [37]
$\{M(Pz)\}(V_4O_{10})$, M= Ni, Co, Zn	Vanadium oxide layers constructed from corner-shared double metavanadate chains. 5-c V(V)/V(IV)	M(Pz) chains parallel to the vanadium oxide layers (1D)	I^3O^1 3D+1D→3D	XEHYAL, XEHXUE, XEHYEP [38]
$\{Ni_2(H_2O)_2(Pz)\}(V_4O_{12})$	$\{V_4O_{12}\}$ cycles. 4-c V(V)	Ni(Pz) chains (1D)	I^2O^1 2D+1D→3D	GICDEC [39,40]
$\{Ni_3(Pz)_3\}(V_8O_{23})$	Metavanadate chains of corner-sharing VO_4 tetrahedra, linked through V_2O_7 dimers. 4-c V(V)	Ni(Pz) chains (1D)	I^3O^1 3D+1D→3D	GICDAY [39]
$[\{Cu(Pz)_2\}(V_6O_{16})]\cdot 0.22H_2O$	Vanadium oxide layers constructed from corner-sharing double metavanadate chains. 5-c V(V)	$Cu(Pz)_2$ square like metal-organic layers (2D)	I^3O^2 3D+2D→3D	IJUCIZ [41]
$\{Cu_2(Pz)\}(V_4O_{12})$	$\{V_4O_{12}\}$ cycles. 4-c V(V)	$Cu_2(Pz)$ discrete units (0D)	I^3O^0 3D+0D→3D	MUJSAL [42]
Pyrimidine (Pym)				
$\{Co(Pym)\}(VO_3)_2$	Metavanadate chains of edge-sharing VO_5 polyhedra. 5-c V(V)	Co(Pym) chains (1D)	I^1O^3 3D + 1D→3D	[43]

When the ligand acts as a bridge between metal centres a polymeric metal-organic substructure is generated and the crystal architectures are classified as **I^3O^1**, when the linkage between metal centres and bridging ligands produces chains, **I^3O^2**, when it generates layers and **I^3O^3**, when it gives rise to 3D metal-organic nets.

Among the **I^3O^1** crystal structures, the disposition of the metal-organic chains with respect to each other and the vanadate substructure are the main characteristics that define the three different types within this group (see Scheme 2). The structural archetypes shown in the Scheme 2 (a) and (b) correspond to three dimensional crystal structures constructed from crossed or parallel metal organic chains linked through the VOS. The connectivity between the VOS and the transition metal centres gives rise to three dimensional inorganic frameworks.

The metal-organic chains can present a crossed disposition (see Scheme 2 (a)), as in $\{M(Pz)\}(VO_3)_2$ M= Ni, Co, $[\{Ni_6(H_2O)_{10}(4Bpy)_6\}(V_{18}O_{51})]\cdot 1.5\cdot H_2O$, and $[\{Ni(H_2O)_2(Bpe)\}(V_4O_{11})]\cdot 0.5\cdot H_2O$ HV, shown in Fig. 11.[36,38,46] The crystal structures of these compounds exhibit a rhombic like inorganic skeleton stabilized by the organic ligands. The Ni-Pz, Ni-4Bpy and Ni-Bpe metal-organic chains show a crossed disposition within the crystal structure. The main difference between these crystal structures lies in the VOS. The $\{Ni_2(H_2O)_4(Bbi)_2\}(VO_3)_4)]\cdot 2H_2O$[61] compound exhibits a similar crystal architecture, however, the metal-organic chains are undulated due to the flexibility of the Bbi ligand.

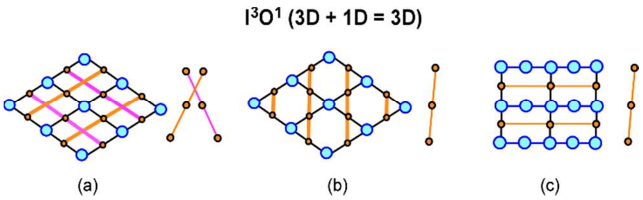

Scheme 2 Structural types in **I^3O^1** group.

A parallel disposition of the metal-organic chains to each other is observed in the second type of **I^3O^1** (see Scheme 2 (b)). In the specific case of $\{Ni_3(Pz)_3\}(V_8O_{23})$[40] HV, the metal-organic chains possess a trans-trans-cis connectivity, instead the linear linkage observed for the previously described compounds. The same structural arrangement showed by the previously described compounds, is observed for $\{Co(H_2O)(Bbi)\}(VO_3)_2$[61] HV, with $\{Co(Bbi)\}$ undulated metal-organic chains.).

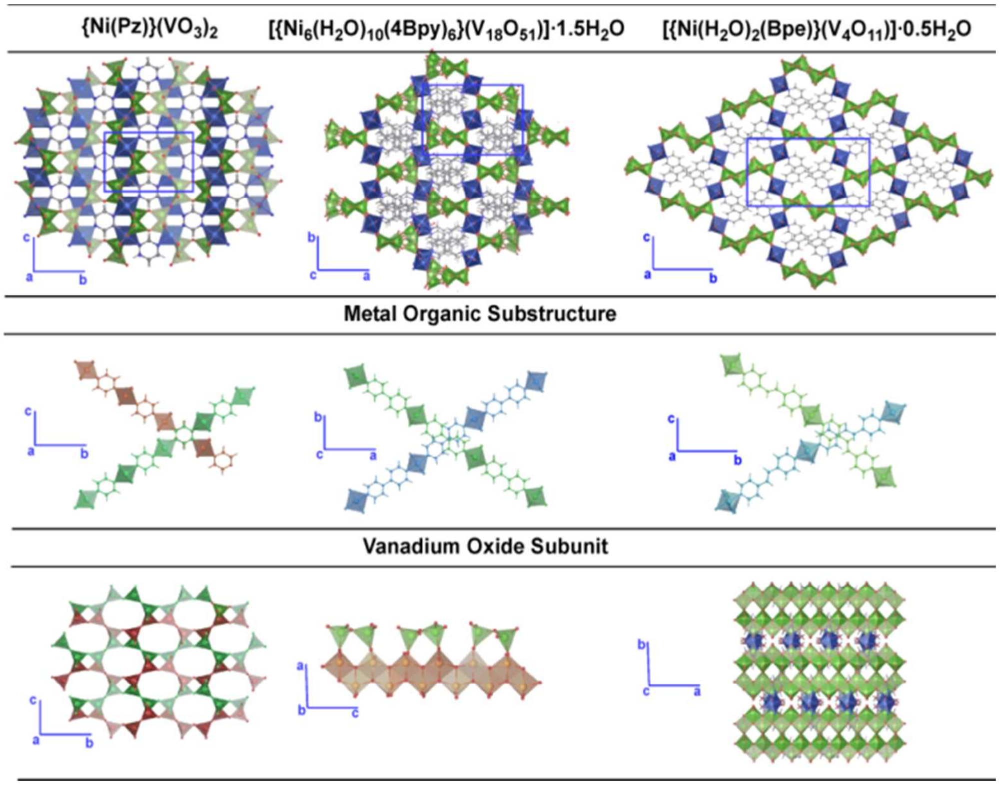

Fig. 11 Crystal structures, metal-organic substructure and vanadium oxide subunit for $\{M(Pz)\}(VO_3)_2$, M=Ni, Co, $[\{Ni_6(H_2O)_{10}(4Bpy)_6\}(V_{18}O_{51})]\cdot1.5\ H_2O$ and $[\{Ni(H_2O)_2(Bpe)\}(V_4O_{11})]\cdot0.5\ H_2O$.[36,40,46]

In $\{Ni_2(H_2O)_2(Bpa)_2\}(V_6O_{17})$,[59] the Ni(II) octahedra are directly coordinated to the Bpa ligands generating $\{NiBpa\}_n$ chains parallel to the vanadium oxide chains. Fig. 12 (a) shows the crystal structure of $\{Ni_2(H_2O)_2(Bpa)_2\}(V_6O_{17})$. Each metal-organic chain is connected to vanadium oxide chains in three different directions, while the VOS are linked to six different metal-organic chains. Fig. 12 (b) shows the connectivity between the V_2O_7 dimers and $\{V_4O_{12}\}$ cycles with the Ni(II) cations. The Bpa organic ligands have been simplified as connectors between the Ni(II) metal centres.

$M_4(2\text{-}Pzc)_4(V_6O_{17})$, M= Ni, Co and $[(NH_4)_2Co_8(H_2O)_2(2\text{-}Pzc)_8(VO_3)_{10}]\cdot xH_2O$ compounds also exhibit **I^3O^1** crystal architecture constructed from $\{M(2\text{-}Pzc)\}$ metal-organic chiral tubes based on metal-ligand helical chains.[79] The disposition of these tubular metal-organic chains (purple polyhedral in Fig. 13) and the double metavanadate chains (green polyhedral in Fig. 13) in the 3D porous crystal structures of $M_4(2\text{-}Pzc)_4(V_6O_{17})$, M= Ni, Co and $[(NH_4)_2Co_8(H_2O)_2(2\text{-}Pzc)_8(VO_3)_{10}]\cdot xH_2O$ are shown in Fig. 13.

Other **I^3O^1** compound is $\{Co_2(H_2O)(2\text{-}Pzc)\}(VO_3)_3$[38]. The metal-organic chains in $\{Co_2(H_2O)(2\text{-}Pzc)\}(VO_3)_3$[38] are constructed from Co(II) dimeric units linked by the 2-Pzc ligand. The metavanadate chains are also parallel to the metal-organic chains, and their linkage generates a 3D compact crystal structure, instead of the porous framework observed within the helical tubes of $M_4(2\text{-}Pzc)_4(V_6O_{17})$, M= Ni, Co and $[(NH_4)_2Co_8(H_2O)_2(2\text{-}Pzc)_8(VO_3)_{10}]\cdot xH_2O$. The choice of unsymmetrical ligands such as 2-Pzc introduces chirality into the structures, demonstrating that this may be a good approach to obtain microporous chiral compounds.[79]

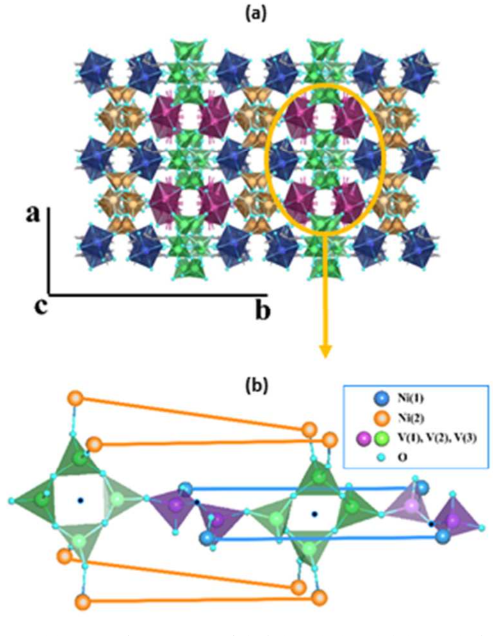

Fig. 12 (a) Crystal structure of $\{Ni_2(H_2O)_2(Bpa)_2\}(V_6O_{17})$ (blue and purple: $NiN_2O_3(H_2O)$ polyhedra, and orange and green, metavanadate chains. (b) Connectivity between the $\{V_4O_{12}\}$ cycles and $\{V_2O_7\}$ dimers and the metal-organic chains in $\{Ni_2(H_2O)_2(Bpa)_2\}(V_6O_{17})$. The Bpa ligands have been simplified as lines.[59]

Cite this: DOI: 10.1039/c0xx00000x

www.rsc.org/xxxxxx

ARTICLE TYPE

Table 2 Hybrid vanadium oxides constructed from 4,4´-bipyridine. (The coordination environment of the vanadium cations has been briefly described as 4-c, 5-c, and 6-c for tetrahedral, square pyramid and octahedral coordination spheres. In the same sense the oxidation states for the vanadium atoms have been depicted as V(V) and V(IV)).

Compound	**Vanadium oxide subunit**	**Metal-organic subnet**	**Class.**	**Ref.**
4,4´-Bipyridine (4Bpy)				
[{$M_2(H_2O)_2(4Bpy)_3$}$(VO_3)_4$]·2.5H_2O M= Ni, Co	Metavanadate chains of corner-sharing VO_4 tetrahedra. 4-c V(V)	Interpenetrated $M_2(4Bpy)_3$ square like metal-organic layers (2D+2D)	I^3O^2 3D + (2D + 2D) → 3D	OCAQOY [44] FIYDOH [45]
{$Ni_6(H_2O)_{10}(4Bpy)_6$}{$V_{18}O_{51}$}]·1.5 H_2O	Metavanadate chains of edge-sharing VO_5 polyhedra, corner linked to V_2O_7 dimers. 4-5-c V(V)	Ni(4Bpy) crossed metal-organic chains (1D)	I^3O^1 3D+ 1D→3D	OHUQUE [46]
[{$Ni_8(4Bpy)_{16}$}$(V_{24}O_{68})$]·8.5H_2O	V_5O_{15} cycles corner linked through single VO_4 tetrahedra, generating chains. 4-c V(V)	Polycatenation of $Ni(4Bpy)_2$ “cds” like 3D metal-organic subnet with two square like $Ni(4Bpy)_2$ metal-organic layers (3D+2D+2D)	I^3O^3 3D + (2D+3D) → 3D	DUXKEN [47]
{Co(4Bpy)}$(VO_3)_2$	{V_4O_{12}} cycles. 4-c V(V)	Co(4Bpy) parallel metal-organic chains (1D)	I^2O^1 2D + 1D→3D	QOXFAK [37]
[{Ag(4Bpy)}$_4$$(V_4O_{12})$]·2$H_2O$	{V_4O_{12}} cycles. 4-c V(V)	Ag(4Bpy) parallel chains (1D)	I^2O^1 2D + 1D→3D	EGOGUD [48]
{M(4Bpy)}(V_4O_{10}) M= Cu, Ag	Vanadium oxide layers constructed from corner-sharing double metavanadate chains. 5-c V(V)	M(4Bpy) parallel chains (1D)	I^3O^1 3D + 1D→3D	WIMHUW [49] WIMJAE [49]
[{Cu(4Bpy)}$_4$$(V_4O_{12})$]·2$H_2O$	{V_4O_{12}} cycles. 4-c V(V)	$Cu_2(4Bpy)_2$ double chains (1D)	I^1O^1 1D + 1D→3D	PAVDAS [50]
[{Mn(4Bpy)}$(VO_3)_2$]·1.16H_2O	Metavanadate chains of edge-sharing VO_5 polyhedra. 5-c V(V)	Mn(4Bpy) layers (2D)	I^2O^2 2D+2D →3D	TAQYER[51]
[{$Mn(4Bpy)_{0.5}$}$(VO_3)_2$]·0.62H_2O	Metavanadate chains of edge-sharing VO_5 polyhedra. 5-c V(V)	$Mn(4Bpy)_{0.5}$ discrete layers (2D)	I^2O^2 2D + 2D →3D	TAQYIV[51]

Cite this: DOI: 10.1039/c0xx00000x

www.rsc.org/xxxxxx

ARTICLE TYPE

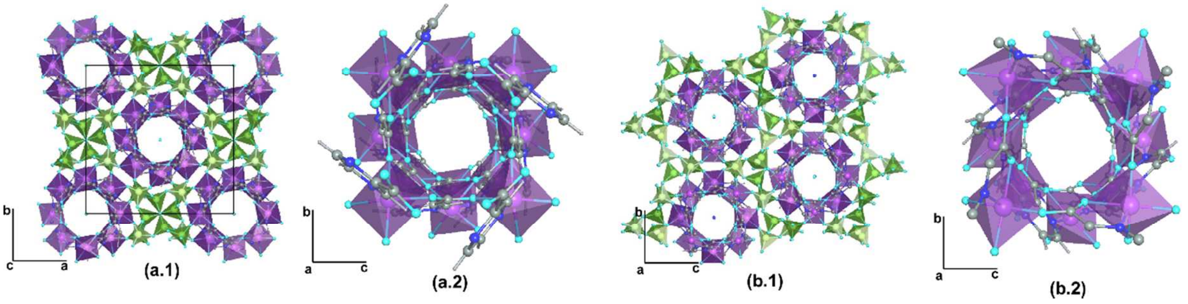

Fig. 13 Crystal structures of (a.1) $M_4(2\text{-Pzc})_4(V_6O_{17})$, M= Ni, Co and (b.1) $[(NH_4)_2Co_8(H_2O)_2(2\text{-Pzc})_8(VO_3)_{10}]$•$xH_2O$ showing the metal-organic chiral tubes ((a.2) and (b. 2)) (purple polyhedra) connected by the metavanadate chains (green polyhedra).[79]

Table 3 Hybrid vanadium oxides constructed from Bpe (1,2-di(4-pyridyl)ethylene) and Bpa (1,2-di(4-pyridyl)ethane. (The coordination environment of the vanadium cations has been briefly described as 4-c, 5-c, and 6-c for tetrahedral, square pyramid and octahedral coordination spheres. In the same sense the oxidation states for the vanadium atoms have been depicted as V(V) and V(IV)).

Compound	**Vanadium oxide subunit**	**Metal-organic subnet**	**Class.**	**Ref.**
1,2-Di(4-pyridyl)ethylene (Bpe)				
$\{Ni(Bpe)\}(VO_3)_2$	Metavanadate chains of corner-sharing VO_4 tetrahedra. 4-c V(V)	Interpenetrated Ni(Bpe) rhombic like metal-organic layers (2D+2D)	I^2O^2 2D + (2D + 2D) → 3D	TIGHOH [52, 53]
$[\{Ni(H_2O)_2(Bpe)\}(V_4O_{11})]\cdot 0.5\ H_2O$	Double metavanadate chain. 5-c V(V)	Crossed Ni(Bpe) metal-organic chains (1D)	I^3O^1 3D + 1D → 3D	OHURAL [46]
$\{Co(HBpe)_2\}(V_4O_{12})$	$\{V_4O_{12}\}$ cycles. 4-c V(V)	$Co(HBpe)_2$ discrete units (0D)	I^1O^0 1D + 0D → 1D	DIWXUD [54, 55]
$[\{M(H_2O)_2(Bpe)_2\}(V_4O_{12})]\cdot 4H_2O\cdot Bpe$; M= Ni, Co	$\{V_4O_{12}\}$ cycles. 4-c V(V)	M(Bpe) metal-organic chains (1D)	I^2O^1 2D + 1D → 3D	DEYJIC, DEYJOI [56]
1,2-Di(4-pyridyl)ethane (Bpa)				
$[\{Ag(Bpa)\}_4(V_4O_{12})]\cdot 4H_2O$	$\{V_4O_{12}\}$ cycles. 4-c V(V)	Ag(Bpa) corner-linked chains giving rise to metal-organic layers (2D)	I^2O^2 2D + 2D → 3D	EGOHAK [48]
$[\{Ni(H_2O)(Bpa)\}(VO_3)_2].2H_2O$	$\{V_4O_{12}\}$ cycles. 4-c V(V)	Ni(Bpa) chains (1D)	I^2O^1 2D + 1D → 3D	ZEFWIS [57]
$[\{Ni_3(H_2O)_3(Bpa)_4\}(V_6O_{18})]\cdot 8H_2O$	$\{V_6O_{18}\}$ cycles. 4-c V(V)	Three $Ni_3(Bpa)_4$ interpenetrated “mot” like 3D nets (3D+3D+3D)	I^3O^3 3D + (3D +3D + 3D) → 3D	CAWZUX[58]
$\{Ni_2(H_2O)_2(Bpa)_2\}(V_6O_{17})$	Metavanadate chains. 4-c V(V)	Ni(Bpa) parallel chains (1D)	I^3O^1 3D + 1D → 3D	[59]
$\{Co(Bpa)\}(VO_3)_2$	$\{V_4O_{12}\}$ cycles. 4-c V(V)	Co(Bpa) parallel chains (1D)	I^2O^1 2D + 1D → 3D	XOJKUD01 [57]

Cite this: DOI: 10.1039/c0xx00000x

www.rsc.org/xxxxxx

ARTICLE TYPE

Table 4 Hybrid vanadium oxides constructed from, Bbi (1,4-bis(imidazol-1-yl)butane), Bpp (1,3-bis(4-pyridyl)propane and Btb (1,4-bis(Triazol-1-yl-methyl)benzene). (The coordination environment of the vanadium cations has been briefly described as 4-c, 5-c, and 6-c for tetrahedral, square pyramid and octahedral coordination spheres. In the same sense the oxidation states for the vanadium atoms have been depicted as V(V) and V(IV)).

Compound	Vanadium oxide subunit	Metal-organic subnet	Class.	Ref.
1,4-bis(imidazol-1-yl)butane (Bbi)				
$\{Cd(HBbi)_2\}(V_4O_{12})$	$\{V_4O_{12}\}$ cycles. 4-c V(V)	$Cd(HBbi)_2$ discrete units (0D)	I^1O^0 1D + 0D → 1D	AHAXOX [60]
$\{Co(H_2O)(Bbi)\}(VO_3)_2$	Metavanadate chains of corner-sharing VO_4 tetrahedra. 4-c V(V)	Parallel corrugated Co(Bbi) chains (1D)	I^3O^1 3D + 1D → 3D	TOHQAJ [61]
$\{M_2(H_2O)_2(Bbi)\}(VO_3)_4$ M = Co, Mn	Metavanadate chains of corner-sharing VO_4 tetrahedra. 4-c V(V)	Parallel M_2(Bbi) chains (1D)	I^2O^1 2D + 1D → 3D	VUTLAY, VUTLEC [62]
$[\{M_2(Bbi)_3\}(V_4O_{12})]\cdot 4H_2O$ M= Ni, Co	$\{V_4O_{12}\}$ cycles. 4-c V(V)	Two 3D $M_2(Bbi)_3$ interpenetrated metal-organic subnets. (3D+3D)	I^1O^3 1D + (3D+·3D) → 3D	VIRYOL [63], VUTLIG [62]
$\{Ni_2(H_2O)_4(Bbi)_2\}(VO_3)_4)]\cdot 2H_2O$	Metavanadate chains of corner-sharing VO_4 tetrahedra. 4-c V(V)	Perpendicular Ni(Bbi) chains (1D)	I^3O^1 3D + 1D → 3D	TOHPUC [61]
$[\{Cu(Bbi)_2\}(V_4O_{12})]\cdot 4H_2O$	$\{V_4O_{12}\}$ cycles. 4-c V(V)	$Cu(Bbi)_2$ layers (2D)	I^0O^2 0D + 2D → 2D	NUXXUA [64]
$\{Cu_2(Bbi)_3\}(V_4O_{12})$	$\{V_4O_{12}\}$ cycles. 4-c V(V)	$Cu(Bbi)_2$ layers (2D) + Cu(Bbi) (1D) chains	I^1O^2 1D + (2D+1D) → 2D	VIRYIF [63]
$[\{Ag(Bbi)_4\}\{Ag_3(V_4O_{12})_2\}]$ $[Ag(Bbi)]\cdot 2H_2O$	$\{V_4O_{12}\}$ cycles. 4-c V(V)	Ag(Bbi) chains	I^1O^1 1D + 1D → 2D	EHODIP [65]
1,3-bis(4-pyridyl)propane (Bpp)				
$\{M_2(Bpp)_4\}(V_4O_{12})$ M= Co, Ni	$\{V_4O_{12}\}$ cycles. 4-c V(V)	Two interpenetrated $M(Bpp)_2$ layers (2D+2D)	I^3O^2 3D + (2D + 2D) → 3D	SAZSOC [66], DIXNII [67]
$\{Zn(Bpp)\}(VO_3)_2$	Metavanadate chains of corner-sharing VO_4. 4-c V(V)	Perpendicular Zn(Bpp) chains (1D)	I^3O^1 3D + (1D+1D+1D) → 3D	HISWUC [68]
$[\{Cu_4(Bpp)_4\}(V_4O_{12})]\cdot 3H_2O$	$\{V_4O_{12}\}$ cycles. 4-c V(V)	Cu(Bpp) metal-organic chains (1D)	I^0O^1 0D + 1D → 3D	LIGPUN [69]
1,4-bis(triazol-1-ylmethyl)benzene (Btb)				
$\{Co_3(H_2O)(Btb)_5\}(V_8O_{23})$	$\{V_8O_{23}\}$ units constructed from two $\{V_5O_{15}\}$ fused rings. 4-c V(V)	Polycatenated $Co_2(Btb)_3$ and $Co(Btb)_2$ layers (2D+2D)	I^3O^2 3D + (2D + 2D) → 3D	MUTZEH [70]

Cite this: DOI: 10.1039/c0xx00000x

www.rsc.org/xxxxxx

ARTICLE TYPE

Table 5 Hybrid vanadium oxides constructed from Bpq (6',6''-Bis(2-pyridyl)-2,2':4',4'':2'',2'''-quaterpyridine), Btpt (tetra-2-pyridylpyrazine), Tpp (2,4,6-tri(4-pyridyl)-1,3,5-triazine), Trz (Triazol), Ptrz (5-(Pyrimidin-2-yl)tetrazol), , and. (The coordination environment of the vanadium cations has been briefly described as 4-c, 5-c, and 6-c for tetrahedral, square pyramid and octahedral coordination spheres. In the same sense the oxidation states for the vanadium atoms have been depicted as V(V) and V(IV)).

Compound	Vanadium oxide subunit	Metal-organic subnet	Class.	Ref.
6',6''-Bis(2-pyridyl)-2,2':4',4'':2'',2'''-quaterpyridine (Bpq)				
[{Cu_2(Bpq)}(V_4O_{12})]·$2H_2O$	{V_4O_{12}} cycles. 4-c V(V)	Cu_2(Bpq) discrete units (0D)	I^1O^0 1D +0D → 2D	TIJHAW [71]
tetra-2-pyridylpyrazine (Btpt)				
{Zn_2(Btpt)}(V_4O_{12})	{V_4O_{12}} cycles. 4-c V(V)	Zn_2(Btpt) discrete units (0D)	I^1O^0 1D +0D → 2D	ATAGUX [72]
{Co_2(Btpt)$_2$}(V_4O_{12})	{V_4O_{12}} cycles. 4-c V(V)	Co_2(Btpt)$_2$ discrete units (0D)	I^1O^0 1D + 0D → 1D	ATAGEH [72]
{Cu_2(Btpt)$_2$}(V_4O_{12})	{V_4O_{12}} cycles. 4-c V(V)	Cu_2(Btpt)$_2$ discrete units (0D)	I^0O^0 0D + 0D → 0D	MUJSEP [73]
[{Cu_2(Btpt)$_2$}(V_4O_{12})]·$2H_2O$	{V_4O_{12}} cycles. 4-c V(V)	Cu_4(Btpt)$_2$ chains (1D)	I^0O^1 0D + 1D → 2D	ATAGOR [72]
2,4,6-tri(4-pyridyl)-1,3,5-triazine (Tpp)				
{Zn(Tpp)$_2$}(VO_3)$_2$	Metavanadate chains of corner-sharing VO_4. 4-c V(V)	Zn(Tpp)$_2$ discrete units (0D)	I^2O^0 2D + 0D → 2D	EHODEK [74]
[{Cu_3(H_2O)$_2$(Tpp)$_2$}(V_8O_{23})]·$3H_2O$	Metavanadate chains of corner-sharing VO_4. 4-c V(V)	Two parallel interpenetrated Cu_3((Tpp)$_2$ layers (2D+2D)	I^3O^2 3D + (2D + 2D) → 3D	EHODOU [74]
[{Zn_3(H_2O)$_2$(Tpp)$_2$}(VO_3)$_6$]·$6H_2O$	Metavanadate chains of corner-sharing VO_4. 4-c V(V)	Parallel and corrugated Zn_3(Tpp)$_2$ layers (2D+2D)	I^3O^2 3D + (2D+2D) → 3D	EHODIO [74]
Triazol (Trz)				
{Cu_3(1,2,3-Trz)$_2$}(V_4O_{12})	{V_4O_{12}} cycles. 4-c V(V)	Cu_3(Trz)$_2$ chains (1D)	I^2O^1 2D + 1D → 3D	MUJSIT [73]
{Cu_3(1,2,4-Trz)$_2$}(V_4O_{12})	Metavanadate chains of corner-sharingVO_4. 4-c V(V)	Cu_3(Trz)$_2$ layers (2D)	I^3O^2 3D + 2D → 3D	LOQKIL [75]
5-(Pyrimidin-2-yl)tetrazol (Ptrz)				
{Cu_3(Ptrz)$_2$}(VO_3)$_4$	Metavanadate chains of corner-sharing VO_4. 4-c V(V)	Cu_3(Ptrz)$_2$ layers (2D)	I^1O^2 1D + 2D → 3D	CIXPAD [76]

Cite this: DOI: 10.1039/c0xx00000x

www.rsc.org/xxxxxx

Table 6 Hybrid vanadium oxides constructed from carboxylate based ligands. (The coordination environment of the vanadium cations has been briefly described as 4-c, 5-c, and 6-c for tetrahedral, square pyramid and octahedral coordination spheres. In the same sense the oxidation states for the vanadium atoms have been depicted as V(V) and V(IV)).

Compound	Vanadium oxide subunit	Metal-organic subnet	Class.	Ref.
Oxalate (Ox)				
(en)[{Co_2(Ox)}(V_4O_{12})]	{V_4O_{12}} cycles. 4-c V(V)	Co_2(Ox) discrete dimers	I^3O^0 $3D+0D \rightarrow 3D$	HUVLUF [77]
(H_2pn)[Mn_2(Ox)(V_4O_{12})]	{V_4O_{12}} cycles. 4-c V(V)	Mn_2(Ox) discrete dimers	I^3O^0 $3D+0D \rightarrow 3D$	XIRCIK [78]
2-pyrazinecarboxylate (2-Pzc)				
{$Co_2(H_2O)$(2-Pzc)}$(VO_3)_3$	Metavanadate chains of corner-sharingVO_4. 4-c V(V)	Co_2(2-Pzc) chains	I^3O^1 $3D+1D \rightarrow 3D$	QOFIS [37]
M_4(2-Pzc)$_4$(V_6O_{17}), M=Ni, Co	Double {V_6O_{17}} metavanadate chains of corner-sharingVO_4. 4-c V(V)	Connected M_4(2-Pzc)$_4$ helical chains giving rise to chiral helical tubes	I^3O^1 $3D + 1D \rightarrow 3D$	WOWHEV, WOWHAR [79]
[$(NH_4)_2Co_8(H_2O)_2$(2-Pzc)$_8(VO_3)_{10}$]·xH_2O	Metavanadate chains of corner-sharingVO_4. 4-c V(V)	Connected M_4(2-Pzc)$_4$} helical chains giving rise to chiral helical tubes	I^3O^1 $3D + 1D \rightarrow 3D$	WOWHIZ [79]
{Ag_4(2-Pzc)$_2$}(V_2O_6)	Metavanadate chains of corner-sharingVO_4. 4-c V(V)	Three dimensional Ag_4(2-Pzc)$_2$ metal-organic net	I^2O^3 $2D + 3D \rightarrow 3D$	EGOHEO [48]
Terephthalate (Tp)				
{Zn_2(Tp)(4-Bpy)}$(VO_3)_2$	{V_4O_{12}} cycles. 4-c V(V)	Zn_2(Tp)(4-Bpy) layers	I^0O^2 $0D + 2D \rightarrow 2D + 2D$	XENCUO [80]
4,4´-bipyridine-2-carboxylate (Pcca)				
[{Co_2(Pcca)$_2(H_2O)$}$(VO_3)_2$]	{V_4O_{12}} cycles. 4-c V(V)	Co_2(Pcca)$_2$ layers	I^1O^1 $1D + 1D \rightarrow 2D$	SAVWIN [81]
[{Co(Pcca)$_2(H_2O)$}$(VO_3)_2$]·3.62H_2O	Metavanadate chains of corner-sharingVO_4 4-c V(V)	Double chains constructed from corner-linked Co(Pcca)$_2$ chains	I^1O^2 $1D + 2D \rightarrow 3D$	SAVWAO [82]

Finally, there are some $\mathbf{I^3O^1}$ architectures exhibiting metal-organic chains arranged parallel between vanadium oxide layers (see Scheme 2 (c)). There is only one example lying in this group, the {M(Pz)}(V_4O_{10}) (M= Ni(II), Co(II), Zn(II)) HV. This family of compounds is characterized by its vanadium oxide layers formed by the corner linkage of double zig-zag chains of edge-sharing VO_5 polyhedra. The layers contain a mixture of V(V)/V(IV) with five coordination environment. The VO_5 polyhedra are connected to the metal centres through oxo groups, giving rise to a three dimensional inorganic framework.

Within the $\mathbf{I^3O^2}$ archetype, two different arrangements of the metal-organic layers have been observed, interpenetrated (Scheme 3 (a)) and parallel (Scheme 3 (b) and (c)) metal-organic layers. The main difference between the structural models shown in Scheme 3 (b) and (c) is the VOS. In the type shown in the Scheme 3 (b) the parallel metal-organic layers are connected through the VOS generating a three dimensional inorganic framework. In the structural type shown in Scheme 3 (c) the metal-organic layers are parallel to the vanadium oxide layers. The metal centres act as bridges between adjacent vanadium oxide layers, establishing a three dimensional inorganic framework.

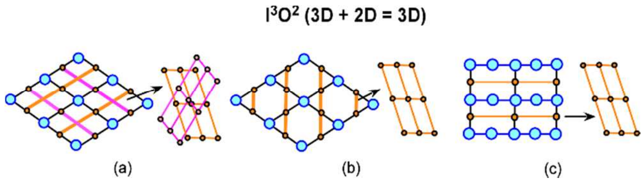

Scheme 3 Structural types in **I^3O^2** group.

In the first group of **I^3O^2** architectures (Scheme 3 (a)), the metal centres are connected in two different directions through a dipodal ligand, generating square-like in ($\{M_2(Bpp)_4\}(V_4O_{12})$ (M= Ni,Co) and $\{Co_3(H_2O)(Btb)_5\}(V_8O_{23})$), or rectangular-like tilted interpenetrated metal-organic sheets in ($[\{M_2(H_2O)_2(4Bpy)_3\}(V_4O_{12})]\cdot 2.5H_2O$ M= Ni(II), Co(II))[44,45,66,67,70] The crystal structure and metal-organic network of the latest compound are observed in the Fig. 14. The vanadate chains (green polyhedra in Fig. 14 (a)) are located between the metal centres of different metal-organic layers, connecting them to generate a three dimensional inorganic framework. The crystal structure shows rhombic channels along the [001] direction in which crystallization water molecules are located (red spheres). The interpenetration between the rectangular like metal-organic layers is observed in the Fig. 14 (b).

The $[\{Cu_3(H_2O)_2(Tpp)_2\}(V_8O_{23})]\cdot 3H_2O$ and $[\{Zn_3(H_2O)_2(Tpp)_2\}(VO_3)_6]\cdot 6H_2O$[74] compounds exhibit three dimensional inorganic framework and parallel interpenetration of hexagonal like metal-organic layers (3D+(2D + 2D) → 3D), instead of the previously described inclined interpenetration (see Scheme 3 (b)).

Fig. 15 (a) shows the crystal structure of $[\{Cu_3(H_2O)_2(Tpp)_2\}(V_8O_{23})]\cdot 3H_2O$.[74] The three dimensional inorganic framework is similar to those observed in **I^3O^1** structural group, with honey-comb like arrangement of the metal centres and the VOS. As shown in Fig. 15 (b), the hexagonal-like metal-organic substructures are clearly related with the geometry of the Tpp ligand. The crystal structure contains two parallel interpenetrated hexagonal metal-organic nets (Fig. 15 (b)). $[\{Cu_3(H_2O)_2(Tpp)_2\}(V_8O_{23})]\cdot 3H_2O$ is the unique HV that exhibits 2D undulated vanadium oxide layers constructed exclusively from four coordinated vanadium (Fig. 15 (c)) and (d)). These inorganic layers are interconnected with the interpenetrated metal-organic sheets, generating one of the most amazing and complicated examples of crystal structures observed in HV.

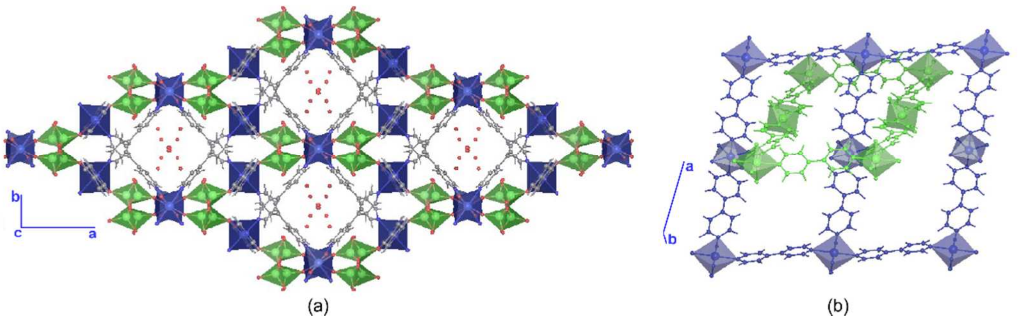

Fig. 14 (a) 3D porous crystal structure of $[\{M_2(H_2O)_2(4Bpy)_3\}(VO_3)_4]\cdot 2.5H_2O$ (M= Ni, Co) (green polyhedra: metavanadate chains, blue polyhedra: Ni(II) octahedra, red spheres: crystallization water molecules). (b) Metal-organic substructure constructed from the interpenetration of two rectangular-like layers. The metal-organic layers have been represented with different colours (green and blue) in order to visualize easier the interpenetration of the nets.[44,45]

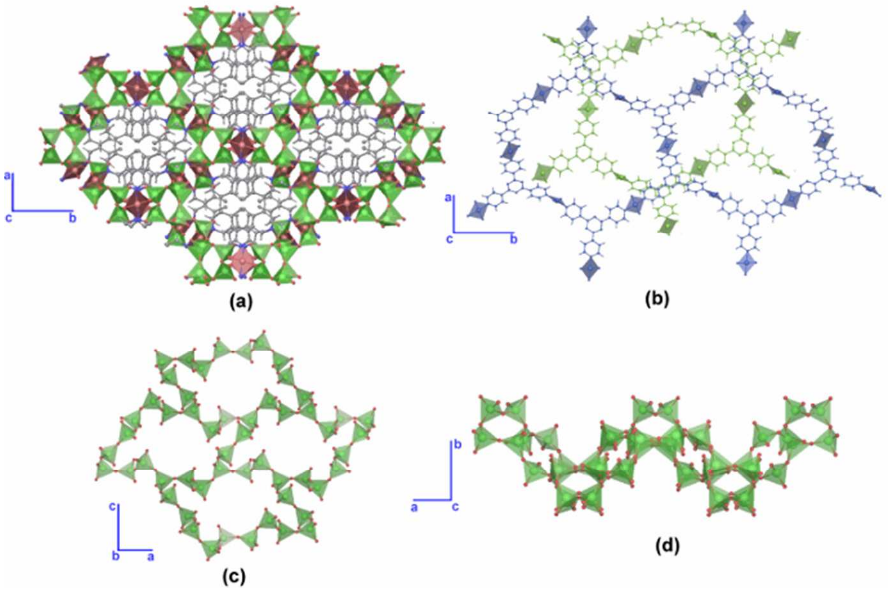

Fig. 15 (a) Crystal structure of $[\{Cu_3(H_2O)_2(Tpp)_2\}(V_8O_{23})]\bullet 3H_2O$. (green polyhedra: metavanadate chains, brown polyhedra: copper square planar polyhedra). (b) Parallel interpenetration of hexagonal-like metal-organic layers. (c) and (d) Vanadium oxide layers constructed from corner-sharing VO_4 tetrahedra.[74]

Cite this: DOI: 10.1039/c0xx00000x

www.rsc.org/xxxxxx

ARTICLE TYPE

While the previous examples of **I^3O^2** crystal architectures are constructed from interpenetrated metal-organic frameworks, the $\{Cu_3(1,2,4Trz)_2\}(V_4O_{12})$ compound possesses parallel non-interpenetrated $\{Cu_3(1,2,4Trz)_2\}$ metal-organic layers (Scheme 3 (b)). Fig. 16 (a) shows the six-coordinated copper cations. These octahedra share edges to form trimeric units. Each trimetric unit is connected to other four via triazol ligands, giving rise to two dimensional $\{Cu_2(1,2,4\text{-}Trz)_3\}$ ruffling layers with an amplitude of about 4.75 Å and a period of 8.87 Å (Fig. 16 (b)). Metavanadate chains are located between adjacent ruffled layers connecting Cu(II) metal centres (Fig. 16 (c)). The linkage between the vanadate chains and the copper cations generates a three dimensional inorganic framework.

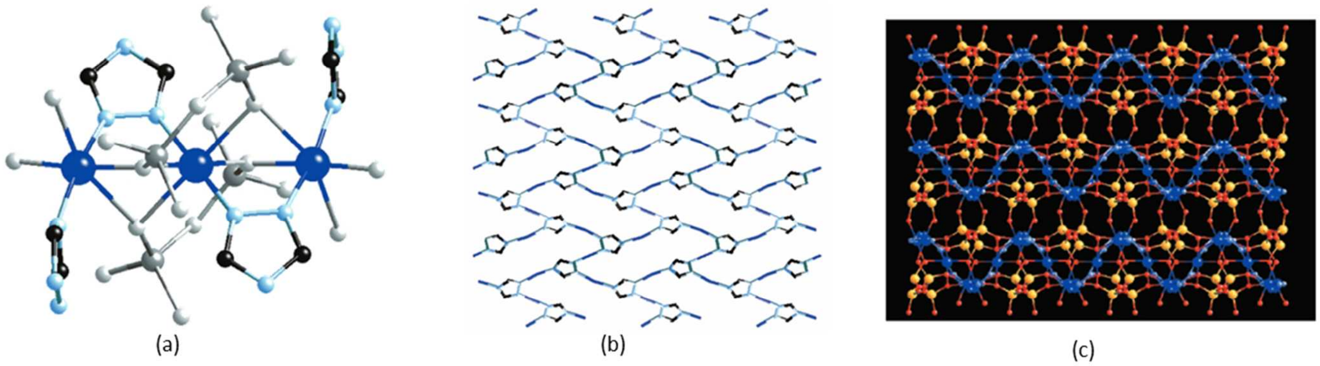

Fig. 16 (a) Trimeric units of $\{Cu_3(1,2,4\text{-}Trz)_2\}(V_4O_{12})$ (blue: copper atoms, grey: VO_4 tetrahedra, pale blue: nitrogen atoms, black: carbon atoms) (b) $\{Cu_3(1,2,4Trz)_2\}$ metal-organic layers, and (c) Crystal structure of $\{Cu_3(1,2,4Trz)_2\}(V_4O_{12})$ (blue: metal-organic layers, yellow: metavanadate chains). Reproduced from Ref. 75 with permission of The Royal Society of Chemistry.

In $[\{Cu(Pz)_2\}(V_6O_{16})]\cdot 0.22H_2O$, an example of the third type of **I^3O^2** structural group (Scheme 3 (c)), there are no interpenetrated layers. In contrast, the metal-organic sheets are disposed between the vanadium oxide layers and parallel to them. In the $[\{Cu(Pz)_2\}(V_6O_{16})]\cdot 0.22H_2O$ structure,[41] Cu(II) cations are linked in two directions through the Pz ligands, generating square-like metal-organic layers. The octahedral coordination environment of the Cu(II) cations is completed by two oxygen atoms shared by the adjacent vanadium oxide layers.

The **I^3O^3** archetype is characterized by the coexistence of both 3D inorganic and metal-organic substructures (Scheme 4).

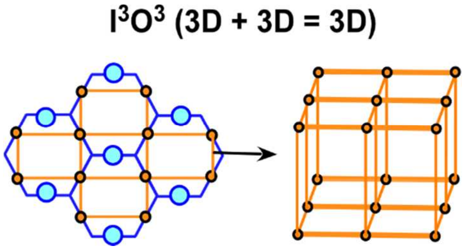

Scheme 4 Structural type in **I^3O^3** group.

$\{Ni_8(4Bpy)_{16}\}(V_{24}O_{68})]\cdot 8.5H_2O$[47] and $[\{Ni_3(H_2O)_3(Bpa)_4\}(V_6O_{18})]\cdot 8H_2O$[58] are examples of this structural group. The metal-organic substructure of $[\{Ni_8(4Bpy)_{16}\}(V_{24}O_{68})]\cdot 8.5H_2O$ consists of the polycatenation of cadmium sulphate "cds" like 3D metal-organic net with two square-like metal-organic layers (Fig. 17 (a)). The vanadium oxide chains are located in the channels of the metal-organic substructure and linked *via* corners to the Ni(II) cations (Fig. 17 (b)). Figs. 17 (c.1) and (c.2) depict the connectivity between the VO_4 tetrahedra belonging to the metavanadate chains and the Ni(II) metal centres within the metal-organic substructure.

The metal-organic substructure of $[\{Ni_3(H_2O)_3(Bpa)_4\}(V_6O_{18})]\cdot 8H_2O$[58] is constructed from the interpenetration of three 3D metal-organic nets. The VOS consists of $\{V_{12}O_{36}\}$ vanadate cycles, which act as four connectors between metal centres of two different metal-organic nets. The combination of both the 3D metal-organic and inorganic scaffolds generates ten connected porous crystal structure. Remarkable characteristics of this compound are the coexistence of Bpa ligand in both "gauche" and "trans" conformations , and that the Ni(II) dimers belonging to the metal-organic nets lie inside the $\{V_{12}O_{36}\}$ cycles connected to them via oxo groups.

3.2.- I^2O^n (n=0-3) Architectures: Hybrid Vanadates Archetypes Containing Two-Dimensional Inorganic Layers.

In **I^2O^n** architectures, the inorganic substructure is 2D. Depending on the dimensionality of the metal-organic substructures, four archetypes can be described, **I^2O^0**, **I^2O^1**, **I^2O^2** and **I^2O^3**.

Two major types of **I^2O^0** architectures can be distinguished (Scheme 5). In the first arrangement of **I^2O^0** archetype the secondary metal is bonded to the vanadate layers and the ligand acts chelating the metal, generating 2D inorganic-organic layers stabilized by weak interactions (Scheme 5 (a)), while the second arrangement is characterized by having discrete metal-organic complexes between the vanadate layers (Scheme 5(b)).

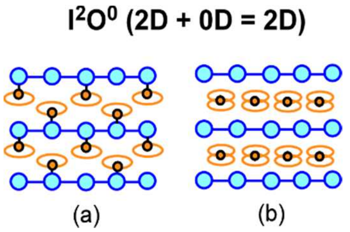

Scheme 5 Structural types in **I^2O^0** group.

Examples of these kind of architectures are: $\{Co(Phen)_3\}(V_{10}O_{27})$,[83] $\{Co_2(2Bpy)_2\}(V_6O_{17})$,[84] $\{Co_2(Phen)_4\}(V_8O_{23})$[85] and $\{Zn(Tpp)_2\}(VO_3)_2$,[74] among others.[86]

In **I^2O^1** and **I^2O^2** structural groups three closely related types have been observed. (see Schemes 6 and 7). The main difference between the **I^2O^1** and **I^2O^2** structures is the existence of metal-organic chains or metal-organic layers within the crystal framework.

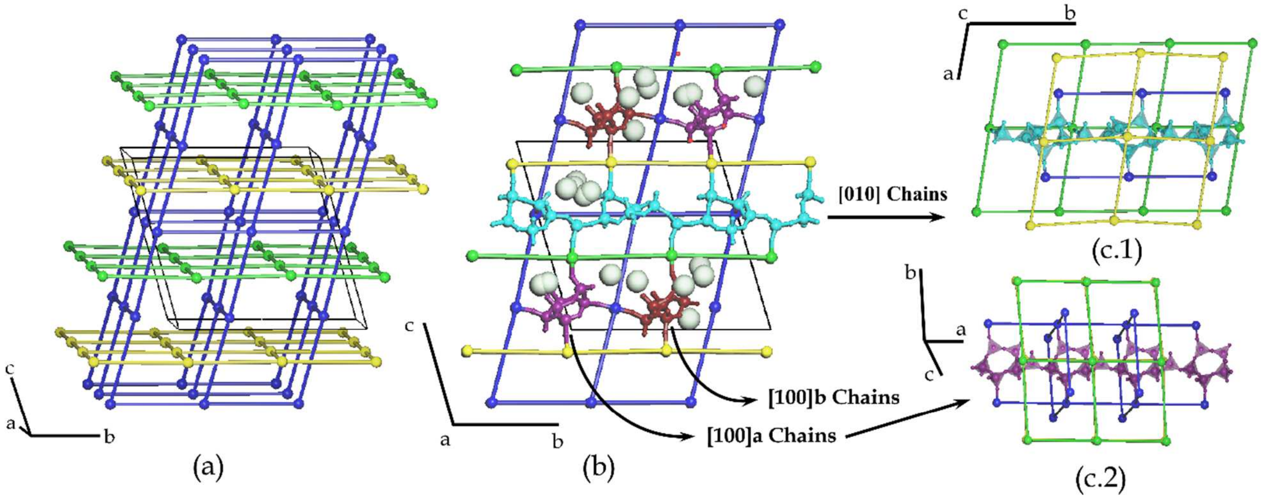

Fig. 17 (a) Metal-organic substructure of $[\{Ni_8(4Bpy)_{16}\}(V_{24}O_{68})]\cdot 8.5H_2O$ constructed from “cds” like 3D net (blue), and two square like (4,4)-c nets (yellow and green nets). (The Bpy organic ligands have been simplified as connectors, while the NiN_2O_4 octahedra have been simplified as the nodes of the metal-organic nets). (b) View of the crystal structure of $[\{Ni_8(4Bpy)_{16}\}(V_{24}O_{68})]\cdot 8.5H_2O$. The metavanadate chains (cyan, purple and maroon atoms) are located into the [100] and [010] channels. (c.1) and (c.2) View of the connectivity between the metavanadate chains and the Ni(II) metal centres belonging to the metal-organic nets.

In the **I^2O^1** and **I^2O^2** structures observed in Schemes 6 (a)-(b) and 7 (a)-(b) the VOS are linked to the metal centres generating inorganic layers. The ligand is directly attached to the metal centres and acts as a pillar between the inorganic layers. The metal-organic chains or layers can acquire a crossed (schemes 6(a) and 7(a)) or a parallel disposition (Schemes 6(b) and 7(b)) within the crystal structures.

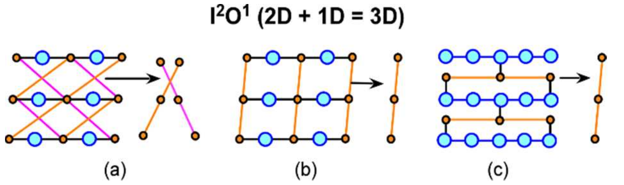

Scheme 6 Structural types in **I^2O^1** group.

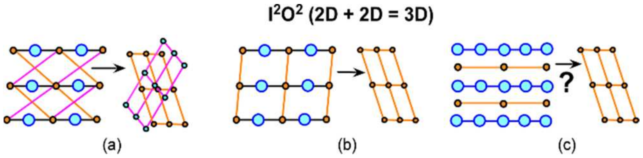

Scheme 7 Structural types in **I^2O^2** group.

An example of **I^2O^1** structural archetype shown in the Scheme 6(a) are the $[\{M(H_2O)_2(Bpe)_2\}(V_4O_{12})]$•$4H_2O$•Bpe; M= Ni, Co hybrid vanadates. These compounds exhibit a crossed disposition of the M(Bpe) chains within the crystal structure. Moreover, the crystal structure possess Bpe solvent molecules located into the channels between the inorganic layers. The hydrogen bonding network between the Bpe guest molecules and crystallization and coordination water molecules is a key factor in the stabilization of the crystal framework.

$\{Ni_2(H_2O)_2(Pz)\}(V_4O_{12})$, $\{Co(4Bpy)\}(VO_3)_2$, $\{Co(Bpa)\}(VO_3)_2$, $[\{Ni(H_2O)(Bpa)\}(VO_3)_2]\cdot 2H_2O$, $\{M_2(H_2O)_2(Bbi)\}(VO_3)_4$ (M=Mn(II), Co(II)), $[\{Ag(4Bpy)\}_4(V_4O_{12})]\cdot 2H_2O$ and $\{Cu_3(Trz)_2\}(V_4O_{12})$ HV belong to the **I^2O^1** structural types shown in the Scheme 6 (b).[39,40 57,48,73] Fig. 18 (a.1), (b.1) and (c.1) show the crystal structures of $\{Co(4Bpy)\}(VO_3)_2$, $\{Co(Bpa)\}(VO_3)_2$ and $[\{Ni(H_2O)(Bpa)\}(VO_3)_2]\cdot 2H_2O$, respectively. The inorganic layers of these three compounds are constructed from $\{V_4O_{12}\}$ cycles connected to six metal centres, and each metal centre linked to three $\{V_4O_{12}\}$ cycles (Fig. 18 (a.2), (b.2) and (c.2)). The most remarkable differences between these crystal structures are the coordination environment of the metal centres and the tilt angle of the organic ligand.

In $\{Ni(Bpe)\}(VO_3)_2$[52,53] the metal centres are sharing edges with each other, generating dimeric units. Each dimeric unit is connected to another four through the organic ligand, giving rise to an interpenetration of two square-like metal-organic layers within the crystal structure (Fig. 19). The metal centres are also connected through the metavanadate chains, giving rise to a ten-connected self-catenated crystal structure. This compound is an example of the **I^2O^2** structural group with interpenetrated metal-organic layers shown in Scheme 7 (a). Fig. 19 shows the crystal structure of $\{Ni(Bpe)\}(VO_3)_2$, as well as the crossed disposition of the Bpe organic ligands between the inorganic layers.

The second type of **I^2O^2** compounds presents parallel instead of crossed metal-organic layers (see Scheme 7 (b)). Examples of this **I^2O^2** architectures are $[\{Mn(4Bpy)\}(VO_3)_2]\cdot 1.16H_2O$, $[\{Mn(4Bpy)_{0.5}\}(VO_3)_2]\cdot 0.62H_2O$ (see Fig. 29, in section 4) and $[\{Ag(Bpa)\}_4(V_4O_{12})]\cdot 4H_2O$[51,48] These structures present metal organic Mn(4Bpy) and $\{Ag(Bpa)\}_4$ layers which metal centres are connected through the vanadium oxide subunit, giving rise also to inorganic sheets.

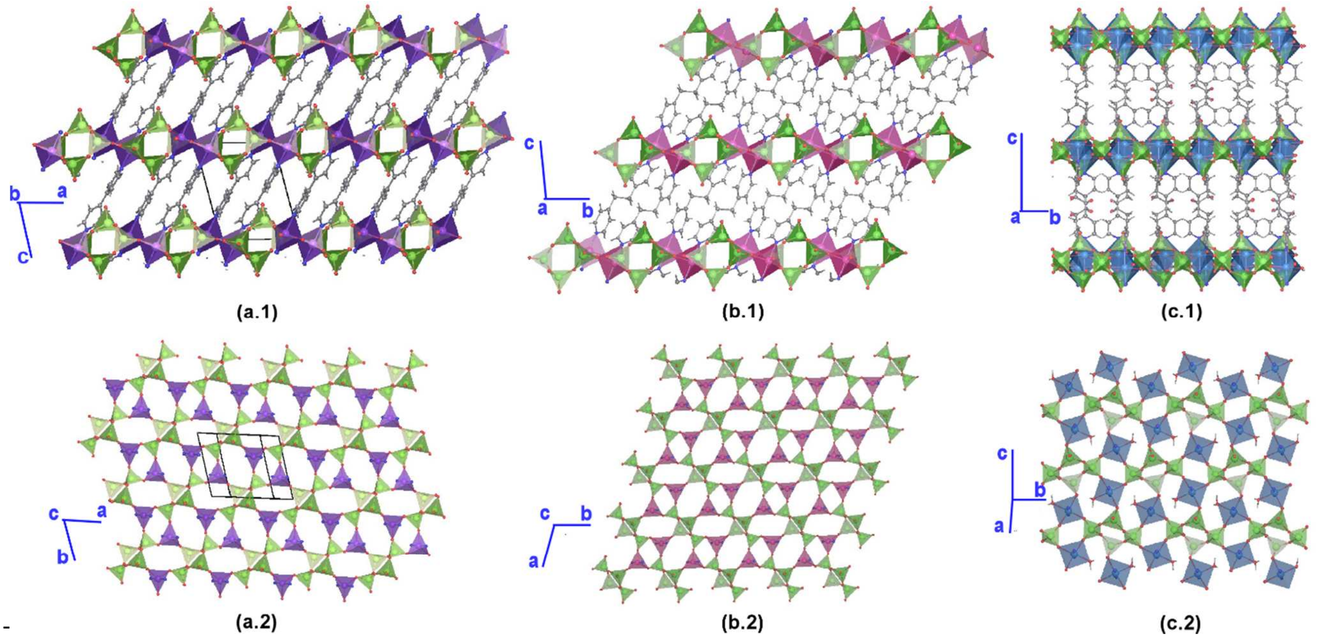

Fig. 18 (a.1), (b.1) and (c.1): Crystal structures of $\{Co(4Bpy)\}(VO_3)_2$, $\{Co(Bpa)\}(VO_3)_2$ and $[\{Ni(H_2O)(Bpa)\}(VO_3)_2]\cdot 2H_2O$. (a.2) and (b.2) Inorganic layers constructed from CoN_2O_3 and $\{V_4O_{12}\}$ cycles. (c.2) Inorganic layers constructed from $Ni(H_2O)N_2O_3$ octahedra and $\{V_4O_{12}\}$ cycles. (green polyhedra: $\{V_4O_{12}\}$ cycles, purple, pink and blue polyhedra: coordination spheres of the secondary metal centres (Ni(II) and Co(II)).**Error! Bookmark not defined.**[57]

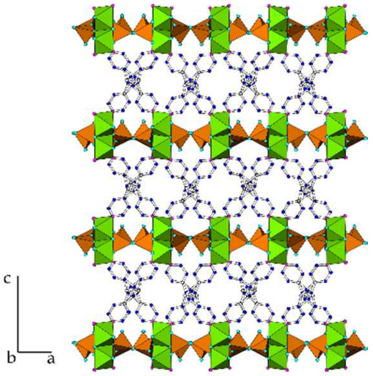

Fig. 19 Crystal structure of $\{Ni(Bpe)\}(VO_3)_2$ (green polyhedra: nickel octahedra, orange polyhedra: metavanadate chains).

In the third arrangement observed for $\mathbf{I^2O^1}$ and $\mathbf{I^2O^2}$ structural archetypes, the metal organic chains or layers are disposed between vanadium oxide layers (see Schemes 6(c) and 7(c)). In the specific case of this kind of $\mathbf{I^2O^2}$ architectures we have not found real examples. Regarding the third type of $\mathbf{I^2O^1}$ (Scheme 6 (c)) only one example is known, $\{M(4Bpy)\}(V_4O_{10})$ (M= Cu(I), Ag(I)). [38,49] Fig. 20 (a) shows the crystal structure of $M(4Bpy)\}(V_4O_{10})$ (M= Cu(I), Ag(I)) HV. Cu(I)-Bpy metal-organic chains are located between the vanadium oxide layers, and the copper metal centres are connected via oxo groups to the VO_5 polyhedra of one layer. If the connectivity through the organic ligand is taken into account the crystal structure is three dimensional, but the inorganic framework is two dimensional, because the copper atoms only connect one of the layers through oxo groups. The disposition of the Cu-Bpy metal-organic chains in the vanadium oxide layers is shown in Fig. 20 (b).

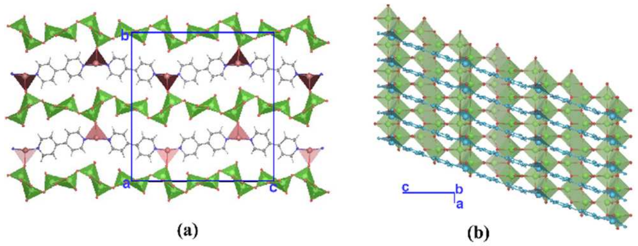

Fig. 20 (a) Crystal structure of $\{M(4Bpy)\}(V_4O_{10})$ (M= Cu, Ag). (b) Connectivity between the metavanadate layers (green polyhedra) and the metal-organic chains (brown polyhedra linked by the (Bpy) organic ligand in the figure (a) and blue spheres in the figure (b)).[49]

There is only one example of $\mathbf{I^2O^3}$ architecture, $\{Ag_4(2\text{-}Pzc)_2\}(V_2O_6)$ (see Scheme 8). In this HV clusters of four Ag atoms (Ag4) are linked through two multipodal 2-Pzc ligands giving rise to a three dimensional metal-organic framework. The metavanadate chains are located in the channels of the metal-organic substructure sharing corners with the silver clusters. In this case, the connectivity between the silver Ag4 clusters and the metavanadate chains generates inorganic layers.

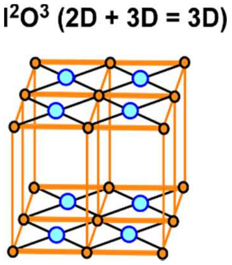

Scheme 8 Structural types in $\mathbf{I^2O^3}$ group.

3.3.-I^1O^n (n=0-3) Architectures: Hybrid Vanadates Archetypes Containing One-Dimensional Inorganic Chains.

There are few examples of HV containing 1D inorganic chains combined with different metal-organic units (**I^1O^0**), chains (**I^1O^1**), layers (**I^1O^2**) or nets (**I^1O^3**). The presence of dipodal ligands seems to favour the crystallization of the previously described structural archetypes instead of crystal structures containing one-dimensional inorganic substructures. Despite this fact, this kind of HV shows very interesting crystal structures, and has more in common with the classic MOFs than the previous described HV.

In **I^1O^0** archetypes discrete metal-organic units are connected through discrete vanadium oxide units giving rise to bimetallic inorganic chains (Scheme 9 (a)) or layers (Scheme 9 (b)).

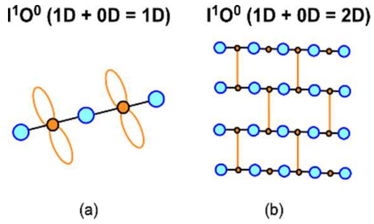

Scheme 9 Structural types in **I^1O^0** group.

Examples of the first type of **I^1O^0** (Scheme 9 (a)) are $\{Co(HBpe)_2\}(V_4O_{12})$,[54,55] $\{Cd(HBbi)_2\}(V_4O_{12})$,[60] $[\{Mn(Phen)\}(V_4O_{12})]\cdot 0.5H_2O$,[87] $\{Co(2Bpy)_2\}(V_4O_{12})$,[88] among others. In these crystal structures metal organic complexes are joined through VOS giving rise to one dimensional inorganic framework. The second type of **I^1O^0** architecture (Scheme 9 (b)) is observed in $[\{Cu_2(Bpq)\}(V_4O_{12})]\cdot 2H_2O$, $\{Zn_2(Btpt)\}(V_4O_{12})$ and $\{Co_2(Btpt)_2\}(V_4O_{12})$ HV.[72] In these structures, the metal centres of adjacent inorganic chains are connected through the organic ligand. The metal-organic substructure is 0D, but the connectivity through the organic molecule generates an increase of the crystal structure dimensionality, 1D+0D → 2D.

Two different arrangements have been described for **I^1O^1** (Scheme 10). Both types of **I^1O^1** architectures consist of inorganic chains connected by the ligand. The linkage between the metal centres and the ligand also gives rise to 1D metal-organic chains. Consequently, an increase in the dimensionality of the crystal structure is observed. The difference between the crystal arrangements within this group lies in the final dimensionality of the crystal structure. The connectivity between metal-organic and inorganic chains could give rise to 3D (Scheme 10 (a)) or 2D (Scheme 10 (b)) crystal structures.

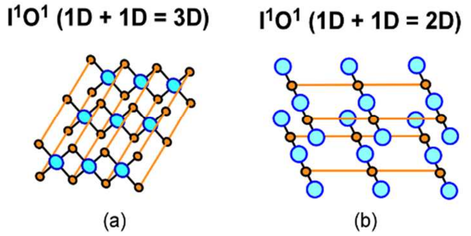

Scheme 10 Structural types in **I^1O^1** group.

$[\{Cu(4Bpy)\}_4(V_4O_{12})]\cdot 2H_2O$ compound[50] (Fig. 21) is an example of the first type of **I^1O^1** architecture (Scheme 10 (a)). The inorganic chains of $[\{Cu(4Bpy)\}_4(V_4O_{12})]\cdot 2H_2O$ are formed by $\{V_4O_{12}\}$ cycles linked through Cu(I) cations, as shown in Fig. 21 (a). A single inorganic chain is observed in Fig. 21(b) and a view of the structure of $[\{Cu(4Bpy)\}_4(V_4O_{12})]\cdot 2H_2O$ is shown in Fig. 21 (c). Each inorganic chain is connected to another six through the organic ligand, generating a 3D crystal structure 1D + 1D = 3D (Fig. 21 (c)).

$[\{Co_2(Pcca)_2(H_2O)\}(VO_3)_2]$ is the unique example of the second type of **I^1O^1** (Scheme 10 (b))**.** This compound contains double metal-organic chains of $Co_2(Pcca)_2$. The metavanadate chains are parallel to the metal-organic chains and connect four $Co_2(Pcca)_2$ adjacent metal-organic chains giving rise to a 2D inorganic-organic structure.[81]

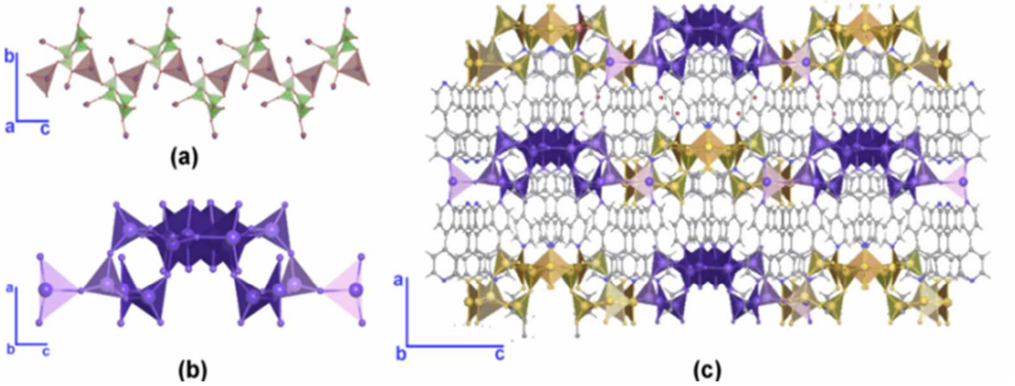

Fig. 21 (a) Inorganic chains (green polyhedra: $\{V_4O_{12}\}$ cycles, brown polyhedra: coordination sphere of copper cations). (b) View of the inorganic chains along the [010] direction. (c) Crystal structure of $[\{Cu(4Bpy)\}_4(V_4O_{12})]\cdot 2H_2O$. The inorganic chains have been represented with two different colours in order to help the reader to visualize the crystal structure.[50]

The **I^1O^2** crystal structures combine both inorganic chains and metal-organic layers. Two different arrangemetas have been observed for **I^1O^2** archetype (Scheme 11).

Only one example of the first type of **I^1O^2** group (Scheme 11 (a)) has been described: $\{Cu_2(Bbi)_3\}(V_4O_{12})$[76]. The inorganic-organic layer of $\{Cu_2(Bbi)_3\}(V_4O_{12})$ HV has copper(II) cations that are linked alternatively to $\{V_4O_{12}\}$ cycles *via* vertexes, generating 1D inorganic chains (Fig. 22 (a.1)). The copper(II) cations of adjacent inorganic chains are connected by Bbi ligands, as shown in Fig. 22 (a.1). The metal-organic layer is a $\{Cu(Bbi)_2\}$ rhomboid-like sheet (Fig. 22 (a.2)). Fig. 22 (a.3) and **(a.4)** show two different views of the interpenetration between the $Cu(Bbi)(V_4O_{12})$ inorganic-organic layers and the $Cu(Bbi)_2$ metal-organic layers. The layers have been represented with different colours (blue: inorganic-organic layers, green: metal-organic layers) in order to visualize better the arrangement between the two kind of sheets. The interpenetration of these two kinds of layers generates a 3D framework without an increase of the dimensionality for the inorganic substructure because the metal-organic layers are not directly attached to the inorganic-organic ones, being the interpenetration what generates the increase of the dimensionality (Fig. 22 (a.3) and (a.4)).

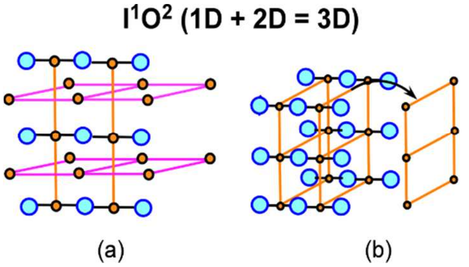

Scheme 11 Structural types in **I^{1}O^2** group.

Two examples of the second type of **I^{1}O^2** architecture (Scheme 11 (b)) have been reported, $\{Cu_3(Ptrz)_2\}(VO_3)_4$[76] and $[\{Co(Pcca)_2(H_2O)\}(VO_3)_2]\cdot 3.62H_2O$.[82] $\{Cu_3(Ptrz)_2\}(VO_3)_4$ compound combines $\{Cu_3(PTrz)_2\}$ undulated layers (Fig. 22 (b.2)) linked through metavanadate chains (Fig. 22 (b.1)). The copper(II) metal centres connect the metavanadate chains, generating also 1D inorganic chains (Fig. 22 (b.3)). The crystal structure is also described as 1D+2D → 3D. $[\{Co(H_2O)(Pcca)_2\}(VO_3)_2]\cdot 3.62H_2O$ compound contains $\{Co(H_2O)(Pcca)_2\}$ metal-organic layers pillared by the $\{V_4O_{12}\}$ cycles, giving rise to a 3D architecture. The linkage between the Co(II) cations and the $\{V_4O_{12}\}$ cycles generates $\{Co(V_4O_{12})\}$ inorganic chains running perpendicular to the metal-organic sheets (see Fig. 28).

The **I^{1}O^3** structural group is similar to the **I^{1}O^2** one, however, the metal centres are connecting parallel metal-organic layers through the ligands generating a 3D metal-organic substructure (Scheme 12).

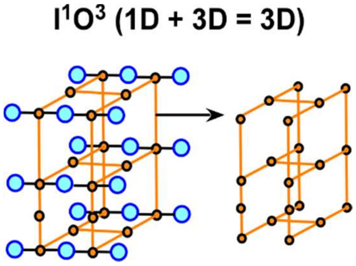

Scheme 12 Structural archetypes in **I^{1}O^3** group.

Concerning this kind of architecture, $[\{M_2(Bbi)_3\}(V_4O_{12})]$ $4H_2O$, M= Ni(II), Co(II)[62,63] possesses two interpenetrated 3D six-connected metal-organic nets (Fig. 23 (a) and (b)). The dimers, belonging to the metal-organic substructure are connected through $\{V_4O_{12}\}$ cycles giving rise to inorganic chains (Fig. 23 (c)). Each dimer connects also six dimers through the organic linker. The crystal structure can be described as an eight connected and self-catenated net, shown in Fig. 23 (d).

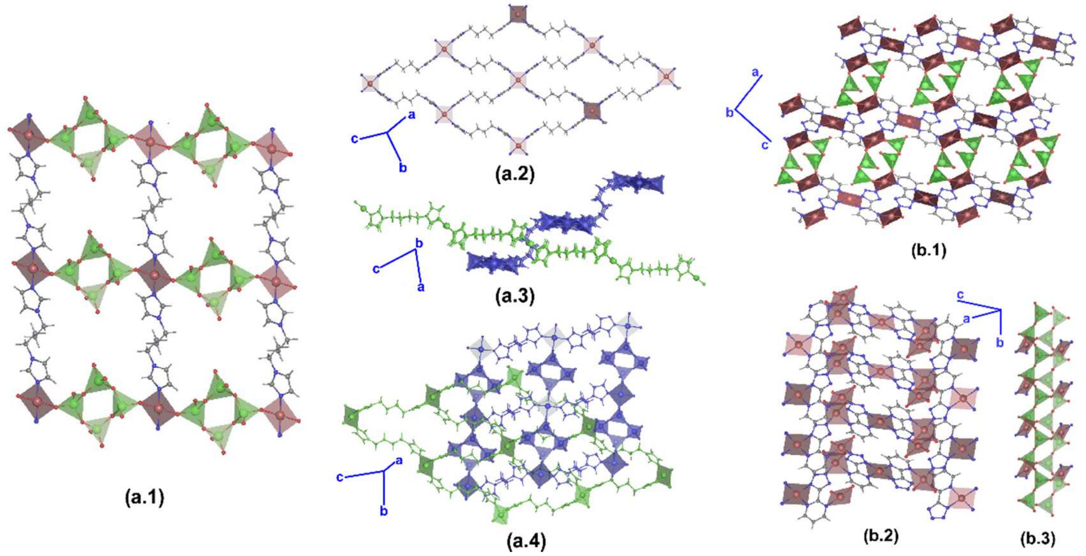

Fig. 22 (a.1) Inorganic-Organic layers. (b.2) $\{Cu(Bbi)_2\}$ metal-organic layers. (a.3) and (b.4) Interpenetration of the metal-organic and inorganic-organic layers of $\{Cu_2(Bbi)_3\}(V_4O_{12})$.[60] (b.1) Crystal Structure of $\{Cu_3(PTrz)_2\}(VO_3)_4$[76]. (b.2) $\{Cu_3(PTrz)_2\}$metal-organic layers. (b.3) Inorganic chains (green polyhedra: $\{V_4O_{12}\}$ cycles, brown polyhedra: coordination environment of the copper cations. For (a.3) and (a.4) figures, blue: inorganic-organic layers and green: metal-organic layers of $\{Cu_2(Bbi)_3\}(V_4O_{12})$.

3.4.-I^{0}O^n (n=0-3) Architectures: Hybrid Vanadates Archetypes Containing Discrete Inorganic Units

In the **I^{0}O^m** architectures, the inorganic substructure is 0D and acts as a node connected through the ligand, like in MOFs. Four different archetypes are described according to the metal-organic dimensionality, **I^{0}O^0**, **I^{0}O^1**, **I^{0}O^2** or **I^{0}O^3**, for discrete, one-dimensional, two-dimensional or three-dimensional metal-organic substructures, respectively.

The **I^{0}O^0** archetype are discrete coordination complexes commonly generated from chelating ligands (Scheme 13). The metal centres are linked to discrete VOS. For HV, this kind of structural archetype in HV was deeply described by Zubieta *et al.*7 An example of this architecture is the $[\{Cu_2(Btpt)_2\}(V_4O_{12})]$ compound.[73]

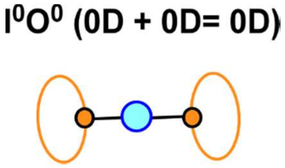

Scheme 13 Structural type in **I^{0}O^0** group.

Cite this: DOI: 10.1039/c0xx00000x

www.rsc.org/xxxxxx

The $\mathbf{I^0O^1}$ crystal structures contain metal-vanadate discrete units linked through the organic ligand. The connectivity between the metal centres and the organic ligand generates metal-organic chains. Two different types have been described (see Scheme 14).

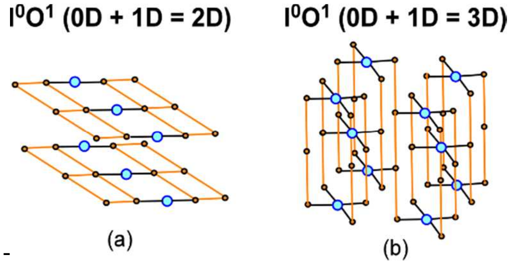

Scheme 14 Structural type in $\mathbf{I^0O^1}$ group.

The unique example of the first type of $\mathbf{I^0O^1}$ archetype (see Scheme 14 (a)) is $[\{Cu_2(Btpt)_2\}(V_4O_{12})]\cdot 2H_2O$. The main building block of this crystal structure is the Cu(Btpt) metal organic chains, which are linked through $\{V_4O_{12}\}$ cycles giving rise to a 2D framework.

A very interesting example of $\mathbf{I^0O^1}$ group is the $[\{Cu_4(Bpp)_4\}(V_4O_{12})]\cdot 3H_2O$ vanadate.[71] This is the second type of $\mathbf{I^0O^1}$ crystal architecture shown in the Scheme 14 (b). Each $Cu_4(V_4O_{12})$ inorganic cluster is connected to another eight, generating an unprecedented eight-connected self-catenated crystal structure (Fig. 24). The connectivity between the copper cations and the ligand generates metal-organic chains, being necessary the linkage through the $\{V_4O_{12}\}$ cycles to obtain the 3D eight connected crystal structure.

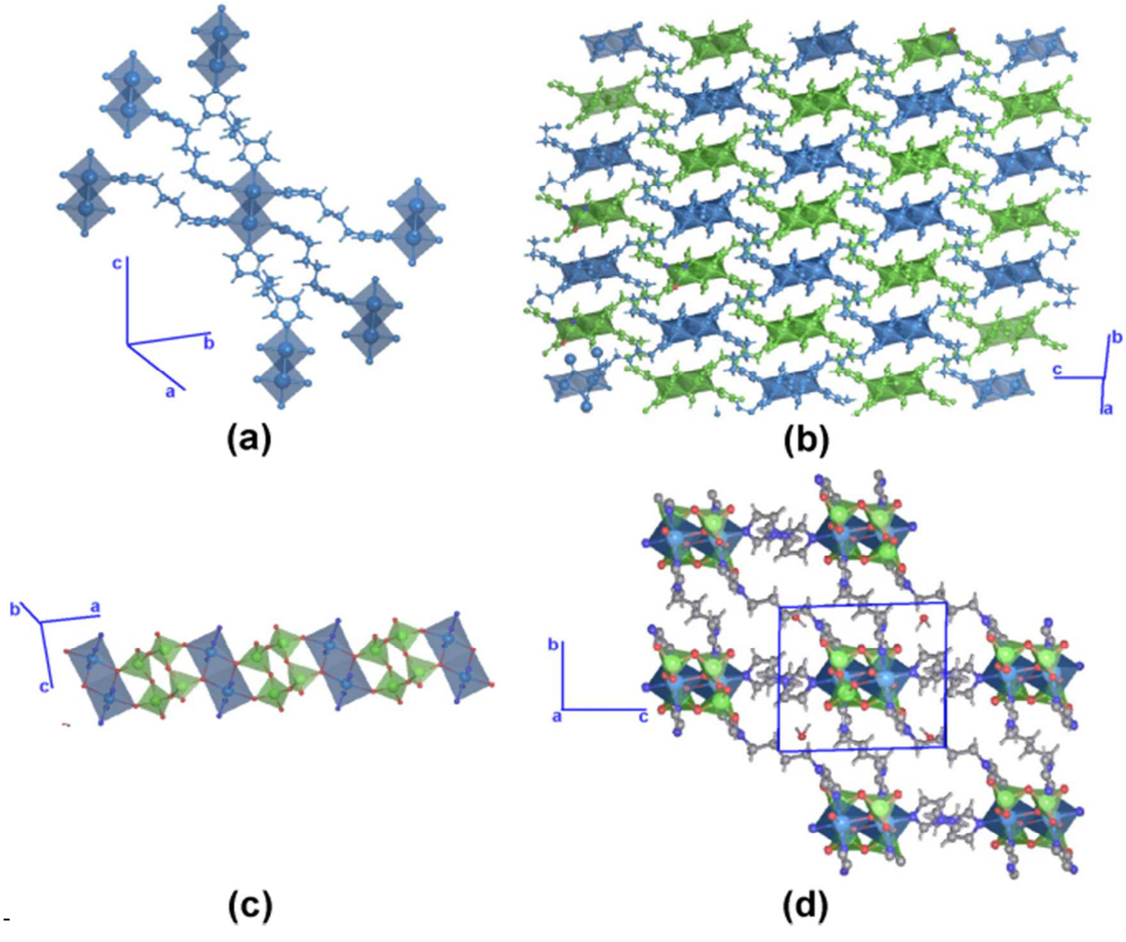

Fig. 23 (a) Six-connected dimeric units. (b) Two interpenetrating 3D metal-organic substructure. (c) Inorganic chains (green polyhedra: $\{V_4O_{12}\}$ cycles, blue polyhedra: Ni(II) octahedral coordination environment). (d) Eight-connected self-catenated structure constructed from inorganic chains and metal-organic net of $[\{M_2(Bbi)_3\}(V_4O_{12})]\cdot 4H_2O$, M=Ni(II), Co(II).[62,63]

The $\mathbf{I^0O^2}$ architectures are very common in MOFs, however, only two examples are known in HV (Scheme 15).

In the first $\mathbf{I^0O^2}$ structural archetype the metal centres or clusters are linked through ligands in two different directions generating metal-organic layers, while VOS are discrete and isolated into the structure (Scheme 15 (a)) or act as connectors between the metal-organic layers (Scheme 15 (b)).

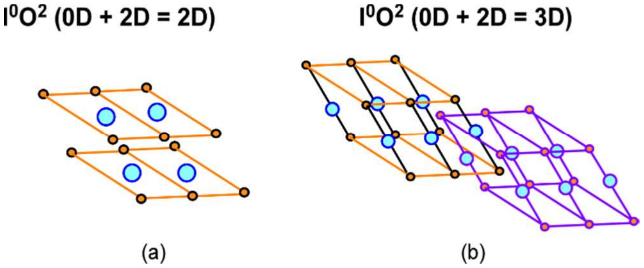

Scheme 15 Structural type in **I^{0}O^2** group.

Examples of **I^{0}O^2** archetypes are [{Cu(Bbi)$_2$}(V$_4$O$_{12}$)]·4H$_2$O^{64} and {Zn$_2$(Tp)(4-Bpy)}(VO$_3$)$_2$^{80}. [{Cu(Bbi)$_2$}(V$_4$O$_{12}$)]·4H$_2$O is an example of the first type of **I^{0}O^2** architecture (Scheme 15 (a)). The crystal structutre consists of {Cu(Bbi)$_2$} metal-organic layers linked through weak interactions to {V$_4$O$_{12}$} cycles. A very different **I^{0}O^2** crystal structure is that of {Zn$_2$(Tp)(4-Bpy)}(VO$_3$)$_2$, the unique example of the second type of **I^{0}O^2** crystal frameworks (see Scheme 15 (b)). This compound combines both carboxylic terephthalate and nitrogen based 4,4´-bipirydine ligands. The mixed organic bridges interlink the Zn(II) dimers to generate cationic rectangular metal-organic grids. Zn ions of two adjacent metal-organic grids are connected through the {V$_4$O$_{12}$} cycles to form a pillared double-layered sheet. As in many other MOF compounds, the double layers are polycatenated.

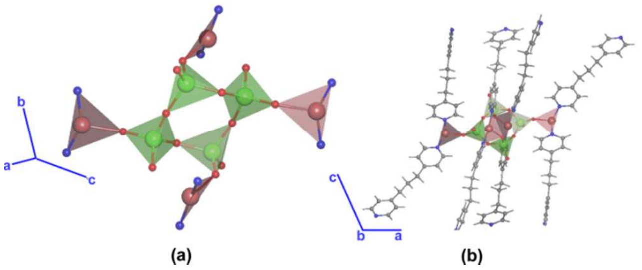

Fig. 24 (a) Cu$_4$V$_4$O$_{12}$ inorganic clusters present in [{Cu$_4$(Bpp)$_4$}(V$_4$O$_{12}$)]·3H$_2$O structure. (b) Eight connected nodes (green polyhedra: {V$_4$O$_{12}$} cycles, brown polyhedra: coordination polyhedra of the copper atoms).^{71}

Despite the **I^{0}O^3** crystal structures are extensively represented in MOFs, there are no examples in HV. In MOFs, the combination of metal centres or metal clusters and carboxylic ligands generates different families of coordination polymers exhibiting **I^{0}O^3** architectures with very interesting physicochemical properties. A hypothetical HV **I^{0}O^3**structural archetype is shown in the Scheme 16.

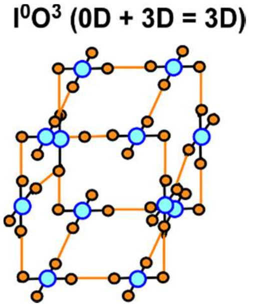

Scheme 16 Structural type in **I^{0}O^3** group.

Hypothetically, the construction of **I^{0}O^3** HV is possible through clusters constructed from discrete vanadium oxide subunits linked to secondary metal centres. This kind of MOFs would be build up from hetero-metallic clusters.

4.-Physicochemical Properties of Hybrid Vanadates

Physicochemical properties of HV depends on the crystal structures itself, and on the fundamental building blocks used for the construction of those architectures. Establishing direct structure-properties relationships that comprise the majority of the compounds is difficult, due to the great structural diversity observed in these materials, but in the case of magnetic and thermal properties some general trends can be suggested. Besides the classical studies on magnetic and thermal properties, recently several research groups have been started to test the hybrid vanadates as catalysts and photo-catalysts. In this section the physicochemical properties of HV are described, and in the concrete case of the thermal properties, future trends and scopes are suggested.

4.1.-Thermal Properties

The thermal properties of HV will be focused on the 3D and 2D crystal structures. Unfortunately, most of the thermal studies carried out on HV consist on thermogravimetric measurements, which only give information about the temperature ranges in which the different decomposition processes (such as, loss of crystallization or coordination water molecules or calcination of the organic ligand) occur. There are few examples in which temperature dependent X-ray diffratometry studies (thermodiffractometry) have been carried out. These measurements complement the thermogravimetric studies, and give a lot of information about the thermal response of the crystal structure to the loss of solvent or coordinated species, or simply, to the increase of temperature (thermal expansion or structural transitions).

The thermal properties of HV are going to be discussed in two different subsections, related to the structural response of the crystal frameworks to the loss of coordinated water molecules and to the reversible release of solvent water molecules. Several examples of thermal response of different 3D and 2D HV are going to be described.

4.1.1-Thermal response to the loss and uptake of coordinated water molecules

The crystal structures of [{Ni$_6$(H$_2$O)$_{10}$(4Bpy)$_6$}(V$_{18}$O$_{51}$)]·1.5 H$_2$O and [{Ni(H$_2$O)$_2$(Bpe)}(V$_4$O$_{11}$)]·0.5 H$_2$O^{46} are classified as **I^{3}O^1** (for more information see Fig. 9, section 2), being the rigid inorganic frameworks stabilized by crossed organic ligands their most relevant characteristic (Fig. 14, section 3.1). The crystallization water molecules are encapsulated between the inorganic scaffold and the organic ligand, and the coordination environment of the metal centres is completed by water molecules. For both compounds the loss of crystallization water molecules finishes at high temperatures (180ºC). No structural response of the crystal structures to the loss of crystallization water molecules is observed. The removal of coordinated water molecules is a continuous and irreversible process (180-280ºC) that involves a drastic crystallinity reduction, and important changes in the IR absorption bands related to the V=O and V-O-V stretching vibration modes.

In that regard, Fig. 25 shows the progressive replacement of the most intense maximun of [{Ni(H$_2$O)$_2$(Bpe)}(V$_4$O$_{11}$)]·0.5 H$_2$O HV (2θ= 8.2º) by the maximun located at 9.0º in 2θ(º), related to the high temperature anhydrous compound. The evolution of the position for the (020) and (011) reflections indicates a contraction of "c" and an increase of "b" parameters.

Taking into account the changes in the XRD patterns and IR spectra, Fernández de Luis *et. al.*[46] proposed a transformation mechanism, involving the generation of two new Ni-O bonds with the V=O terminal oxygen atoms of the VO_5 polyhedra. As shown in Fig. 25 (Inset), the equatorial plane of the Ni(II) coordination environment is completed establishing two new bonds with terminal oxygen atoms belonging to VO_5 polyhedra within the adjacent metavanadate chain.

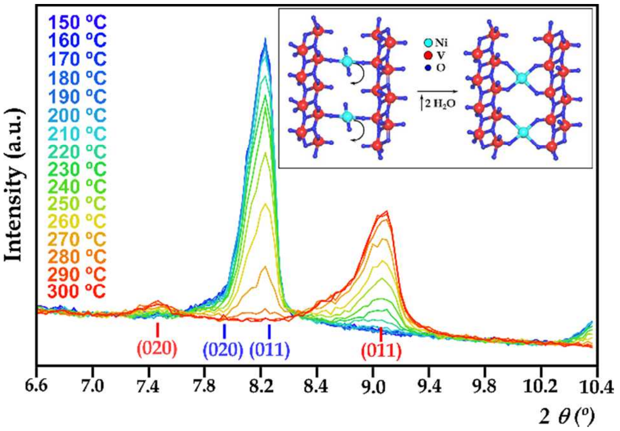

Fig. 25 Displacement of the (020) and (011) reflections during the structural transformation of $[\{Ni(H_2O)_2(Bpe)\}(V_4O_{11})]\cdot 0.5H_2O$. Inset: Qualitative model for the transformation due to the loss of coordinated water molecules. Reproduced with permission from Ref. 46 Copyright (2009) Wiley-VCH Verlag GmbH and Co. KGaA.

Another irreversible structural transformation due to the loss of coordinated water molecules is also observed in $\{Ni_2(H_2O)_2(Pz)\}(VO_3)_2$.[39,40] This HV possess a $\mathbf{I^2O^1}$ crystal architecture (see Fig. 9, Section 2). As it is observed in Fig. 26, the inorganic layers are constructed from two edge-sharing Ni(II) octahedra corner linked to $\{V_4O_{12}\}$ cycles. The inorganic layers are linked through Pz ligands. The coordination environment of the Ni(II) atoms is completed by one coordination water molecule. An important feature stand out in Fig. 26 is the hydrogen bond established between the coordinated water molecule and the terminal oxygen atom belonging to the V=O terminal groups within the (VO_4) tetrahedra.

The crystal structure of the anhydrous compound could not be solved due to the loss of crystallinity resulting from the removal of the coordinated water molecules. However, according to the X-ray diffractograms, it is very likely that the six-coordination environment of the nickel(II) atoms is maintained during the structural transformation through a slight rotation of the nickel dimers along the hydrogen bond, and towards the V=O vanadyl groups, which allows the generation of a new Ni-O bond, compensating the loss of coordinated water molecules. This transformation mechanism is pointed in the Fig. 26 with arrows.

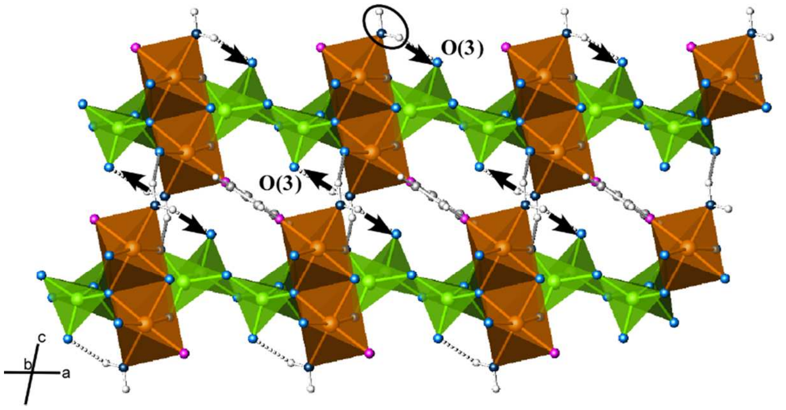

Fig. 26 Structural transformation pathway proposed for the dehydration of $\{Ni_2(H_2O)_2(Pz)\}(V_4O_{12})$. Adapted from Ref. 39 with permissions of Elsevier Copyright {2007}

This solid state transformation mechanism was confirmed by synchrotron radiation X-ray diffraction in the case of $\{Ni_2(H_2O)_2(Bpa)_2\}(V_6O_{17})$ compound (Fig. 27). This I^3O^1 HV (see Fig. 9) retains its crystallinity after the loss of coordinated water molecules. The thermodiffractometry shows a solid state reaction involving a strong structural transformation. The crystal structure of the anhydrous compound could be solved by rigid body refinement of the room temperature model. Figs. 27 (a) and (b) depict the transformation mechanism in this compound. The main difference between the hydrated and anhydrous crystal structures lies in the connectivity between the Ni(II) cations and the VOS. The loss of coordination water molecules from the Ni(II) metal centres is compensated by the incorporation of the terminal oxygen atoms belonging to the VO_4 tetrahedra into the coordination sphere of the Ni(II) cations (Fig. 27 (b)).[59] The structural transformation also involves changes in the cell parameters and the reorientation of the Bpa ligand and the $\{V_4O_{12}\}$ cycles and $\{V_2O_7\}$ dimers that form the vanadate chains (see Fig. 12, section 3.1).

Dynamic structural changes induced by the removal/readsorption of coordinated species from the framework itself are rare, and certain thermal stability after the removal of coordinated water molecules is necessary. In this sense, $[\{Co_2(Pcca)_2(H_2O)\}(V_4O_{12})_{0.5}]\cdot 3.62H_2O$ $\mathbf{I^1O^2}$ vanadate (see structural description on section 3.3) undergoes two distinct reversible single-crystal to single-crystal transformations.

The removal of the guest molecules generates the shrinkage of the framework, while the loss of the coordinated water molecule involves an unusual change in the coordination environment of the cobalt centre, from six (octahedral) to five (bipyramidal). Fig. 28(a) and (b) show the crystal structure of the hydrated and anhydrous compounds, pointing the coordination environment of the Co(II) cations in both crystal structures. Together with this change in the cobalt coordination environment, there is a colour change of the compound from red to brown. Whereas the removal of the guest water molecules leads to a small decrease in volume, it is the removal of the coordinated water molecules what initiates the more substantial channel collapse.

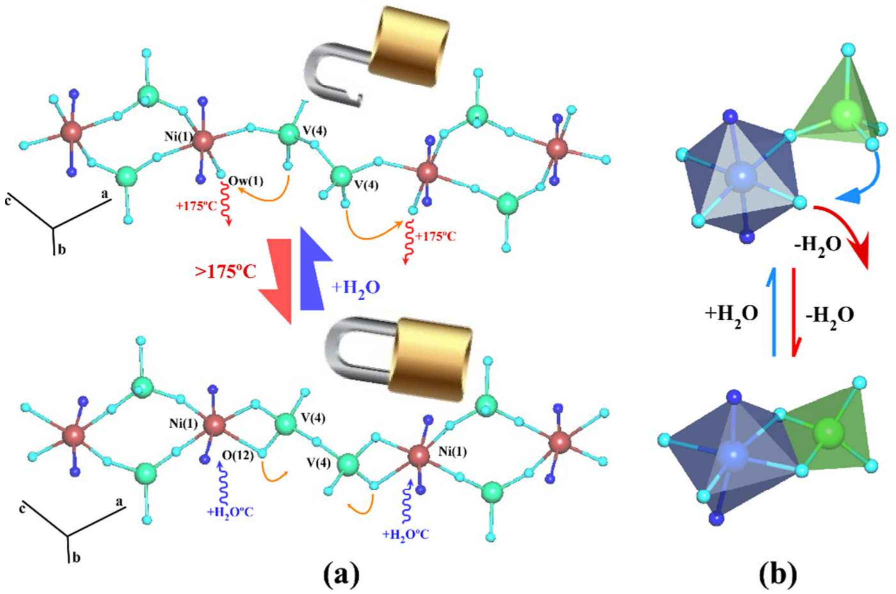

Fig. 27 (a) Structural transformation pathway proposed for the dehydration of $\{Ni_2(H_2O)_2(Bpa)_2\}(V_6O_{17})$. Adapted from Ref. 59 with permissions of American Chemical Society Copyright {2014}.(b) Coordination polyhedra involved in the transformation mechanism observed in $\{Ni_2(H_2O)_2(Bpa)_2\}(V_6O_{17})$

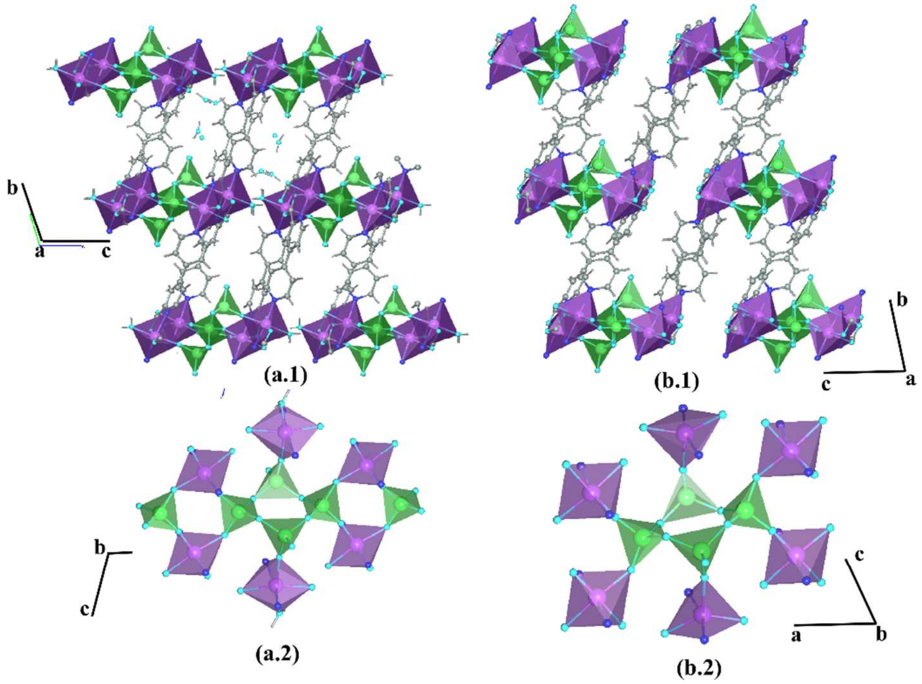

Fig. 28 (a) View of the $[\{Co_2(Pcca)_2(H_2O)(V_4O_{12})_{0.5}\}_n]$ framework containing hydrated Co(II)in an octahedral coordination environment; and (b) of the dehydrated $[\{Co_2(Pcca)_2(V_4O_{12})_{0.5}\}_n]$ framework containing Co(II) in a trigonal-bipyramidal coordination environment. Copyright (2005) Wiley-VCH Verlag GmbH and Co. KGaA. Reproduced with permission from Ref. 81.

4.1.2-Thermal response to the loss of crystallization water molecules

The effect of the crystallization water molecules loss in **I^{3}O^3** compounds $[\{Ni_8(4Bpy)_{16}\}(V_{24}O_{68})]\cdot 8.5H_2O$ and $\{Ni_3(H_2O)_3(Bpa)_4\}(V_6O_{18})]\cdot 8H_2O$ is related with the rigid and flexible natures of the 4Bpy and Bpa organic ligands, respectively. The crystal structures have been previously described in section 3.1 (see Fig. 17).

For $[\{Ni_8(4Bpy)_{16}\}(V_{24}O_{68})]\cdot 8.5H_2O$, despite having a 3D inorganic scaffold, and a rigid ligand such as 4Bpy, the crystal structure volume is contracted a 0.6% during the loss of crystallization water molecules. Fig. 29(a) shows the thermal evolution of the cell volume obtained from a cyclic Rietveld refinement. The initial contraction is ascribed to the loss of crystallization water molecules.

The **I^{3}O^3** [{$Ni_3(H_2O)_3(Bpa)_4$}(V_6O_{18})]·$8H_2O$ framework possesses a more dynamic structural response to the loss of solvent, probably due to the presence of more flexible Bpa organic ligand in the crystal structure. The thermal evolution of the 2θ(°) position and intensity for the (110) reflection is shown in Fig. 29(b). The intensity variation suggets the existence of three different processes, the first one between 25ºC and 80ºC, the second one in the 80ºC to 200ºC range, and a third one above 200ºC.

The removal of eight crystallization water molecules per formula unit takes place between room temperature and 80 ºC and involves a contraction of the [100] channels in which the guest is located. After the loss of crystallization water molecules, and in the second temperature range, between 80 and 200ºC, the crystal structure continues its contraction showing a negative thermal expansion. In a third step (200-275ºC) the loss of coordinated water molecules takes place, generating an irreversible and strong structural transformation, which promotes a reduction of the crystal domains, lowering the crystallinity of the compound (Fig. 29(b)). The main difference between the thermal response of [{$Ni_8(4Bpy)_{16}$}($V_{24}O_{68}$)]·$8.5H_2O$ and [{$Ni_3(H_2O)_3(Bpa)_4$}(V_6O_{18})]·$8H_2O$ compounds to the loss of solvent is the range of cell volume contraction. Both compounds exhibit a reversible and dynamical structural response, however while the crystal framework of [{$Ni_8(4Bpy)_{16}$}($V_{24}O_{68}$)]·$8.5H_2O$ responses with a 0.6 % of cell volume reduction, the [{$Ni_3(H_2O)_3(Bpa)_4$}(V_6O_{18})]·$8H_2O$ compound exhibits a contraction of approximately 6 %. Both compounds possess complex 3D structures combining both 3D inorganic and metal-organic substructures, however, the flexibility of the Bpa ligand is larger than the 4Bpy one. While the pyridyl rings of the Bpa organic molecules could rotate and orientate itself through the ethane group, giving rise to a reduction of the distance between the nitrogen donor atoms, the 4Bpy ligand acts as a rigid pillar.

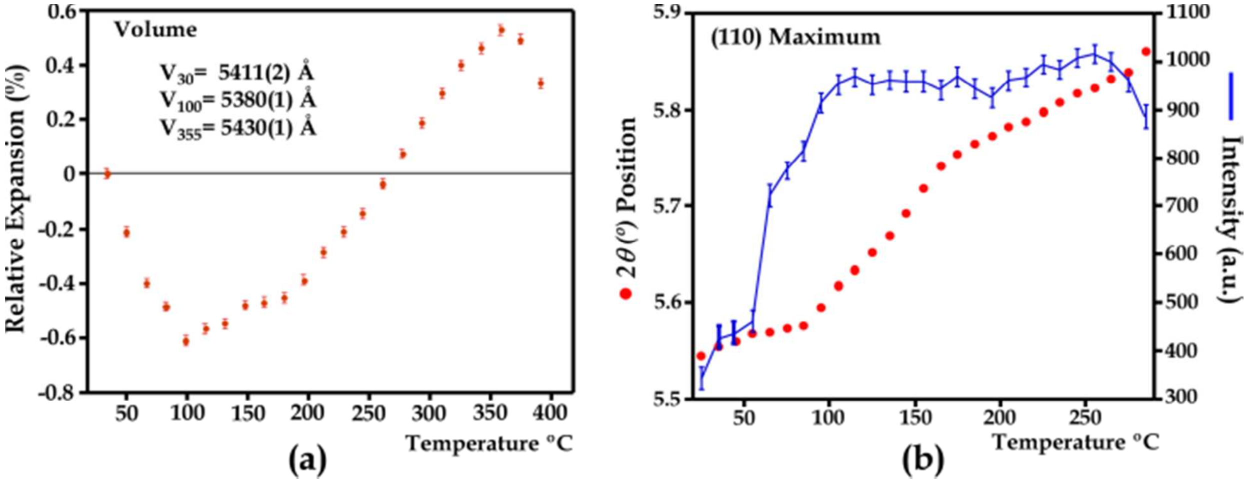

Fig. 29 (a) Thermal evolution of the cell volume for [{$Ni_8(4Bpy)_{16}$}($V_{24}O_{68}$)]·$8.5H_2O$. (b) Thermal displacement of the (110) reflection for the [{$Ni_3(H_2O)_3(Bpa)_4$}(V_6O_{18})]·$8H_2O$ hybrid vanadate. Adapted from Refs. 47, 58 with permission of The Royal Society of Chemistry Copyright {2010} and the American Chemical Society, Copyright {2012}

An amazing example of dynamical and reversible response of the crystal structures due to the loss of guest water molecules are the manganese HV [{$Mn(4Bpy)$}($VO_3)_2$]·$1.16H_2O$ and [{$Mn(4Bpy)$}$_{0.5}$($VO_3)_2$]·$0.62H_2O$.[51]

As it has been described previously, these **I^{2}O^2** crystal architectures are constructed from inorganic layers pillared by the 4Bpy organic ligand (see section 3.2). The crystallization water molecules are located between the organic pillars and the inorganic layers The crystal structures of both compounds after and before the loss of crystallization water molecules are shown in Fig. 30. The changes in the unit cell parameters and angles are represented in the same figure. The response of the different structural subunits during the transformation is also indicated by arrows.

For both compounds, two important displacements and intensity changes of some X- ray diffraction reflections take place in the heating process near room temperature. The loss of solvent gives rise to a tilting of the 4Bpy pillars between the inorganic layers, and hence, an increase of the "β" angle value. However, surprisingly, the major structural changes are directly associated with the compression of the inorganic layers, which generates the reduction of the "a" parameter. In this way, the opposite tilt of the vanadate and manganese octahedra chains explains, qualitatively, the variation in the unit cell parameters for both compounds due to the removal of the solvent (Fig. 30).

Cite this: DOI: 10.1039/c0xx00000x
www.rsc.org/xxxxxx

ARTICLE TYPE

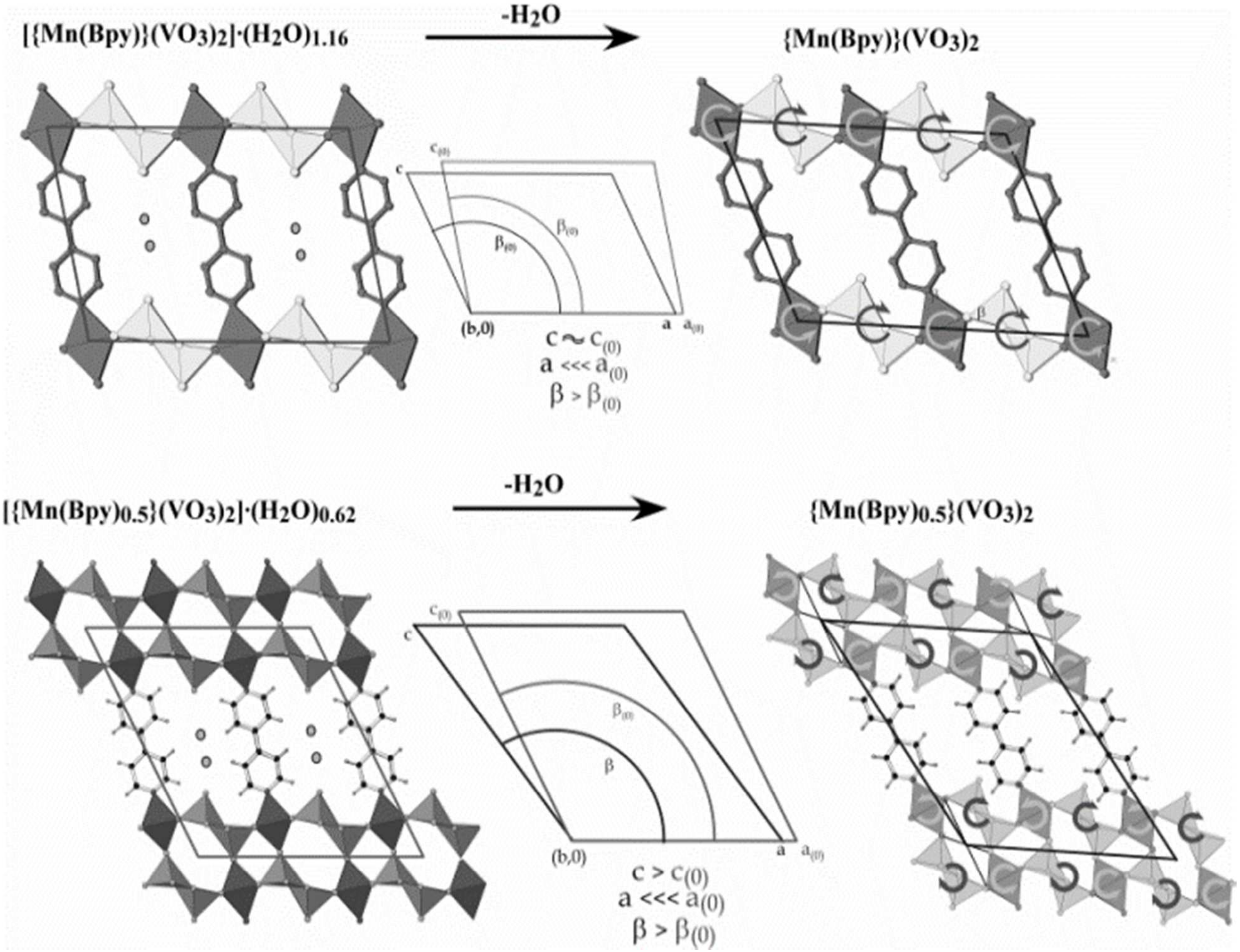

Fig. 30 Qualitative description of the crystal response to the loss of crystallization water molecules in $[\{Mn(4Bpy\}(VO_3)_2]\cdot 1.16H_2O$ (top) and $[\{Mn(4Bpy\}_{0.5}(VO_3)_2]\cdot 0.62H_2O$ (botton). Reprinted with permission from Ref. 51. Copyright {2010} American Chemical Society.

It is difficult to establish general temperature ranges for the loss of crystallization and coordinated water molecules, because these processes strongly depend on the crystal structure itself. In the same way, it is also difficult to predict the crystal structure response to the loss of crystallization and/or coordinated water molecules. From a general point of view, those vanadates containing rigid organic linkers and compact inorganic frameworks, such as $[\{Ni_6(H_2O)_{10}(4Bpy)_6\}(V_{18}O_{51})]\cdot 1.5H_2O$ and $[\{Ni(H_2O)_2(Bpe)\}(V_4O_{11})]\cdot 0.5H_2O$, do not show strong structural responses to the loss of guest molecules, but the crystal structures are not able to accommodate the removal of coordination water molecules, giving rise to an irreversible amorphization of the compounds.

In the case of HV containing less rigid inorganic frameworks and organic linkers, such as $[\{Ni_3(H_2O)_3(Bpa)_4\}(V_6O_{18})]\cdot 8H_2O$ the loss of crystallization water molecules induces a dynamic response of the crystal structures, and the removal of coordinated water molecules is reversible, even when the process gives rise to amorphous or poor crystalline compounds. In those processes involving the removal and uptake of species that form an integral part of the crystal framework, the crystal structure adaptability is a key point to get crystalline compounds after the transformations. In fact, the $\{Ni_2(H_2O)_2(Bpa)_2\}(V_6O_{17})$ and $[\{Co_2(Pcca)_2(H_2O)\}(V_4O_{12})_{0.5}]\cdot 3.62H_2O$ crystal structures are example of this. The rational design of the crystal structures and more specifically, the rational choice of initial structural building blocks with enough degree of freedom to establish new weak interactions and/or bonds, are essential tasks to avoid the crystalline to pseudoamorphous transformations after the loss of coordinated species. Different possible strategies can be adopted, such as: (i) the synthesis of crystal structures containing not rigid inorganic substructures formed by corner-sharing polyhedra. For more information about the hydrothermal synthesis of HV the reader is referred to the works of Fernández de Luis *et. al.*[59,89], Livaje *et. al.*[90] and Chirayil *et. al.* [91]. (ii) The choice of secondary metal centres that could adopt different coordination environments, such as Co(II) and Cu(II); and (iii) the use of flexible organic ligands, that not only could adopt different conformations, but also do not incorporate extra donor atoms that could complete the coordination sphere of the secondary metal centres.

4.2.- Magnetic Properties

4.2.1-Hybrid vanadates with diamagnetic V(V) vanadium oxide subunits.

The connectivity of the metal centres in HV usually takes place through VO_4 tetrahedra and organic linkers, so the length of the M-O-V-O-M magnetic exchange pathways and the length and electronic structure of the organic ligands play a crucial role in the magnetic coupling of the metal centres. Even for those species showing polymerization, the connectivity of the polymerized units occurs *via* vanadate bridges and/or organic ligands. This has an obvious consequence in the magnetic behaviour of those systems, in such a way that the strength of the magnetic exchange along these pathways is inevitably reduced compared with that in a M-O-M link.

Several HV are constructed from magnetically isolated atoms showing a typical paramagnetic behaviour. Common magnetic structural buildings are the dimeric units constructed from metal octahedra sharing an edge. Example of those are the $\mathbf{I^2O^1}$ $\{Ni_2(H_2O)_2(Pz)\}(V_4O_{12})$ and $\mathbf{I^2O^2}$ $\{Ni(Bpe)\}(VO_3)_2$ crystal structures, that contains inorganic layers interconnected by metal-ligand chains (see Fig. 26 and 19 and sections 4.1 and 3.1 for more information about the crystal structures).[39,53] The Ni(II) octahedra share one edge, giving rise to dimeric units in both crystal structures. However, the distance and number of atoms between adjacent dimeric units are large enough to avoid any inter-dimer magnetic interaction. The magnetic susceptibilities are well fitted to typical intradimer antiferromagnetic (AF) interactions with J/k values of -22.4 and -59.4 K for $\{Ni_2(H_2O)_2(Pz)\}(V_4O_{12})$ and $\{Ni(Bpe)\}(VO_3)_2$, respectively. The magneto-structural correlations in dimeric complexes show that the *J* exchange parameter is directly connected with the Ni-O-Ni bridging angle with a crossover value of 97 º between the ferromagnetic (F) and AF behaviour.[92]. The Ni-O-Ni angle for $\{Ni_2(H_2O)_2(Pz)\}(V_4O_{12})$ (95.95º) and $\{Ni(Bpe)\}(VO_3)_2$ (92.80º) may favour the F interaction between metal centres, but the out-of-plane Ni-O-V angles and the connectivity between the metal centres and the vanadium atoms have a great influence in the final magnetic behaviour, as observed in the susceptibility measurements.[93,94]

Dimeric units of Co(II) centres linked by VO_4 tetrahedra have been reported in $\{Co(4Bpy)\}(VO_3)_2$**Error! Bookmark not defined.** and $\{Co(Bpa)\}(VO_3)_2$.[57] As it has been previously described (see Fig. 18, section 3.2), the $\mathbf{I^2O^1}$ $\{Co(4Bpy)\}(VO_3)_2$ and $\{Co(Bpa)\}(VO_3)_2$ HV contain inorganic $\{CoV_2O_6\}$ layers interconnected by Co(4Bpy) and Co(Bpa) chains. The magnetic exchange across the organic ligand is expected to be very weak, so the overall AF interaction should be mainly attributed to the superexchange coupling within the inorganic layers (see Fig. 18). The Co(II)···Co(II) distances within the layers suggest that the effective magnetic coupling is given between Co(II) atoms linked through one (VO_4) tetrahedron, generating magnetic dimeric AF units. The adjacent dimeric unit are far enough to avoid significant inter-dimer magnetic couplings (see Fig. 18 (b)). The thermal evolution of the magnetic susceptibilities for $\{Co(4Bpy)\}(VO_3)_2$ [37] and $\{Co(Bpa)\}(VO_3)_2$ [57] show broad maxima located at 36 and 20K, respectively. The susceptibility curves can be explained based on dimeric AF interactions plus the spin-orbit coupling typical for Co(II) d^7 cations.

The metal centres can also be magnetically coupled through the VOS or organic ligand giving rise to one dimensional systems, such as in $[\{Ni(H_2O)_2(Bpe)\}(V_4O_{11})]\cdot0.5H_2O$ and $\{Co_2(2\text{-}Pzc)(H_2O)\}(VO_3)_3$ compounds.[37,46] For $[\{Ni(H_2O)_2(Bpe)\}(V_4O_{11})]\cdot0.5H_2O$ the magnetic susceptibility shows a continuous increase of its value in the 300 to 2 K temperature range. Fig. 31 shows the thermal evolution of χ_m and χ_mT product. The VO_5 polyhedra and $Ni(H_2O)_2N_2O_2$ octahedra are corner-sharing, giving rise to 1D chains, with a Ni(II)···Ni(II) shortest distance of 6.26 Å. The inset of Fig. 31 shows the connectivity between the Ni(II) metal centres through VO_5 polyhedra. The magnetic susceptibility was analysed with Heisenberg isotropic AF S=1 chain model. The fitting is shown in the Fig. 31. The best fitting gives rise to g= 2.27 and J= -5.83K values, corroborating the existence of a weak AF interaction between the metal centres through the vanadate subunit.

The $\{Co_2(2\text{-}Pzc)(H_2O)\}(VO_3)_3$ $\mathbf{I^3O^1}$ structure (see Section 3.1 for more information about the crystal structure) is composed of infinite $\{Co_2(2\text{-}Pzc)(H_2O)\}$ metal-organic chains isolated by diamagnetic metavanadate chains. The $\{Co_2(2\text{-}Pzc)(H_2O)\}$ paramagnetic chains contains corner-sharing dimers of cobalt octahedra. The magnetic data was analysed by an isotropic dimer model for S= 3/2 ions with the inclusion of inter-dimer interaction (θ). The magnetic exchange coupling is mainly attributed to the intradimer AF exchange of the Co(II) metal centres through the Co-O-Co bridges (g= 2.52, J=-14.8 cm^{-1}). The weak inter-dimer interaction through the pyrazine group (θ= -0.9 K) is in good agreement with the other pyrazine bridged compounds where only very weak AF interactions occur between the magnetic centres.

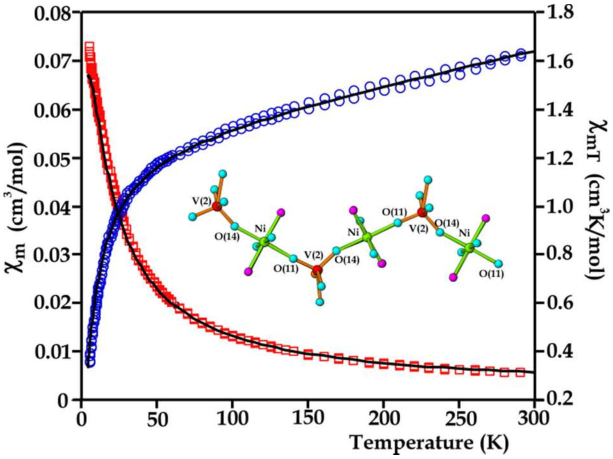

Fig. 31 χ_m and χ_mT curves for $[\{Ni(H_2O)_2(Bpe)\}(V_4O_{11})]\cdot0.5H_2O$. The lines are the best fit for a Heisenberg isotropic AF S=1 chain model. Inset: One dimensional magnetic exchange pathway between Ni(II) cations through the VO_5 polyhedra. Copyright (2009) Wiley-VCH Verlag GmbH and Co. KGaA. Reproduced with permission from Ref. 46

An interesting example of magnetically isolated $\{Cu(Pz)_2\}$ metal-organic layer between diamagnetic $\{V_6O_{16}\}^{2-}$ layers is the $[\{Cu(Pz)_2\}(V_6O_{16})]\cdot0.22H_2O$ $\mathbf{I^3O^2}$ vanadate. The $\{Cu(Pz)_2\}$ layers exhibit an AF ordering of the square lattice of Cu(II) ions, with a χ_{max} at 8 K.[41]

Magnetic trimers of edge-sharing Cu(II) cations have been reported in the $\{Cu_3(1,2,3\text{-}Trz)_2\}(V_4O_{12})$ $\mathbf{I^2O^1}$ and $\{Cu_3(1,2,4\text{-}Trz)_2\}(V_4O_{12})$ $\mathbf{I^3O^2}$ (see Section 3.1, Fig. 16) HV.[73,75] For $\{Cu_3(1,2,3\text{-}Trz)_2\}(V_4O_{12})$, the χ_m shows a continuous increase with a maximum at 12 K, then falling down until 2 K, while the χ_mT product decrease continuously with temperature. The χ_m and χ_mT evolution suggest AF interactions between the Cu(II) metal centres. The magnetic data was first fitted to a relatively isolated trimeric linear units of Heissenberg S= 1/2 (S_{A1}-S_B-S_{A2}) model with one nearest interaction J and two different values of the g factor. Fig. 32 (a) and (b) shows the trimeric units linked through the trizolate organic ligand and the magnetic exchange pathways within the Cu(II) cations in the trimeric units. The fitting of the thermal evolution of the magnetic susceptibility and the thermal evolution of the magnetic susceptibility are shown in the Fig. 32 (c). The best fit was obtained for g_A= 2.44, g_B= 2.27, J= -66 K and θ= -26K. The high value of the interdimer magnetic exchange (θ) indicates strong interactions between trimers.

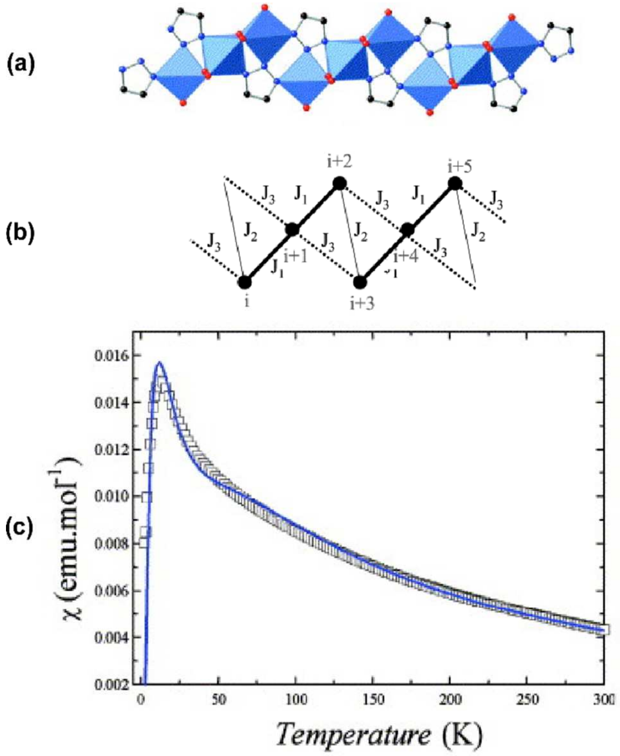

Fig. 32 (a) A view of a $\{Cu_3(1,2,4\text{-}Trz)_2\}_n^{4n+}$ chain of $\{Cu_3(1,2,4\text{-}Trz)_2\}(V_4O_{12})$, showing the bridging of Cu(II) trinuclear units by the triazolate ligands. (b) Magnetic model of chain of trimers with two inter-trimer exchange pathways (J_2 and J_3) (c) Plot of susceptibility vs. *T* with the blue line showing the fit to the trimer chain model. Adapted from Ref. 75 with permission of The Royal Society of Chemistry.

Devi *et. al.*[75] described the magnetic behaviour based on a chain of trimers with two inter-trimer exchange pathways (J_2 and J_3) (Fig. 32 (b)). The best fitting values are g= 2.3, J_1= -98, J_2= -37, J_3= -16K, θ= -6.6K, and TIP (Temperature Independent magnetism) = 2 x 10^{-5} emu·mol^{-1}. If the crystal structure is taken into account, inter-trimer magnetic exchange can be mainly attributed to the magnetic exchange through the triazolate bridges between trimers. The linkage of $\{Cu_3(1,2,3\text{-}Trz)_2\}$ metal-organic chains through the $\{V_4O_{12}\}$ cycles involves a very long exchange pathway (Cu-O-V-O-V-O-Cu), so the magnetic interactions are not expected to be very strong. For $\{Cu_3(1,2,4\text{-}Trz)_2\}(V_4O_{12})$ similar shape of the χ_m curve is observed, in good agreement with the existence of AF coupled trimetric units in the crystal structure. In comparison with the previously described copper vanadate, the Cu(II) cations within the trimetric units are linked through the triazolate and VO_4 bridges. Each trimetric unit connects to other four via triazolate ligands, giving rise to two dimensional $\{Cu_2(1,2,4\text{-}Trz)_3\}$ ruffling layers with an amplitude of about 4.75 Å and a period of 8.87 Å. (see Fig. 16, Section 3.1) In the same way that for $\{Cu_3(1,2,3\text{-}Trz)_2\}(V_4O_{12})$ compound, attempts to fit the data for non interacting trimetric units were unsuccessful, suggesting strong inter-trimer magnetic coupling. Moreover, the susceptibility exhibits a sharp drop below 6 K and FC-ZFC divergence, suggesting long-range AF ordering.

The comparative study of the magnetic properties of $[Co(H_2O)_2(VO_3)_2]\cdot 2H_2O$ and the $\{Co(Pym)\}(VO_3)_2$ **I^3O^1** HV reveals the importance of including M-L-M magnetic exchange pathway in competition with the magnetic coupling established by the metal centres in the purely inorganic framework.[43] The inorganic scaffolds of both compounds are very similar, and contain cobalt metal centres connected though double metavanadate chains giving rise a 3D scaffold. Fig. 33(a) shows a comparative view of the crystal structures of $\{Co(Pym)\}(VO_3)_2$ and $[Co(H_2O)_2(VO_3)_2]\cdot 2H_2O$, respectively. In the hybrid compound the metal centres are connected through the pyrimidine organic ligand, giving rise to metal-organic chains aligned in the [100] crystallographic direction. The possible magnetic exchange pathways between Co(II) cations have been represented in Fig. 33 (b). There are two common magnetic exchange pathways across the metavanadate chains for both crystal structures, defined as J_1 and J_2. For the hybrid compound a third magnetic pathway through the organic ligand take place (J_3).

Fig. 34 (a) and Fig. 34 (b) show the thermal evolution of χ_m and $\chi_m T$ measured at a magnetic field of 1 kOe for $\{Co(Pym)\}(VO_3)_2$ and $[Co(H_2O)_2(VO_3)_2]\cdot 2H_2O$, respectively. For the inorganic compound the negative value of the Weiss temperature θ= -33.7 K and the decrease of the $\chi_m T$ product indicate the AF coupling of the Co(II) octahedral through the double metavanadate chains. The thermal dependence of the magnetic susceptibility χ_m for the inorganic compound shows a maximum at 2.5 K indicating the existence of a 3D AF ordering (Fig. 34 (b)). The small change of curvature in the magnetization curve registered at a critical field Hc= 6kOe is also in good agreement with the establishment of the 3D AF ordering at low temperatures. The λ peak observed in the magnetic specific heat measurements at low temperatures and its shift to lower temperatures by increasing the magnetic field, confirm the AF ordering. At magnetic fields higher than 30 KOe, the maximum is shifted to higher temperatures, indicating a F ordering. The broad maximum could be related with a F component in the inorganic scaffold.

The hybrid $\{Co(Pym)\}(VO_3)_2$ vanadate possess the same connectivity and structural units that $[Co(H_2O)_2(VO_3)_2]\cdot 2H_2O$ in the inorganic scaffold, except for the pyrimidine ligand. The linkage of the Co(II) metal centres through the pyrimidine bridges introduce a competition between the AF coupling of the Co(II) cations of the inorganic scaffold and the magnetic exchange through the organic ligand, as it is suggested by the irreversibility of the magnetic susceptibility at low temperatures which indicates the existence of a -weak F component. The decrease of the $\chi_m T$ product and the negative value of the Weiss temperature θ= -34.5 K indicates the existence of AF interactions in the high temperature range (Fig. 34 (a)). The magnetization measurements carried out at 2 K show hysteresis loop with a coercive field value of 330 Oe and a remnant magnetization of 1604 emu mol^{-1}. The hysteresis decreases with increasing temperature, disappearing at 4.5 K. The general shape of the *M(H)* curve, with hysteresis at low fields, and then AF behaviour at higher fields, is characteristic of soft ferromagnets.

The F contribution at low temperatures is favoured by the Co-pym-Co bridges, which compete with the AF coupling of the inorganic scaffold. The increase of the applied field or the temperature favours the AF ordering of the inorganic scaffold, in -good agreement with the AF ordering observed in the inorganic compound, revoking the F component associated to the Co-Pym-Co metal-organic chains.

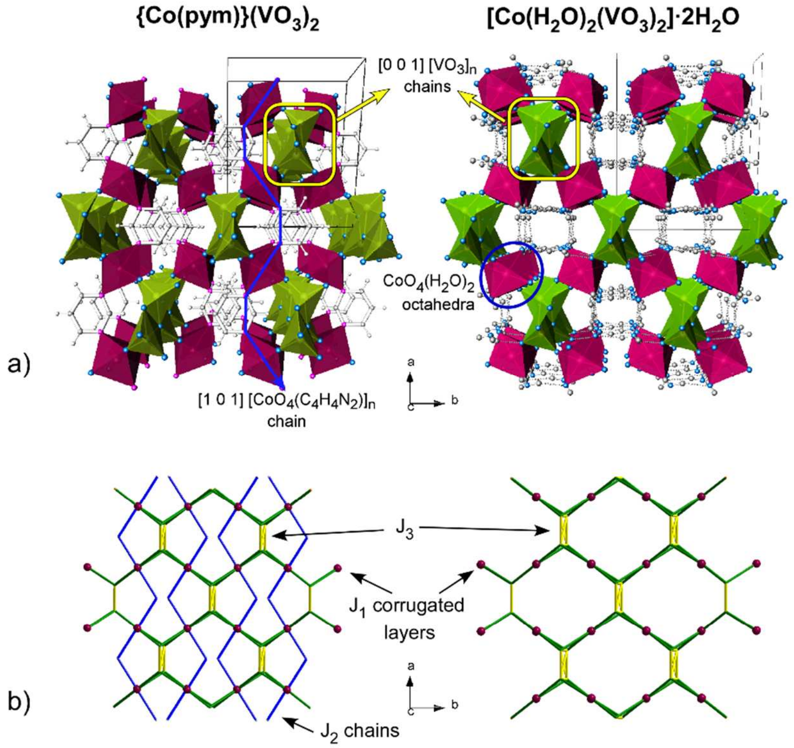

Fig. 33 (a) Polyhedral view of the three-dimensional crystal structures of {Co(Pym)}$(VO_3)_2$ and $[Co(H_2O)_2(VO_3)_2]\cdot 2H_2O$ in the ab-plane. (maroon polyhedral: CoN_2O_4 octahedra; green polyhedra: metavanadate chains) (b) Schematic representation of the magnetic exchange pathways in 1 and 2. Reproduced from Ref. 43.with permission of The Royal Society of Chemistry.

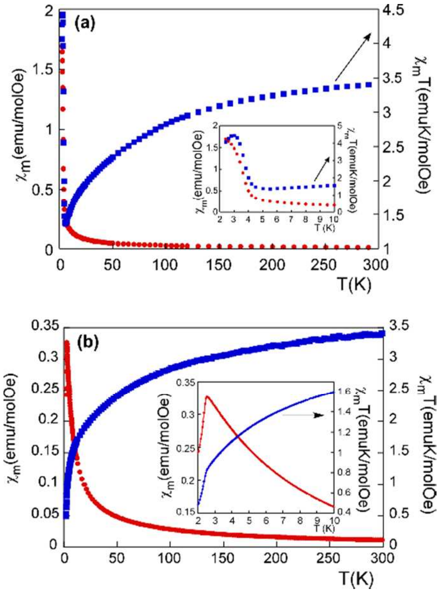

Fig. 34 Thermal evolution of χ_m and χ_mT measured at a magnetic field of 1 kOe for {Co(Pym)}$(VO_3)_2$ (a) and $[Co(H_2O)_2(VO_3)_2]\cdot 2H_2O$. (b) The insets show the low temperature region. Reproduced from Ref. 43.with permission of The Royal Society of Chemistry.

Other very interesting examples of the introduction of organic molecules in inorganic scaffolds are the $[\{Mn(4Bpy)\}(VO_3)_2]\cdot 1.16H_2O$ and $[\{Mn(4Bpy)\}_{0.5}(VO_3)_2]\cdot 0.62H_2O$ **I^{2}O^2** hybrid Brannerites (hereafter denoted as MnBpy and MnBpy$_{0.5}$), structurally closely related with the inorganic MnV_2O_6 vanadate.[51] In all the crystal structures the Mn(II) octahedra are edge-sharing, giving rise to chains extended along the "b" axis. It is well known that, in the different reported Brannerite inorganic compounds, the metal cations are F coupled within the chains and AF ordering of the adjacent chains is achieved at low temperatures. In the hybrid MnBpy and MnBpy$_{0.5}$ Brannerites, the vanadate and manganese chains are connected giving rise to inorganic layers. Those are pillared by the organic ligand (see Fig. 30). In that respect, the interchain distances, from 4.964 Å in MnV_2O_6 to 5.471 Å in MnBpy$_{0.5}$ and 8.537 Å in MnBpy, are related to the Néel temperature, from 20 K in MnV_2O_6 to 7.5 and 4 K in MnBpy$_{0.5}$ and MnBpy, respectively.

The maxima observed at 7.5 and 4 K in the χ_m and χ_mT curves also indicate the establishment of 3D AF at low temperatures. The data above the maxima are well fitted to Curie-Weiss law, and also to a one dimensional homogeneous S=5/2 chain ($H=-JS_i+S_{i+1}$) with positive Weiss temperatures of 16.9K for MnBpy and 16.3K for MnBpy$_{0.5}$ and magnetic couplings of J= 1.142(4) and J= 1.516(7) K for MnBpy and MnBpy$_{0.5}$, respectively. Those fittings are in good agreement with the F coupling of the Mn(II) cations within the chains. The AF ordering is overcome at applied fields as low as 0.2 T for MnBpy and 0.4 T for MnBpy$_{0.5}$. In this sense, the specific heat measurements show λ type peaks at low temperatures, shifted to lower temperatures when higher fields are applied, in good agreement with an AF ordering. The AF structure for MnBpy was determined by neutron diffraction, showing the AF ordering of F chains. The Fig. 35 (a) and (b) shows the orientation of the manganese spins in the magnetic cell and in the crystal structure of MnBpy, respectively.

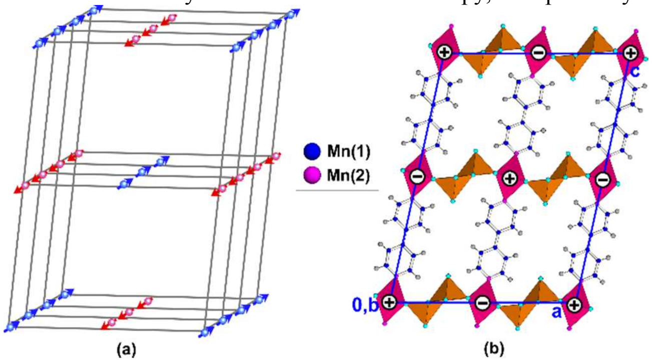

Fig. 35 (a) Magnetic ordering in [{Mn(4Bpy)}$(VO_3)_2$]·1.16H_2O. (b) Magnetic structure for [{Mn(4Bpy)}$(VO_3)_2$]·1.16H_2O. Reprinted with permission from Ref. 51 Copyright {2010} American Chemical Society.

-

The ability of vanadium atoms to adopt different oxidation states takes an important role in the magnetic properties of the HV. {M(Bpy)}(V_4O_{10}) (M=Ag(I), Cu(I)) **I^3O^1** compounds present $(V_4O_{10})^-$ reduced layers constructed from corner- and edge-sharing VO_5 distorted square base pyramids.[49] The layers can also be described as zigzag chains of edge-shared VO_5 square base pyramids corner linked to the adjacent chains (see Fig. 20 Section 3.2). In both crystal structures the V(1) and V(2) belonging to the same zigzag chain have slightly reduced positions +4.5, while the V(3) and V(4) cations exhibit higher valences of +5. Thus, the chains of partially reduced VO_5 polyhedra are structurally isolated from each other. The electric conductivity of both compounds exhibit positive temperature dependence that is consistent with semiconducting behaviour. The non-linear relationship of log(ρ) *vs.* 1/T indicates that the thermally activated hopping is not characterized by a constant activation energy. The modelling of the electrical conductivity to Mott´s variable-range-hopping model indicates that the energetically favourable electron hopping also occurs between more remote V sites rather than solely nearest- neighbour V cations. The magnetic susceptibilities show strong temperature dependences consistent with random localization of unpaired electrons. The Curie-Weiss fits indicate negative Weiss temperatures of θ= -25 and θ= -31 K for Cu(I) and Ag(I) compounds, respectively. The Curie constants are close to that expected for one unpaired spin per formula (C= 0.374 emu K $\cdot mol^{-1}$). The magnetic data were also fitted to a Heissenberg linear AF chain model for V^{4+} (S=1/2) with final values of g= 1.81(2) and J= -6.8(2) cm^{-1} for the Cu(I) compound and g= 1.90(1) and J= 9.01(8) cm^{-1} for the Ag(I) vanadate. These results suggest a gradual localization of the electrons along isolated vertex shared chains of VO_5 pyramids at the lowest temperatures.

Another interesting strategy is to combine magnetically active transition metal cations with reduced vanadate groups in the same crystal structure, giving rise to the competition between the magnetic properties related with the randomly or fully delocalized electrons of the reduced VOS and the unpaired electrons of the transition metal centres. That is the example of the reduced hybrid layered {M(pz)}(V_4O_{10}) (M=Zn(II), Co(II), Ni(II)) vanadates.[38] The crystal structure of these compounds can be envisioned as arising from an in situ intercalation and polymerization of cationic $\{M(pz)\}^{2+}$ chains between the $(V_4O_{10})^{-2}$ layers. Due to the mixed valence V^{4+}/V^{5+} of the $(V_4O_{10})^{-2}$ layers, the compounds exhibit electrical conductivity, with apparent activation energy values of 0.36, 0.46 and 0.59 eV for the Co, Ni and Zn(II) vanadates, respectively. The average vanadium oxidation state is +4.5 and implies two unpaired electron per $(V_4O_{10})^{-2}$ unit. The observed Curie-Weiss constant for the Zn(II) vanadate (0.79(2) emu K /mol) is consistent with two randomly localized S= 1/2 spins per $(V_4O_{10})^{-2}$ unit. The magnetic susceptibility shows a maximum located at 22 K, that provides unequivocal evidence of the presence of a single ground state and the formation of a spin gap at low temperatures. The V^{4+}/V^{5+} charge ordering seems to play an important role in the long range order AF transition of the Zn(II) hybrid reduced vanadate. The spin-dimer analysis method within the extended Hückel approximation was employed to determine the possible spin lattices for the $(V_4O_{10})^{-2}$ layers, and the AF spin-exchange interaction. The interaction energies suggest the possibility of the coexistence of both F and AF exchange within a triangular spin arrangement. The charge ordering to low temperatures could lead to magnetic structures showing both AF and F spin interactions or only AF order intra and inter magnetic dimers. The Fig. 36 shows the temperature dependence of the magnetic susceptibility for {Zn(pz)}(V_4O_{10}). As the Zn(II) cation is diamagnetic, the AF couplings observed in the thermal susceptibility evolution is ascribed to the presence of V^{4+} cations in the crystal structure. The inset of Fig. 36 shows the possible arrangement of the V^{4+} cations within the $(V_4O_{10})^{2-}$ layers (Fig. 36 (Inset)).

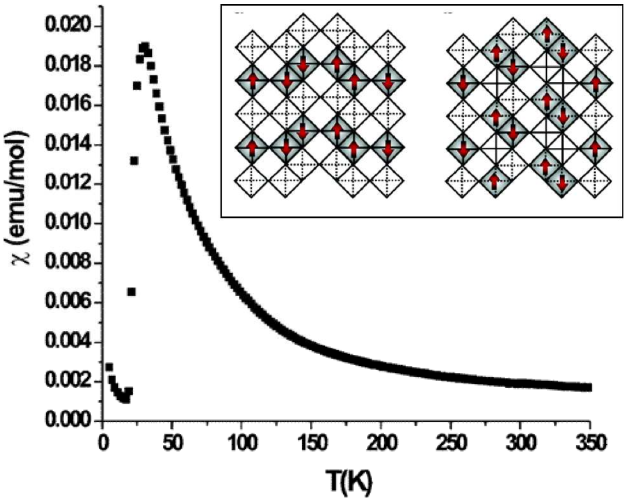

Fig. 36 Magnetic susceptibility versus temperature for {Zn(pz)}(V_4O_{10}). The measuring field was 0.1 T. Inset: two possible spin lattices for the charge localization of V^{4+} sites (shaded) exhibiting both F and AF or only AF V^{4+}–V^{4+} interactions. Adapted with permission Ref. 38 Copyright {2013} American Chemical Society.

In the specific case of the {Ni(pz)}(V_4O_{10}) and {Co(pz)}(V_4O_{10}), the χ_m values obtained for Ni(II) (1.72(3) emu K /mol) and Co(II) (4.302(4) emu K /mol) compounds take also into account the temperature independent paramagnetism for the Ni(II) cation and the spin-orbit coupling effect for the Co(II) metal centres. The magnetic susceptibilities for the Ni(II) and Co(II) compounds show no sharp peak at low temperatures, suggesting that there is not long range AF order, destroying the spin gap state. The ZFC/FC divergences below 10 K may indicate a spin glassy ground state for both compounds.

Most of the HV constructed from dipodal ligands present magnetically isolated transition metal cations. The distance between the metal centres connected through the vanadate oxoanion and/or organic ligand are too long, hindering the magnetic coupling between the cations, and giving rise to paramagnetic behaviours. However, when the distance between metal centres is short enough and the magnetic super-exchange pathway does not involve many atoms, the magnetic interaction through the vanadate groups could lead to dimeric, one dimensional coupling, and even three dimensional long range AF orders. Another strategy is to bridge the metal centres through short organic linkers that favours the magnetic couplings. In several HV, the magnetic metal-organic unit are isolated by the vanadate groups, giving rise to cluster or one-dimensional magnetic coupling similar to that showed by purely metal-organic or coordination compounds. But the competition between the magnetic super-exchange pathways within the metal-organic scaffolds and the inorganic framework could give rise to metamagnetic compounds. In these, the increase of the magnetic field favours the coupling of the metal centres through the vanadate groups instead of across the ligand, or vice versa, giving rise to field induced magnetic transitions.

4.3- Catalytic and Photocatalitic Properties

It is well known that vanadium based materials are active heterogeneous catalysts for several reactions. In fact, since the discovery of vanadate dependent enzymes from various algae and terrestrial fungi, the coordination chemistry of this element has received increasing interest.[95] Moreover, recently several studies reveal that HV could act as visible light catalyst for water splitting or degradation of pollutants.[96]

Despite several examples of this section are focused on HV with chelating ligands, we consider that this is a very interesting starting point for future research on catalytic and photo-catalytic studies on HV constructed from organic connectors.

As far as we are aware, the first catalytic test on HV was done with the family of compounds $M(HAep)_2(VO_3)_4$, M= Co(II), Ni(II), Cu(II), H_2Aep= 1-(2-amoethyl)piperazine. These iso-structural $\mathbf{I^2O^0}$ materials possess a 2D crystal structure, constructed from inorganic layers based on metavanadate chains of VO_4 tetrahedra linked through metal centres. The coordination environment of the metal centres is completed by the chelating HAep ligand. The layers of the crystal structure are stacked establishing hydrogen bonds with the adjacent layers along the [010] crystallographic direction.[97]

The activity of this HV was probed towards oxidation of sulfides. Various catalytic essays were performed with different oxidizing agents (H_2O_2 and TBHP) and substrates (methyl phenyl sulfide, ethylbutyl phenyl sulfide, p-chlorophenyl methyl sulfide and methyl p-tolyl sulphide).

The Fig. 37 shows the kinetic profile of the studied catalysts for the oxidation of methyl phenyl sulfide with H_2O_2 as oxidizing agent. The behaviour of all of the catalysts is very similar, reaching conversions between 83 and 64 %, with selectivity rates towards the sulfoxide over 94 %.

The second example of catalytic activity in HV was reported on the $[\{CoNi(H_2O)_2(Bpe)_2\}(V_4O_{12})]\cdot 4H_2O\cdot Bpe$ compound.[56] This was probed in the cyanosilylation reaction of aldehydes with trimethylsilyl cyanide (TMSCN) under solvent-free conditions. Benzaldehyde was used to fit the best starting conditions, and then establishing the conditions for different aldehydes. When using aromatic aldehydes, the conversion decreases in the order p-methylbenzaldehyde > benzaldehyde > p-fluorobenzaldehyde, in agreement with their corresponding electronic effects. When using an aliphatic aldehyde as heptaldehyde, the reaction takes place faster than when using aromatic aldehydes. The catalyst loss progressively efficiency in successive recycling runs. The X-ray diffraction and IR studies show that despite the loss of crystallinity after the reactions, the compound maintain the layered crystal structure, and its basic initial building blocks $\{V_4O_{12}\}$ cycles, metal centres and Bpe organic ligands. However, the existence of extra bands in the IR spectra, suggest that the active centres are blocked progressively by cyanide groups during the catalytic reactions.

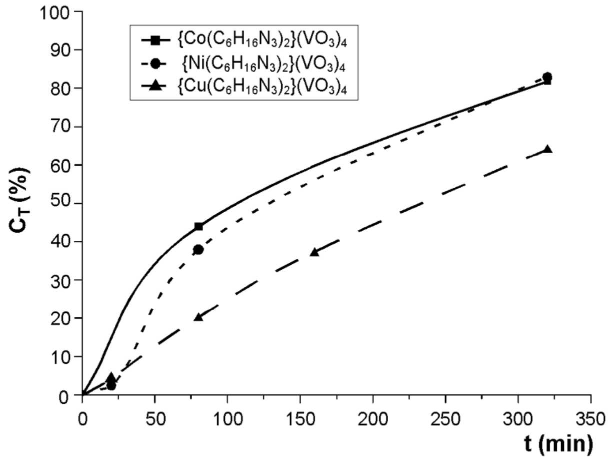

Fig. 37 Kinetic profile for the oxidation reaction of methyl phenyl sulfide with $M(HAep)_3(VO_3)_4$, M= Co^{2+}, Ni^{2+}, Cu^{2+}. Reproduced from Ref.97 with permission of The Royal Society of Chemistry.

Lin and Maggard have synthesized three silver vanadates with 4Bpy, Bpa and pyrazinedicarboxylate Pzc as ligands, whose formulas are: $[\{Ag(4Bpy)\}_4(V_4O_{12})]\cdot 2H_2O$ **($\mathbf{I^2O^1}$)**, $[\{Ag(Bpa)\}_4(V_4O_{12})]\cdot 4H_2O$ **($\mathbf{I^2O^2}$)** and $\{Ag_4(2\text{-}Pzc)_2\}(V_2O_6)$ **($\mathbf{I^2O^3}$)**.[48] $[\{Ag(4Bpy)\}_4(V_4O_{12})]\cdot 2H_2O$ and $[\{Ag(Bpa)\}_4(V_4O_{12})]\cdot 4H_2O$ crystal structures are composed of neutral $\{Ag_4V_4O_{12}\}_n$ layers that are pillared by the organic ligands, 4Bpy or Bpa, coordinated to the Ag(I) sites. The layers consist of isolated $\{VO_{12}\}$ rings that are linked together by eight Ag^+ cations per ring. The third compound is composed of a 3D $\{Ag_2(Pzc)^+\}_n$ metal-organic network that contains $\{VO_3^-\}_n$ double chains within its open channels.

On the other hand, Han et al., have recently obtained a new silver(I) HV with 1,4-Bis(N-imidazolyl)butane, Bbi, $[Ag(Bbi)][\{Ag(Bbi)\}_4\{Ag_3(V_4O_{12})_2\}].2H_2O$.[65] The phase crystallizes in the triclinic space group P-1 and the most fascinating feature is the 1D chains containing $\{Ag_7\}$ clusters with Ag···Ag interactions based on dicyclic rings of $\{V_4O_{12}\}$.

All these silver(I) vanadates show photocatalytic activity and were tested for the decomposition of methylene blue (MB) under ultraviolet and/or visible light. MB is commonly used as a representative of widespread organic dyes that contaminate textile effluents and that are very difficult to decompose in waste streams. In Fig. 38 changes in the concentration of the aqueous MB solution vs. irradiation time with ultraviolet light were plotted. All of them are active for the decomposition of MB under UV light irradiation.

The photocatalytic rates of $\{Ag_4(2\text{-}Pzc)_2\}(V_2O_6)$ and $[Ag(Bbi)][\{Ag(Bbi)\}_4\{Ag_3(V_4O_{12})_2\}]. 2H_2O$ are notably higher than either $[Ag(4Bpy)]_4V_4O_{12}.2H_2O$ or $[\{Ag(Bpa)\}_4V_4O_{12}].4H_2O$. $\{Ag_4(2\text{-}Pzc)_2\}(V_2O_6)$ is also active under visible light, decomposing an 80% of the MB after 3 h.

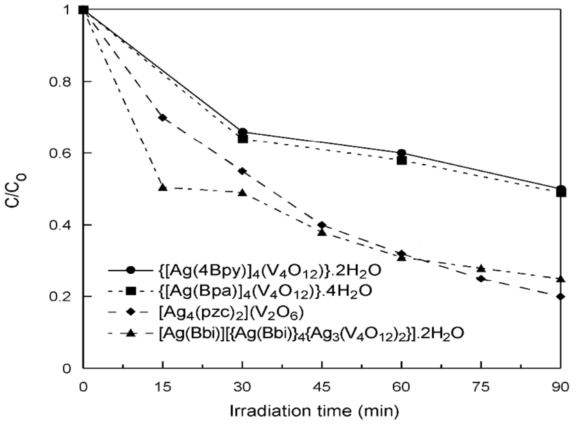

Fig. 38 Photocatalytic decomposition of MB solution under UV light with the use of hybrid silver(I) vanadates.

Some silver and manganese HV also present photo-catalytic properties. A synergistic effect between silver ions and vanadates allows tuning the band-gap improving their catalytic activity for the photocatalytic splitting of water or photocatalytic degradation of pollutants.

The first example of water splitting by a hybrid compound was reported recently by Luo and Maggard in Mn(Bpy)(V_4O_{11})(Bpy) vanadate.[98] This compound was found to exhibit photocatalytic activity for the production of hydrogen, as well as for total water splitting into both hydrogen and oxygen. The photocatalitic tests were carried out with water, in methanol solutions (Fig. 39 (a) and (b)), and after coating the material with a 1% Pt co-catalyst (Fig. 39 (c) and (d)). This HV is an effective photocatalyst, with production of hydrogen ranging from 16 μmol H_2 $g^{-1}h^{-1}$ in 20% methanol solution to 71 μmol H_2 $g^{-1}h^{-1}$ per Pt coated samples under ultraviolet light.

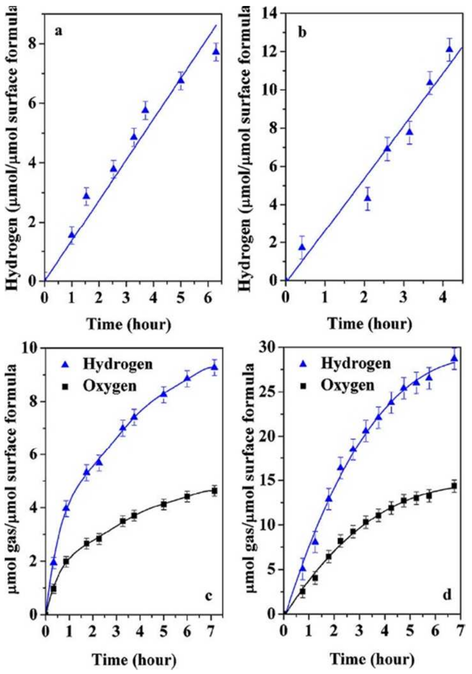

Fig. 39 Amount of hydrogen molecules per surface sites of Mn(Bpy)(V_4O_{11})(Bpy) undervisible light (420−800 nm) and different photocatalytic testing conditions: (a and b) with methanol as a scavenger or (c and d) with 1% Pt as a surface cocatalyst. Reprinted with permission from Ref. 98. Copyright {2013} American Chemical Society.

Concluding Remarks

The great structural diversity of transition metal hybrid vanadium oxides is clearly related with the ability of vanadium to adopt different coordination environments and to polymerize giving rise to different vanadium structural subunits. The hydrothermal synthesis conditions influence drastically the obtained vanadium building blocks, promoting in some cases the partial or complete reduction of V^{5+} to V^{4+}. If at those points, the possibility to adopt different coordination environment by the secondary transition metal centres, the diversity in metal-organic substructures, the rigidity/flexibility of the organic molecules, or the possibility of multiple modes of coordination for the mixed carboxylic-nitrogen donor ligands are added; the scope of possible structural archetypes becomes enormous, hindering the predictability of the obtained frameworks. But, due to these degrees of freedom, the complexity of the crystal chemistry of HV is amazing, sharing common characteristics with the classical inorganic-organic materials and present metal-organic frameworks.

Despite that the studies of the thermal responses of HV to the loss of guest and coordinated species are scarce, a great range of behaviours have been reported, mainly dependent on the crystal structures. It would be very interesting to study the thermal response of several reported HV constructed from flexible and rigid organic connectors. And more concretely, it would be very clarifying to determine the transformation mechanisms involved in the reversible removal and uptake of coordinated water molecules in HVs. Up to now, the V=O terminal bonds seems to takes an important role in the formation of new metal-oxygen bonds after the coordination water removal. Another possibility is to incorporate ligands with non-bonded donor atoms that could complete the coordination environment of the metal centre after the loss of coordinated species, and or metal centre that could adopt different coordination environments. Moreover, the crystal structure has to possess enough degree of flexibility to assume these strong atomic motions during the transformation.

With regard to the magnetic properties, different strategies have been proposed. The most important strategy is to obtain structural building blocks constructed from corner- or edge-sharing metal centre polyhedra, because the magnetic exchange through the VOS usually gives rise to AF couplings or orderings. Strategies such as mixing reduced VOS with metal centres linked through short organic linkers, have allowed obtaining very interesting magnetic competitions within the same structure. A very interesting future scope could include hybrid vanadates constructed from short carboxylate ligands that could promote the magnetic exchange between metal centres.

The use of short, long bipodal or multipodal carboxylate based ligands could enlarge greatly the crystal chemistry of this amazing family of hybrid materials, focusing the compounds on specific properties and applications.

A new amazing field of study is being developed by different research groups. The use of HV as catalyst and/or photo-catalyst is a very interesting research field for the green and effective degradation of pollutants. Other interesting and emerging research area is the splitting of water in H_2 and O_2, tested for several inorganic silver vanadates, is one of the promising fields for testing HV as new photo-catalysts.

Acknowledgments

This work has been financially supported by the "Ministerio de Ciencia e Innovación" (MAT2010-15375 and MAT2013-42092-R) and the "Gobierno Vasco" (IT630-13), which we gratefully acknowledge. The authors thank the technicians of SGIker

(UPV/EHU). R. Fernández de Luis thanks to the MICINN (Madrid, Spain) for funding. E. S. Larrea and J. Orive thanks the UPV/EHU for funding.

Notes and references

[a] Departamento de Mineralogía y Petrología, Facultad de Ciencia y Tecnología, Universidad del País Vasco (UPV/EHU), Apdo. 644, 48080 Bilbao, Spain. Fax:+34 946 013 500; Tel: +34 946 015 984
[b]BCMaterials (Basque Centre for Materials, Applications & Nanostructures). Technological Park of Zamudio, Camino de Ibaizabal, Bndg. 500-1st, 48160, Derio, Spain. E-mail: roberto.fernandez@ehu.es, edurne.serrano@ehu.es, joseba.orive@ehu.es karmele.urtiaga@ehu.es, maribel.arriortua@ehu.es.

---

1 G. Férey; *C. R. Acad. Sci.* Paris, **1998**, *1*, 1.

2 (a) S. T. Wilson, B. M. Lok, C. A. Messina, T. T. Cannan and E. M. Flanigen, *J. Am. Chem. Soc.* 1982, **104**, 1146-11XX. (b) M. Estermann, L. McCusker, C. Baerlocher, A. Merrouche and H. Kesseler, *Nature*, 1991, **352**, 320-32X. (c) G. Ferey, *J. Fluorine Chemistry*, 1995, **72**, 187-18X. (d) S. Natarajan and S. Mandal, *Angew. Chem. Int. Ed.* 2008, *47*, 4798-4828.

3 T. Rojo, J. L. Mesa, J. Lago, B. Bazán, J. L. Pizarro and M. I. Arriortua, *J. Mater. Chem.* 2009, **19**, 3793-3818.

4 (a) Z.-E. Lin and G.-Y. Yang, *Eur. J. Inorg. Chem.*, 2010, **19**, 2895-2902. (b) M. E. Medina, M. Iglesias, N. Snejko, E. Gutierrez-Puebla and M. A. Monge, *Chem. Mater.* 2004, **16**, 594-599. (c) N. Snejko, M. E. Medina, E. Gutierrez-Puebla and M. A. Monge, *Inorg. Chem.* 2006, **45**, 1591-1594.

5 C. N. R. Rao, J. N. Behera and D. Meenakshi, *Chem. Soc. Rev.* 2006, **35**, 375-387.

6 O. M. Yaghi, M. O´Keefee, N. W. Ockwig, H. K. Chae, M. Eddaoudi and J. Kim, *Nature,* 2003, **423**, 705-714.

7 P. J. Hargrman, R. C. Finn and J. Zubieta, *Solid State Sciences*, 2001, **3**, 745-774.

8 C. Janiak and J. K. Vieth, *New J. Chem.* 2010, **34**, 2366-2388.

9 Z.-H. Yi, X.-B. Cui, X. Zhang, J. Yu, J. Lu, J.-Q. Xu, G.-D. Yang, T.-G. Wang, H.-H. Yu and W.-J. Duan, *Dalton Trans.* 2007, 2115.

10 R. C. Finn, J. Sims, C. J. O`Connor and J. Zubieta, *J. Chem. Soc., Dalton Trans.* 2002, 159.

11 C. M. Liu, Y.-L., Hou, J. Zhang and S. Gao, *Inorg. Chem.* 2002, **41**, 140.

12 R. N. Devi and J. Zubieta, *Inorg. Chim. Acta*, 2003, **342**, 313.

13 P. J. Hargman and J. Zubieta, *Inorg. Chem.*, 2001, **40**, 2800.

14 C.-M. Liu, S. Gao, H.-H. Hu and Z.-M. Wang, *Chem. Commun.*, 2001, 1636.

15 (a) X. Qu, L. Xu, G. Gao, F. Li and Y. Yang, *Inorg. Chem*. 2007, **46**, 4775-4777. (b) D. L. Long, A. J. Blake, N. R. Champness, C. Wilson and M. Schröder, *Angew. Chem. Int. Ed.* 2001, **40**, 2443-2447.

16 M. Schindler, F. C. Hawthorne and W. H. Baur, *Chem. Mater*. 2000, **12**, 1248-1259.

17 A.F. Wells, *Structural Inorganic Chemistry*, Claredon Press, Oxford, **1984**.

18 P. Y. Zavalij and M. S. Whittingham, *Acta. Crystallogr*. 1999, **B55**, 627-663.

19 B. L. Ulická, F. Pavelcík and K Huml, *Acta Crystallogr*. 1987, **C43**, 2266-2268.

20 L. Shi-Xiong, L. Bi-Zhou and L. Shen, *Inorg. Chim. Acta* 2000, **304**, 33-37.

21 D. Riou and G. Férey, *J. Solid State Chem*. 1996, **124**, 151-154.

22 R. L. La Duca, R. S. Rarig, and J. Zubieta, *Inorg. Chem*., 2001, **40**, 607-612.

23 J. R. D. Debord, Y. Zhang, R. C. Haushalter, J. Zubieta, and C. J. O`Connor, *Solid State Chem.* 1996, **122**, 251-258.

24 R. L. La Duca, R. Ratkoski, R. S. Rarig and J. Zubieta, *Inorg. Chem. Commun.* 2001, **4**, 621-625.

25 J.-Y. Xie and J.-G. Mao, *J. Mol. Struct.* 2005, **750**, 186-189.

26 C.-M. Liu, Y.-L. Hou, J. Zhang and S. Gao, Inorg. Chem. 2002, 41, 140-143.

27 (a) A. K. Cheetham, C. N. T. Rao, R. K. Feller, *Chem. Commun.* 2006, 4780-4795. (b) Rao, C. N. R., Cheetham, A. K., Thirumurugan. *J. Phys.: Condens. Matter*. 2008, **20**, 083202 (21pp).

28 (a) A. Thirumurugan, R., A. Sanguranath and C. N. R. Rao, *Inorg. Chem.* 2008, **47**, 823-831. (b) M. J. Bialek, J. Janczak and J. Zon, *CrystEngComm*, 2013, **15**, 390-399. (c) T. Kurc, J. Janczak, J, Hoffmann and V. Videnova-Adrabinska, *Cryst. Growth Des.*, 2012, **12**, 2613-2624. (d) A. Thirumurugan, K. P. Swapan, M. A. Green and S. Natarajan, *J. Mater Chem.*, 2003, **13**, 2937-2941.

29 I. D. Willians, T. S. Law, H. H.-Y. Sung, G.-H. Wen and X.-X. Zhang, *Solid State Chem.* 2000, **2**, 47-55.

30 Z. Shi, L. Zhang, G. Zhu, G. Yan, J. Huar, H. Ding and S. Feng, *Chem. Mater*. 1999, **11**, 3565-3570.

31 X. Wang, L. Liu, A. J. Jacobson and K. Ross, *J. Mater. Chem.,* 1999, **9**, 859–861.

32 I. D. Willians, T. S.-C. Law, H. H.-Y. Sung, G.-H. Wen and X.-X. Zhang, *Solid State Sci.* 2000, **2**, 47-55.

33 B. F. Abrahams, M. G. Haywood and R. Robson, *Polyhedrom*, 2007, **26**, 300-304.

34 G.-C. Ou, L. Jiang, X.-L. Feng and T.-B. Lu, *Dalton Trans*., 2009, 71-76.

35 (a) J. Do and A. J. Jacobson, *Inorg. Chem*. 2001, **40**, 2468-2469. (b) B.-Z. Lin and S.-X. Liu, *Polyhedron*, 2000, **19**, 2521-2527. (c) B.-Z. Lin and S.-X. Liu, *J. Chem. Soc., Dalton Trans.*, 2002, 865-869. (d) P. Y. Zavalij, F. Zhang and M. S. Whittingham, *Acta Crystallogr.*, 1999, **B55**, 953-962. (e) Z. Shi, L. Zhang, G. Zhu, G. Yang, J. M. Hua, H. Ding and S. Feng, *Chem. Mater.* 1999, **11**, 3565-3570.

36 Y.-Q. Jiang, Z.-H. Xu and Z.-X. Xie, *J. Coord. Chem.* 2008, **61**, 1575-1581.

37 L.-M. Zheng, X. Wang, Y. Wang, and A. J. Jacobson, *J. Mater. Chem*. 2001, **11**, 1100-1105.

38 B. Yan, J. Luo, P. Dube, A. S. Sefat, J. E. Greedan and P. A. Maggard, *Inorg. Chem.* 2006, **45**, 5109-5118.

39 E. S. Larrea, J. L. Mesa, J. L. Pizarro, M. I. Arriortua and T. Rojo, *J. Solid State Chem.* 2007, **180**, 1149-1157.

40 (a) E. S. Larrea, Doctoral thesis, "*New Transition Metal Hybrid Vanadates. Hydrothermal Synthesis, Structural Study and of their Spectroscopic and Magnetic Properties*", Universidad del País Vasco (UPV/EHU), **2009**. (b) E. S. Larrea, J. L. Mesa and M. I. Arriortua, *Mat. Res. Bull.* 2011, **46**, 845-849.

41 P. A. Maggard and P. D. Boyle, *Inorg. Chem*. 2003, **42**, 4250-4252.

42 R. N. Devi, P. Rabu, V. O. Golub, C. J. O'Connor and J. Zubieta, *Solid State Sci.* 2002, **4**, 1095-1102.

43 E. S. Larrea, J. L. Mesa, J. L. Pizarro, R. Fernández de Luis, J. Rodríguez Fernández, T. Rojo, and M. I. Arriortua, *Dalton Trans.* 2012, **41**, 14170-14179.

44 L. Yang, C. Hu, H. Naruke and T. Yanase, *Acta Crystallogr. Sect. C: Cryst. Struct. Commun.* 2001, **57**, 799-801.

45 M. I. Khan, E. Yohannes, R. C. Nome, S. Ayes, V. O. Golub, C. J. O'Connor and R. J. Doedens, *Chem. Mater*. 2004, **16**, 5273-5279.

46 R. Fernández de Luis, J. L. Mesa, M. K. Urtiaga, T. Rojo and M. I. Arriortua, *Eur. J. Inorg. Chem.* 2009, 4786-4794.

47 R. Fernández de Luis, M. K. Urtiaga, J. L. Mesa, A. T. Aguayo, T. Rojo, T. and M. I. Arriortua, *Cryst. Eng. Comm.* 2010, **10**, 1880-1886.

48 H. Lin and P. A. Maggard, *Inorg. Chem*. 2008, **47**, 8044-8052.

49 B. Yan and P. A, Maggard, *Inorg. Chem*. 2007, **46**, 6640-6646.

50 C.-D. Zhang, S.-X. Liu, L.-H. Xie, B. Gao, C.-Y. Sun and D.-H. Li, *J. Mol. Struct.* 2005, **753**, 40-44.

51 R. Fernández de Luis, M. K. Urtiaga, J. L. Mesa, K. Vidal, L. Lezama, T. Rojo and M. I. Arriortua, *Chem. Mater.* 2010, **22**, 5543-5553.

52 C.-C. Wang, Acta Crystallogr., *Sect. E: Struct. Rep. Online* 2007, **63**, m2233.

53 R. Fernández de Luis, J. L. Mesa, M. K. Urtiaga, L. Lezama, L., M. I. Arriortua and T. Rojo, *New. J. Chem.* 2008, **32**, 1582-1589.

54 C.-C. Wang and C. Yin, *Z. Kristallogr. New Cryst. Struct*. 2008, **223**, 13-15.

55 R. Fernández de Luis, M. K. Urtiaga, J. L. Mesa, J. Orive Gómez de Segura, T. Rojo and M. I. Arriortua, *CrystEngComm*, 2011, **13**, 6488-6498.

56 R. Fernández de Luis, M. K. Urtiaga, J. L. Mesa, E. S. Larrea, T. Rojo and M. I. Arriortua, *Inorg. Chem.*, 2013, **52**, 2615-2626.

57 R. Fernández de Luis, M. K. Urtiaga, J. L. Mesa, E. S. Larrea, T. Rojo and M. I. Arriortua, *CrysEngComm*, 2012, **14**, 6921-6933.

58 R. Fernández de Luis, J. L. Mesa, M. K. Urtiaga, E. S. Larrea, T. Rojo, and M. I. Arriortua, *Inorg. Chem.* 2012, **51**, 2130-2139.

59 R. Fernández de Luis, J. Orive, E. S. Larrea, M. K., Urtiaga and M. I. Arriortua, *Cryst. Growth Des.* 2014, **14**, 658−670.

60 X. Wang, H.-L. Hu, B.-K. Chen, G.-C. Liu and J. Li, *Z. Anorg. Allg. Chem*. **2009**, *635*, 2692-2696.

61 Y.-Q. Lan, S.-L. Li, X.-L. Wang, K.-Z. Shao, D.-Y. Du, Z.-M. Su and E.-B. Wang, *Chem. Eur. J.* 2008, **14**, 9999-10006.

62 X.-L. Wang, B.-K. Chen, G.-C. Liu, H.-Y. Lin and H.-L. Hu, *J. Organomet. Chem.* 2010, **695**, 827-832.

63 Y.-F. Qi, D. Xiao, E. Wang, A. Zhang and X. Wang, *Aust. J. Chem*. 2007, **60**, 871-878.

64 X. Wang, B. Chen, G. Liu, H. Lin, H. Hu and Y. J. Chen, *Inorg. Organomet. Polym. Mater.* 2009, **19**, 176-180.

65 Y. Hu, F. Luo and F. Dong, *Chem. Commun.* 2011, **47**, 761-763.

66 M. I. Khan, S. Deb and R. J. Doedens, *Inorg. Chem. Commun*. 2006, **9**, 25-28.

67 L.-J. Zhang, Z.-J. Hu, Z. Zang and H.-Y. Gou, *Chin. J. Chem*. 2007, **25**, 566-569.

68 X. Qu, L. Xu, F. Li, G. Gao and Y. Yang, *Inorg. Chem. Commun*. 2007, **10**, 1404-1408.

69 X. Qu, L. Xu, G. Gao, F. Li and Y. Yang, *Inorg. Chem*. 2007, **46**, 4775-4777.

70 Y.-F. Qi, C.-P. LV, Y.-G. Li, E.-B. Wang, J. Li and X.-L. Song, *Inorg. Chem. Commun.* 2010, **13**, 384-387.

71 W. Ouellette and J. Zubieta, *Solid State Sci*. 2007, **9**, 658-663.

72 W. Ouellette, E. Burkholder, S. Manzar, L. Bewley, R.S. Rarig and J. Zubieta, *Solid State Sci.* 2004, **6**, 77-84.

73 R.N. Devi, P. Rabu, V.O. Golub, C.J. O'Connor and J. Zubieta, *Solid State Sci*. 2002, **4**, 1095-1102.

74 R. S. Jr. Rarig and J. Zubieta, *Dalton Trans*. 2003, 1861-1868.

75 P. J. Hargman, C. Bridges, J. E. Greedan and J. Zubieta, *J. Chem. Soc., Dalton Trans.*, 1999, 2901-2903.

76 J.-R. Li, Q. Yu, E.C. Sanudo, Y. Tao, W.-C Song and X.-H. Bu, *Chem. Mater*. 2008, **20**, 1218-1220.

77 (a) C.-L. Pan, J.-Q. Xu, K.-X. Wang, X.-B. Cui, L. Ye, Z.-L. Lu, D.-Q. Chu and T.-G. Wang, 2003, (b) G. Li, Z. Shi, Y. Xu, S. Feng, *Inorg. Chem.* 2003, **42**, 1170-1174.

78 T. S-C. Law, H. H-Y. Sung and I. D. Williams, *Inorg. Chem. Commun.* 2000, **3**, 420-423.

79 L.-M. Zheng, T. Whitfield, X. Wang and A. J. Jacobson, *Angew. Chem. Int. Ed.* 2000, **39**, 4528-4531.

80 J. Tao, X.-M. Zhang, M.-L. Tong and X.-M. Chen, *J. Chem. Soc., Dalton Trans.*, 2001, 700-771.

81 C.-L. Chen, A. M. Goforth, M. D. Smith, C.-Y. Su, H.-C. zur Loye, *Angew. Chem. Int. Ed.* 2005, **44**, 6673-6677.

82 J. M. Ellsworth, M. D. Smith, H.-C. zur Loye, *Solid State Sci.*, 2008, **10**, 1822-1834.

83 J. Lu, E. Wang, J. Chen, Y. Qi, C. Hu, L. Xu and J. Peng, *J. Solid State Chem*. 2004, **177**, 946-950.

84 D. Xiao, E. Wang, H. An, L. Xu and C. Hu, *J. Molec. Struc*. 2004, **707**, 77-81.

85 D. Xiao, Y. Xu, Y. Hou, E. Wang, S. Wang, Y. Li, L. Xu, C. Hu, *Eur. J. Inorg. Chem*. 2004, 1385-1388.

86 (a) R. N. Devi and J. Zubieta, *Inorg, Chim. Acta*, 2002, **338**, 165-168. (b) L.-M. Zheng, J.-S. Zhao, K.-H. Lii, L. Y. Zhang, Y. Liu and X.-Q. Xin, *J. Chem. Soc*., *Dalton Trans*., 1999, 939–943. (c) C. Sun, E. Wang, D. Xiao, H. An and L. Xu, *J. Mol. Struct.* 2007, **840**, 53-58. (d) D. Xiao, Y. Hou, E. Wang, Y. Li, J. Lu, L. Xu and C. Hu, *J. Mol. Struct.* 2004, **691**, 123-131. (e) S. Natarajan, *Inorg. Chim. Acta*, 2003, **348**, 233-236.

87 Y. Lu, E. Wang, M. Yuan, Y. Li, L. Xu, C. Hu, N. Hu and H. Jia, *Solid State Science* 2002, **4**, 449-453.

88 C.-M. Liu, D.-Q. Zhang, M. Xiong, M.-Q. Dai, H.-M. Hu and D.-B. Zhu, *J. Coord. Chem.* 2002, **55**, 1327-1335.

89 R. Fernández de Luis, M. K. Urtiaga, J. L. Mesa, T. Rojo and M. I. Arriortua, *J. Alloy Compd.* 2009, **480**, 54-56.

90 (a) J. Livaje, Coor. Chem. Rev. 1998, 178, 999-1018. (b) L. Bouhedja, N. Steunou, J. Maquet and J. Livage, J. Solid State Chem. 2001, 162, 315-321.

91 T. Chirayil, P. Y. Zavalij and M. S. Whittingham, *Chem. Mater*. 1998, **10**, 2629-2640.

92 K.K. Nanda, L. K. Thompson, J. N. Bridson, K. J. Nag, *Chem. Soc., Chem. Commun.* 1994, 1337-1341.

93 M.H. Zeng, B. Wang, X. Y. Wang, W. X. Zhang, X. M. Chen and S. Gao, *Inorg. Chem.* 2006, **45**, 7069-7076.

94 (a) J. Cano, G. De Mundo, J. L. Sanz, R. Ruiz, J. Faus, F. Loret, M. Julve and A. Caneschi, *J. Chem. Soc., Dalton Trans.*, 1997, 1915-1924. (b) P. Vitoria, J. M. Gutiérrez-Zorrilla, A. Luque, P. Román, L. Lezama, F. J. Zuñiga and J. I. Beitia, *Inorg. Chem.* 2003, **42**, 960-969.

95 (a) R. A. Shiels, K. Venkatasubbaiah and C.W. Jones, *Adv. Synth. Catal.*, 2008, **350**, 2823; (b) A. Zhang, J. Zhang, N. Cui, X. Tie, Y. An and L. Li, *J. Mol. Catal. A: Chem.*, 2009, **304**, 28; (c) D. E.Katsoulis, *Chem. Rev.*, 1998, **98**, 359; (d) G. Centi and F. Trifiro, *Appl. Catal., A*, 1996, **143**, 3; (e) Y. Idota, *Eur. Pat.*, 0 567 149 A1, 1993; (f) M. S.Whittingham, *J. Electrochem. Soc.: Electrochem. Sci. Tech*, 1976, **123**, 315; (g) S. Denis, E. Baudrin, F. Orsini, G. Ouvrard, M. Touboul and J.-M. Tarascon, *J. Power Sources*, 1999, **81–82**, 79; (h) Y. Ueda, *Chem.Mater.*, 1998, **10**, 2653; (i) L. Liu, X.Wang and A. J. Jacobson, *J. Mater. Res.*, 2009, **24**, 1901.

96 (a) M. Weyad, H. J. Hecht, M. Kiess, M. F. Liaud, H. Vilter and D. Schomburg, *J. Mol. Biol.*, 1999, **293**, 595; (b) J. N. Carter-Franklin, J. D. Parrish, R. A. Tchirret-Guth, R. D. Little and A. Butler, *J. Am. Chem. Soc.*, 2003, **125**, 3688; (c) D. Rechder,G. Santoni,G.M. Licini, C. Schilzke and B. Meier, *Coord. Chem. Rev.*, 2003, **237**, 53.

97 E. S. Larrea, J. L. Mesa, J. L. Pizarro, M. Iglesias, T. Rojo and M. I. Arriortua, *Dalton Trans.*, 2011, **40**, 12690.

98 L. Luo and P. A. Maggard, *Cryst. Growth Des.* 2013, *13*, 5282−5288.

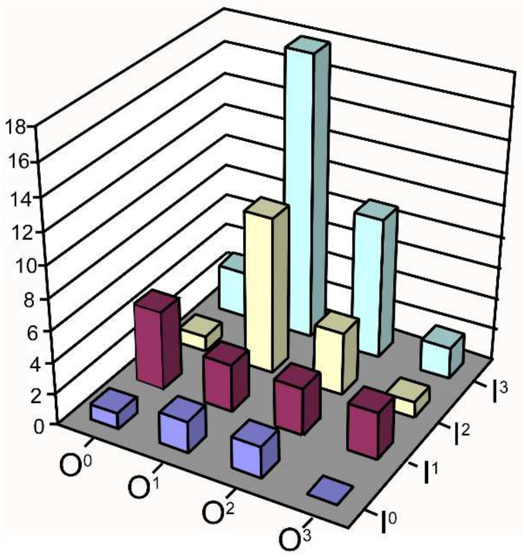

Classification of inorganic-organic vanadates constructed from bridging ligands in function of the metal-organic and inorganic substructures dimensionalities